

REPUBLIQUE DU CAMEROUN  
Paix-Travail-Patrie

-----  
UNIVERSITE DE YAOUNDE I

-----  
CENTRE DE RECHERCHE ET DE  
FORMATION DOCTORALE EN  
SCIENCES, TECHNOLOGIES ET  
GEOSCIENCES

UNITE DE RECHERCHE ET DE  
FORMATION DOCTORALE  
PHYSIQUE ET APPLICATIONS

B.P 812 Yaoundé  
Email: crftstg@uyi.uninet.cm



REPUBLIC OF CAMEROON  
Peace-Work-Fatherland

-----  
THE UNIVERSITY OF YAOUNDE I

-----  
POSTGRADUATES SCHOOL OF  
SCIENCE, TECHNOLOGY AND  
GEOSCIENCES

RESEARCH AND POSTGRADUATE  
TRAINING UNIT FOR PHYSICS AND  
APPLICATIONS

P.O.BOX 812 Yaoundé  
Email: crftstg@uyi.uninet.cm

**LABORATORY OF NUCLEAR, ATOMIC, MOLECULAR  
PHYSICS AND BIOPHYSICS**

**Solitons-like regimes of interaction of bacterial  
chemotaxis**

**THESIS**

Submitted and defended in fulfillment of the requirements for the  
Degree of **Doctorat/Ph.D. in Physics**

**Specialty: ATOMIC, MOLECULAR PHYSICS AND BIOPHYSICS**

By:

**DOMGNO KUIPOU William**

**Registration number: 09W0071**

**Master of Science in Physics**

Under the supervision of  
**MOHAMADOU ALIDOU**

*Professor*  
*University of Maroua*



**YEAR : 2021**



**DEPARTEMENT DE PHYSIQUE**  
DEPARTMENT OF PHYSICS

**ATTESTATION DE CORRECTION DE LA THESE DE**  
**DOCTORAT/Ph.D**

Nous, Professeurs, **DJUIDJE Germaine**, **BEN-BOLIE Germain Hubert**, **FEWO Serge Ibraïd**, **ABDOULKARY SAIDOU**, et Professeur **WOAFO Paul**, respectivement Examineurs et Président du jury de la thèse de Doctorat/Ph.D de Monsieur **DOMGNO KUIPOU William** Matricule **09W0071**, préparée sous la direction du Professeur **MOHAMADOU Alidou** intitulée : « **SOLITON-LIKE REGIMES OF INTERACTIONS OF BACTERIAL CHEMOTAXIS** », soutenue le **Vendredi, 29 Juillet 2022**, en vue de l'obtention du grade de Docteur/Ph.D en Physique. Spécialité **Physique Atomique, Moléculaire et Biophysique**, attestons que toutes les corrections demandées par le Jury de soutenance ont été effectuées.

En foi de quoi, la présente attestation lui est délivrée pour servir et valoir ce que de droit.

Fait à Yaoundé le **20 OCT 2022**.....

Examineurs

Pr. DJUIDJE Germaine

Pr. FEWO Serge Ibraïd

Le Président du Jury

Pr. WOAFO Paul

Pr. ABDOULKARY SAIDOU

Le Chef de Département de Physique

Le Chef de  
Département de  
Physique

Jean-Marie Bienvenu  
Professeur

# Soliton-like regimes of interaction of bacterial chemotaxis

Laboratory of Nuclear, Atomic, Molecular Physics and Biophysics

THESIS

Submitted for the Partial Fulfillment of the Requirements for the  
Award of the Degree of Doctorat/Ph.D in Physics  
Option: Atomic, Molecular Physics and Biophysics

By

**DOMGNO KUIPOU William**

Registration Number: 09W0071

Master of Science in Physics

Under the Supervision of

**MOHAMADOU ALIDOU**

Professor

University of Maroua (UMa)

December 8, 2022

---

# Dedication

✠ To my family **Grand-Mother, Mother, Brothers and Sisters** who have been an active part of this exciting process.

---

---

# Acknowledgments

By the end of this Ph.D. voyage, I am grateful and honored to have walked the steps of intellectual challenges amongst careful and brilliant minds. Under your guidance, I have gained insights. I hereby reiterate my utmost appreciations to all of you.

♣ To **Almighty God the Father** who guides and strengthens me. **Allowed Be Thy Name.**

♣ I hereby thank my Supervisor, **Prof. A. Mohamadou** for his guidance and advices.

♣ I highly acknowledge the work of **Prof. H. P. Ekobena Fouda**, Head of the Biophysics Laboratory, and all the lecturers and teaching staff of the Physics Department for their relentless and combined efforts to providing students with a unique capacity building skills.

♣ I thank **Prof. S. R. Ramaswamy**, and **Dr. H. Soni** for their incessant momenta. They provide me with deep insights on active matter systems.

♣ I specially thank **Prof. E. Kengne** and **Dr. D. Belobo Belobo** for our discussions. Their relentlessness and rainy suggestions shape in great detail my scientific aptitudes. I really hope they will find in this piece of work the expression of my sincere gratitude.

♣ I hereby thank **Prof. Mballa Eloumou Landry**, **Prof. Saïdou**, **Prof. D. Vondou**, **Prof. B. Bodo**, **Dr. A. Dang Koko**, **Dr. M. Teuma**, **Dr. C. D. Bansi Kamdem** for their continue input through these Ph.D years.

♣ I thank my friends, **Njoka Maria Goretti**, **S. Tiakoua**, **E. Tankou**, **J. V. Monepimb**, **R. Tabapsi**, **Dr. Hamadou Issa**, **M. Tatchoua Kamgaing**, **A. P. Ndjawa Yomi** for our constructive discussions.

♣ I am indebted to my friend **M. Kambong Hugues** and his family for providing me with partial fundings to printing this document.

♣ To **Mrs. Mezoh Corentine**, **Mrs. Takodjou Orlette**, **Mrs. Ndikimtum Mathilda** and their respective loving and caring families, thank you. You are sources of inspiration.

♣ I will not forget the advices of my grand-uncle **Mr. Noumsi Jean** and his wife **Mrs. Mafodjui Jeanne D'Arc**.

♣ I would never ever thank enough my family, **Maguemne Marie** (grand-mother), **Joseph Kuipou**

---

**Tueno** (late father), **Djuidje Helene** (mother), **N. Kuipou Tchongui**, **A. Kuipou Maguemne**, **M. G. Kuipou Tienoue**, **Dr. R. M. Toghueo Kouipou**, **H. Kuipou Noumsi** (brothers and sisters). Your unwavering support and unconditional LOVE have fueled my tanks with the supplementary energy I needed to make the extra mile I could not make by my own.

♣ The non-exhaustive list of those not cited here, please, accept my sincere gratitude for your invaluable inputs throughout this learning process.

---

# Contents

<b>Dedication</b>	<b>1</b>
<b>Acknowledgements</b>	<b>i</b>
<b>Résumé</b>	<b>vi</b>
<b>Abstract</b>	<b>vii</b>
<b>Introduction</b>	<b>1</b>
<b>1 Generalities on bacterial chemotaxis and traveling bacterial waves</b>	<b>4</b>
1.1 Introduction . . . . .	4
1.2 The run and tumble dynamic and its biochemical implications . . . . .	4
1.3 From microscopic to emergence of a bulk collective motion . . . . .	7
1.4 Propagation of weakly nonlinear excitations in active systems . . . . .	10
1.5 Experimental and theoretical evidences of chemotactic waves, the outline of the present work . . . . .	11
1.5.1 Experimental and theoretical foundations of chemotactic traveling waves . . . . .	12
1.5.2 Outline and the contribution of the present work . . . . .	13
1.6 Conclusion . . . . .	14
<b>2 Models derivation and methodology</b>	<b>15</b>
2.1 Introduction . . . . .	15
2.2 The Keller-Segel class models: Description, derivation . . . . .	15
2.3 The models investigated in the present study . . . . .	17
2.3.1 The (2+1)-dimensional Keller-Segel model in a uniform flow . . . . .	17
2.3.2 Chemotaxis, traction and long-range diffusion in fluids . . . . .	18
2.3.3 The coupled haptotaxis-chemotaxis model . . . . .	20

---

2.3.4	The hydrodynamic description of chemotactic suspensions . . . . .	24
2.4	Theoretical calculations methods . . . . .	27
2.4.1	The Extended F-expansion method . . . . .	27
2.4.2	The reductive perturbation method and its applications . . . . .	28
2.4.3	The Hirota Bilinear Method (HBM) . . . . .	29
2.5	Numerical methods . . . . .	30
2.5.1	The fourth order Runge-Kutta method (RK4) . . . . .	30
2.5.2	The Fourier Pseudo-spectral . . . . .	30
2.6	Conclusion . . . . .	31
<b>3</b>	<b>Results and Discussion</b>	<b>32</b>
3.1	Introduction . . . . .	32
3.2	(2+1)-Traveling chemotactic waves in fluid . . . . .	32
3.2.1	Exact solutions of Eqs. (2.4) through the F-expansion method . . . . .	32
3.2.2	Existence, dynamical behavior of solutions of Eqs. (2.4) . . . . .	34
3.2.3	Numerical confirmation through the Fourier pseudo-spectral method . . . . .	37
3.3	Bacterial and chemical waves in chemotactic system with long-range diffusion, traction and kinetics . . . . .	39
3.3.1	Analytical solutions of Eqs. (2.11) through an extended F-expansion method . . . . .	39
3.3.2	Existence, dynamical behavior of solutions Eqs. (3.14)-(3.16) . . . . .	41
3.3.3	Numerical experiments with the bell-shape traveling wave . . . . .	46
3.4	Dynamic of nonlinear excitations in coupled haptotaxis-chemotaxis systems . . . . .	47
3.4.1	Results of the application of the reductive perturbation method: The wave frequency, group velocity, and the reduced model . . . . .	47
3.4.2	Analytical solutions of the reduced model: The bilinear approach . . . . .	49
3.4.3	Existence and dynamical behaviors of soliton solutions Eq. (3.37) . . . . .	51
3.4.4	Numerical experiments . . . . .	52
3.5	Nonlinear breathing chemotactic patterns in fluids . . . . .	54
3.5.1	The linear analysis revisited . . . . .	54
3.5.2	Model reduction through the application the reductive perturbation method . . . . .	57
3.5.3	Analytical solutions and dynamical behaviors of bacterial densities in the chemotaxis- fluidss model Eqs. (5) . . . . .	59
3.5.4	Confirmation through direct numerical simulations . . . . .	63
3.6	Conclusion . . . . .	64



Conclusion and future research plans	65
Appendices	66
References	75

---

# Résumé

Ce travail illustre la propagation des ondes de déplacement dans les modèles mathématiques de chimiotaxie. Nous considérons les cellules pouvant proliférer dans un fluide bi-dimensionnel dans lequel la traction, et la diffusion de longue portée sont pris en compte. Une extension des fonctions de type  $F$  nous permet de construire des solutions de type cloches, cloches renversées, escaliers, et périodiques. Nous démontrons que le champ de vitesse du fluide constitue le support compact sur lequel la propagation est possible. Ceci nous permet de déduire la ligne séparant les solutions dynamiques et stationnaires. La vitesse des ondes décroît avec l'augmentation de la traction et la diffusion de longue portée. De plus, les valeurs croissantes de la diffusion de longue portée réduisent la largeur de l'onde tout en favorisant un déplacement dans le sens direct. Cependant, la traction diminue de la largeur de l'onde et du nombre de particules transportées. Plus loin, nous couplons chimiotaxie et l'haptotaxie obtenant ainsi un modèle où traction et adhésion sont prépondérants. Par injection des excitations nonlinéaires, les propriétés visco-élastiques sont établies, et nous prédisons l'existence des zones de paramètres pouvant mener à la génération des ondes expansives ou compressives. La réduction du modèle nous mène à une équation complexe de Ginzburg-Landau dont les solutions nous permettent de montrer que le transport des cellules est optimisé lorsque l'adhésion croît ou la traction décroît. En fluide nonuniforme, le modèle correspondant prend en compte les effets de friction, gravité et traction. En présence des perturbations transversales, nous établissons que le type d'instabilité ne dépend pas de la profondeur d'immersion de cellules. Les perturbations non-transversales mettent en évidence les structures oscillatoires en eau profonde, en plus du fait que le système reste stable pour des grandes valeurs du vecteur d'onde de perturbation. Dans toutes nos analyses, nous observons que les solutions numériques et analytiques restent proches les unes des autres et gardent leur positivité. Ce dernier fait nous permet de dire que les solutions construites sont stables et peuvent être considérées comme des objets physiques.

***Mots clés:** Particules biologiques actives, Mouvement collectif, Interactions Hydrodynamiques, Excitations Nonlinéaires, Ondes de matière bactériennes.*

---

---

# Abstract

The results present in this document broadly describe the propagation of traveling waves in chemotaxis models. Considering cells to be immersed in fluids, and assuming a two-dimensional framework, we introduce models taking into consideration proliferation, long-range diffusion, traction and chemoattractant consumption rate. An extended F-expansion method allows to construct several families of waves, including bell-shaped, dip, step, and periodic profiles. We show that the flow rate of the medium constitutes the compact support through which the propagation is made possible. The later observation allows us to separate stationary and non-stationary states, and we establish the critical line separating forward and backward propagations. It is observed that wave velocity decreases as traction and long-range diffusion increase. Long-range diffusion reduces the wave width accompanied by a forward displacement, while traction decreases wave width and the number cells transported. Coupling chemotaxis and haptotaxis allows to describe the transport of cells in fibrous media. Through nonlinear excitations phenomenology, visco-elastic properties are deduced, and we predict the existence of parameter domains where expansive or compressive waves may be generated. Model reduction yields the complex Ginzburg-Landau equation, whose solutions are used to show that cells transport is optimized when adhesion increases or traction decreases. In a nonuniform fluid, we propose a chemotaxis model where friction, gravity and traction are at play. Transversal perturbations to the y-axis reveal that the type of instability does not depends on depth of the suspension. In presence of non-transversal perturbations, our analysis predict the emergence of stable oscillatory patterns in deep suspensions. Moreover, the system remains stable at long wave-vectors while stability reduces as gravity and friction increase. In our manufacturing, we have performed numerical simulations by using the analytical solutions constructed as initial conditions. We observe that numerical and analytical solutions keep their positivity and remain close to one another. This allows us to confidently assert that our solutions are physically relevant and can therefore be observed in real experimental settings.

**Keywords:** *Active biological particles, Collective behavior, Hydrodynamic interactions, Nonlinear excitations, Bacterial waves.*

---

---

# List of Figures

1.1	Left panel, biochemical transduction path of chemotactic motion in E. Coli [34]. Right panel displays the run-tumble dynamic associated with chemoreceptor states spanning cellular cytoplasm [35]. . . . .	5
1.2	On the left, the simulated path of a single cell dynamics while the right displays the crystalline order of a bacterial flock. . . . .	8
3.1	The temporal evolution of bacterial waves shows that wave thickness and velocity vary as fluid flow (a). Reduction of the carrying capacity increases amplitude and wave thickness. The same observations hold when the chemoattractant consumption's rate decreases as displayed on panels (c), (f). Parameters $D_n = 4 \cdot 10^{-6}$ , $D_c = 8.9 \cdot 10^{-6}$ , $\chi_0 = 3.9 \cdot 10^{-9}$ , $r = 2 \cdot 10^{-4}$ , $\sigma = 3.5$ , $\beta = 1$ , $k = 0.9$ , $l = 0.9$ , $\delta_{0_x} = 1.5 \cdot 10^{-6}$ , $\delta_{0_y} = 1.5 \cdot 10^{-6}$ . . . . .	35
3.2	Stable evolution of traveling bacterial (top) and chemoattractant concentrations (bottom) waves. Parameters are taken as on Fig. 3.1(a), (b). The thickness of chemoattractant waves slightly increases and its amplitude decreases as time evolves. . . . .	38
3.3	Propagation of traveling bacterial-step (top panels), and chemoattractant (bottom panels) waves. Parameters are taken as on Figs. 3.1(c), (d). Chemical wave shifts from step to down-step profile. . . . .	38
3.4	Bell-shape solutions Eqs. (3.18) for density (a) and chemoattractant concentration (b). Wave velocity increase with traction (c), chemotaxis (e), or as long-range diffusion (d) decreases. Parameters are $D_1 = 8.9 \cdot 10^{-6}$ , $D_2 = 1.69 \cdot 10^{-9}$ , $D_3 = 4 \cdot 10^{-6}$ , $\chi_0 = 6.49 \cdot 10^{-5}$ , $\tau_0 = 1.62 \cdot 10^{-3}$ , $\sigma = 2.4231 \cdot 10^8$ , $\beta = 3.5 \cdot 10^{-8}$ , $\delta_{0_x} = 1.5 \cdot 10^{-5}$ , $\delta_{0_y} = 4.5 \cdot 10^{-4}$ , $P_2 = 4$ . . . . .	42
3.5	Influence of long-range diffusion (a), traction (b), chemotaxis (c), short-range diffusion (d) and chemoattractant consumption rate (e) upon the bell-shape bacterial wave at $y = 0$ and time $t = 100$ s Except where mentioned, parameters are taken as in Fig. 3.4. . . . .	43
3.6	Dip traveling waves for bacterial density (a) and chemoattractant concentration (b) given by Eqs. (3.20). Same parameters as in Fig. 1 except for $P_2 = -2$ . . . . .	44

---

3.7	Step traveling waves for bacterial density (a) and chemoattractant concentration (b) (Eqs. (3.22)). $P_2 = 4$ , other parameters taken as in Fig. 1. . . . .	46
3.8	Snapshots of stable numerical bell-shape solutions for bacterial (chemoattractant) wave $att = 0$ s (a) [(d)], $t = 100$ s (b) [(e)], and $t = 200$ s (c) [(f)]. Parameters as in Figs. 3.4. . . . .	47
3.9	The wave frequency, the growth rate and the group velocity as functions of the wave vector. The parameters taken as in [2] are: $D_n = D_c = \alpha_1 = \gamma = \chi_0 = 10^{-3}$ , $\mu = 1$ , $\lambda = 0.12$ , $\beta = 0.05$ , $\alpha = 1$ , $\tau_0 = 1.1$ , $s = 140$ . Panel (a) shows not significant influences on wave frequency, while panel (b), the group velocity switches sign as traction increases, showing an expansive/compressive wave transition point. In panel (c), the group velocity remains positive as adhesion increases. . . . .	48
3.10	Solutions of Eq. (2.14) generated through Eq. (3.37) in the $(\xi, \tau)$ -frame. Top row, in panel (a), solitary pulse experiences amplitude reduction for $k = 1$ while (a1) displays and amplitude increase for $k = 5$ . The bottom row panels show that the wave undergoes flattening and amplitude decrease when traction (b), chemoattractant consumption (d) rate increase, while substrate attachment decreases (c). $k_{1r} = 0.9$ . Parameters as in Fig. 3.9 . . . . .	52
3.11	Numerical solutions of Eq. (2.14) generated through Eq. (3.40) as initial conditions in the $(x, t)$ -plane. Parameters are taken as in Fig. 3.9. Panel (a) depict spatiotemporal evolution of the numerical solution. The other panels compare with great agreement numerical and analytical solutions at different times. . . . .	53
3.12	Growth rate of the linear stability for parameters $\alpha = 1$ , $\beta = 10$ , $\gamma_0 = 10^3$ , $\chi_0 = 10$ , $\nu = 4$ , $P_e = 1$ , $c_0 = 1$ . Left panels, $\gamma = 1$ , $\mu_0 = 1$ , $n_0 = 10$ . Middle panels $\gamma = 10^{-2}$ , $\mu_0 = 1$ , $n_0 = 1$ and right panels $\gamma = 1$ , $\mu_0 = 5 \cdot 10^{-2}$ , $n_0 = 1$ . . . . .	56
3.13	Influence of friction (left), gravity (middle) and traction (right) on stability domains. The magnitudes and the length of the instability domain increase when friction (a), gravity effects (b) decrease, while traction increases (c). Parameters taken as in Fig. 3.12 . . . . .	56
3.14	Influences of traction, friction and amount of cells carried vertically on group velocities $V_{x_r}$ and $V_{y_r}$ . $k_y = 0.9$ (Top panels), $k_x = 0.9$ (bottom panels), parameters taken as in Fig. 1(a). . . . .	58

3.15	Top panels display bacterial waves profile generated by inserting the first order rational solution Eqs. (3.48) into Eq. (3.50). Bottom panels represent the bacterial profile recovered by plugging the second order rational solution Eq. (3.49) into Eq. (3.50). In top and bottom panels, solutions are displayed at the same time $t = 5 \cdot 10^{-3}$ . $L = 0.09, z_0 = 0.1, k_x = 0.01, k_y = 10, \varepsilon = 10^{-3}$ . Left panels $\mu_0 = 1, \nu = 2$ . Middle panels $\mu_0 = 0.1, \nu = 2, L = 0.009$ and right panels $n_0 = 10, \gamma_0 = 1, \gamma = 10, \mu_0 = 0.1; Pe = 100, k_y = 5$ . . . . .	61
3.16	Influences of proportion of cells vertically transported (a), friction (b), traction (c), diffusion ratio (d), chemotaxis (e), and chemoattractant consumption rate (f) on the thicknesses and amplitudes of the wave. Parameters taken as in Fig. 3.14(b). . . . .	62
3.17	Stable numerical solutions for first (second) order bacterial wave at $t = 0$ (a) [(d)], $t = 5 \cdot 10^{-3}$ (b) [(e)], and $t = 0.02$ (c) [(f)]. Parameters as in Figs. 5(b) [(f)]. . . . .	63

---

# Introduction

Studies on active media and innovative trends in biotechnology, have grown increasing attention for researchers from diverse walks of science. Particularly, studies on active biological particles have continuously set the evidence on spatiotemporal symmetry-breaking properties, and pave the way toward their sorting into different classes. A collection of bacteria, spermatozoa, or cells moving towards an energy source, or away from repellent domains constitutes an active system within which particles are continuously and outwardly driven by tuning their orientation through signal sensing, transduction, and adaptation. When the external factor responsible for such a directed motion is a chemical, the process is termed chemotaxis and when it is induced by extracellular medium (ECM) properties, it is known as haptotaxis. Both mechanisms have been studied experimentally, theoretically, and numerically. Though they present some differences at the molecular level, they are commonly capable of assembling cells at favorable environmental locations. In that sense, chemotaxis and haptotaxis have been shown to be at the onset of several biological processes of interest such as organ repair [1], pattern formation [2, 3], wound healing [2, 4], fertilization [2, 5], long-range communication [2, 6], and also pathological conditions including cancer cells invasion [7, 8], metastasis formation/migration [2, 3, 8], and tumour angiogenesis [9, 10]. It is therefore ubiquitous to understand how both phenomena contribute to topological deformations cells induce upon their direct surroundings, the ECM.

Chemical-induced collective motion of a cellular distribution was first studied by Adler [11], Patlak [12], Keller and Segel [13]. The latter proposed the first mathematical models to describe self-assemblies of chemotactic particles, while mathematical models describing haptotaxis were proposed later [2, 4, 7, 10, 14, 15, 16, 17]. Chemotaxis and haptotaxis models have been continuously and independently modified to take into consideration various aspects of bacterial migration including long-range interactions, contact inhibition, proliferation, hydrodynamic events and competitive interactions amongst cells [2, 6, 18, 19, 20, 21, 22, 23]. On the other side, though experimental shreds of evidence reveal that chemotaxis and haptotaxis operate through different biochemical paths, they also occur simultaneously [15, 24], yet no mathematical models taking into consideration both aspects have been consistently provided and analyzed up until now, to the best of our knowledge. Moreover,

---

chemotactic/haptotactic models have been analyzed in one-dimensional settings, however, the spreading behavior of cells and their sudden orientational change suggests that a two-dimensional analysis may be required to access new pieces of information. Mathematical models and theoretical calculations in this end and to the best of our knowledge, have also not yet received much attention. Besides, collective dynamic in cellular networks occurs as traveling bands of matter [2, 13, 19, 20, 21, 25], letting us to think that the use of traveling wave methods may be appropriate to uncover intrinsic salient features embedded in those systems. For example, Keller and Segel [13] showed the existence of traveling waves conditioned by a singular chemotactic drift. A very problematic assumption, since such a singularity, entails an unbounded chemotactic velocity drift and, an infinite cellular density. These observations further encouraged investigations on conditions within which chemotactic/haptotactic systems are globally and locally integrable [11, 26, 27, 28, 29, 30]. The latter results design different physical setups within which traveling bands of matter-wave may be observed. They also lay the mathematical foundations for investigating bacterial spread and invasion within multidimensional biological tissues, thus the aim of our investigations.

Ordinary and partial differential equations have proved their usefulness in formulating various problems under sound and specific physical constraints. This is well visible in reactive systems for example, where deterministic reaction-diffusion equations are often used to describe spatial spread. However, in their natural habitat, cells are subject to the influences of several factors, enforcing the adaptation of their motion to both chemical and mechanical events. The latter observations raise several questions amongst which the prominent are: How reaction-diffusion models may be modified to incorporate physical phenomena relevant to the study of active collective assemblies? In other words, how do particles integrate local and distant sensing pieces of information simultaneously and correlate globally their motion towards the realization of a unique endeavor? How does the collective motion of a given population shape and/or reshapes the topology of the medium within which they are immersed? And finally what are the appropriate structures emanating from generalized reaction-diffusion models responsible for a stable cellular transport in the limit of long-time and large space dimensions? Pieces of information necessary to answering these questions have not yet been provided, to the best of our knowledge. In other words, investigating these questions offers an opportunity to study new directions in the physics of collective behaviors. It opens the doors to many possibilities for analytical as well numerical analyses. We subsequently propose to theoretically assess spatiotemporal evolutions of active particles placed in a medium with dynamics of its own in one and two spatial dimensions. Using traveling wave analysis in some cases and weakly nonlinear excitations in others, we intend to provide in close analytical expressions, the solutions for chemotactic-haptotactic models and use these ones to probe cellular transport across their propagating media.



To the best of our knowledge, the application of exact solutions methods, perturbations techniques coupled with stability and numerical analysis, have not yet been used to decipher the nonlinear dynamics of reactive systems composed of biological particles set into motion by an external energy source in a multi-dimensional space. We lay down in chapter 1, brief generality on chemotaxis is provided. In chapter 2, we proceed with model derivation, and present mathematical and numerical models used to analyzed those models. the third chapter displays our common findings. The F-expansion method is used to construct traveling wave solutions of a two-component chemotaxis models. The RPM is applied to reduce chemotaxis models to cubic complex Ginzburg-Landau and complex Davey-Stewartson equations. The analytical solutions of these equations are later used to probe spatiotemporal evolutions of bacterial densities. The present report is enclosed with a general conclusion and an open door on future research works.

---

# Chapter 1

## Generality on bacterial chemotaxis and traveling bacterial waves

### 1.1 Introduction

Understanding bacterial chemotaxis/haptotaxis has become a paradigm for biology and biomechanic system analysts. Broadly, both mechanisms happen as the signature of local excitations strong enough to trigger an average convergence towards stable configurations. It is therefore reasonable to wonder how an element of a given population senses and integrates external excitations at the molecular level such that the resulting motion at the population scale is coherent. The answer to this question represents a fundamental issue in the sense it requires taking into consideration variants characteristics of cell-cell interactions. Starting at the molecular level, we lay in this chapter, the biochemical foundations of collective motion and expose the main motivation of our investigations.

### 1.2 The run and tumble dynamic and its biochemical implications

Chemotaxis is the ability of a cell to instantaneously direct its orientation directions toward regions with attractive or repulsive chemical properties. It was observed by Engelmann [31, 32] and Pfeffer [33], and has since then received much attention from theoreticians and experimentalists. At the cellular level, this phenomenon is achieved by specific chemoreceptors known as Methyl-accepting Chemotaxis Proteins (MCPs). Each of these receptors respond to specific chemoeffectors. In *E. coli* for example, there are five preponderant receptors, namely: Tar responding to aspartate, Tsr responds

---

to serine, Tap to dipeptides, Trg to galactose and Aer, the less abundant responds to oxygen. The receptors span the cytoplasm and form clusters at both ends of bacteria. Chemoreceptors are highly sensitive to chemoattractant concentration variations, and they each respond to specific attractants. In absence of any external bias, a bacterium moves randomly without a preferred orientation direction. In presence of an attractive chemical, activation of bacterial receptors triggers a set of intracellular biochemical cascades that subsequently monitor the bacterial flagella activity. When several flagella rotate counterclockwise (CCW), they bundle and propel the cell in a quasi straight line forward motion called a run. Clockwise (CW) rotations are at the onset of flagella detachment, and such a process would lead to a tumbling motion. The latter allows a cell to change its primary direction orientation. The process is very transient compared to runs

In the case of *E. coli* specie as depicted on the left panel of Fig. 1, CW and CCW rotations are entertained by a set of specific chemicals known as chemotaxis proteins (Che). These are known to play a linkage role between the receptor and flagella motors situated at the end of the cell body. Though each chemotaxis protein has a specific role, their mutual interactions coupled with production-depletion control both the type and degree of the cellular motion as displayed in Fig. 1. On the left panel of Fig.

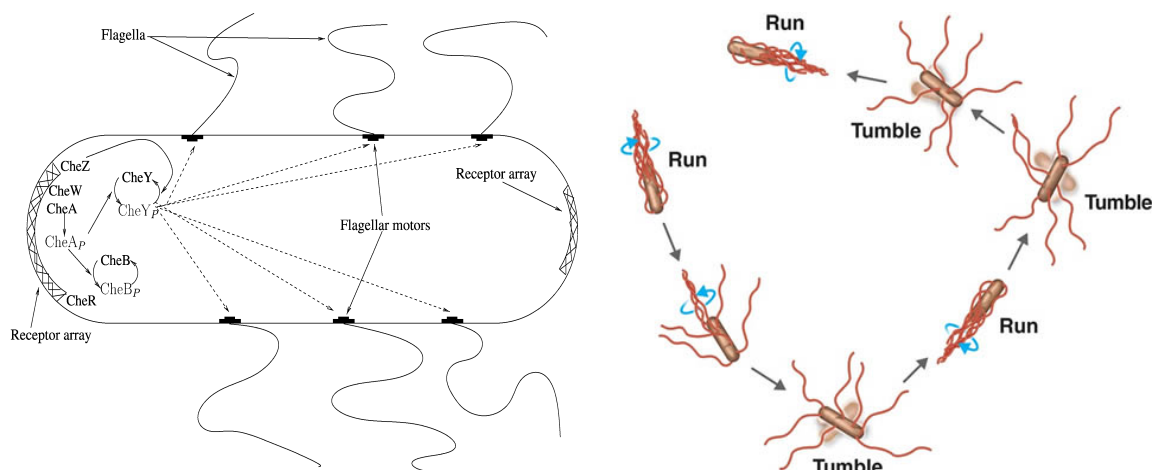


Figure 1.1: Left panel, biochemical transduction path of chemotactic motion in *E. coli* [34]. Right panel displays the run-tumble dynamic associated with chemoreceptor states spanning cellular cytoplasm [35].

1, the chemotaxis proteins Che's provide the necessary path for the biochemical cascade taking place within each cell during a chemotactic event. This enforces that the signal transduction from sensing to the actuation of flagella motors is controlled by a set of well defined intracellular protein-protein interactions. The proteins CheA, CheW and CheZ are located at bacterial receptors level. In presence of a given chemical, receptors produce a signal that is then transmitted within the cell. In order to

translate the detected signal at the intracellular level, the chemoreceptor protein CheW plays a linking role between CheA and the receptors situated at both edges of cells [36]. CheA also interacts directly with the receptors. When the chemoattractant concentration decreases, an autophosphorylation of CheA is triggered by receptors. One of the phosphoryl group is either subsequently transferred to the response regulator CheY or to CheB. The phosphotransfer from CheA<sub>p</sub> to CheY increases the affinity of the latter with flagella motors. Thus CheY<sub>p</sub> diffuses through the cell. Once it reaches flagella, the tumbling rate/probability of the cell increases [37]. As consequence, flagella unbundle. Signal termination happens when CheZ dephosphorylates CheY<sub>p</sub> at the receptors level [38].

Simultaneously on the other side, a slower the phosphotransfer also occurs from CheA<sub>p</sub> to CheB, triggering the process of adaptation. The latter is mediated by the CheB<sub>p</sub> proteins. In fact, the primary role of CheB is to reset the receptors into the unstimulated state, while CheB<sub>p</sub> has the potential to demethylating the receptors, hence counteracting the activity of the methyltransferase CheR. The dual competition between CheY and CheB proteins reveals that receptor methylation leverages the rate of CheA<sub>p</sub> production [34, 35]. When bacteria are in their unstimulated states, the dual competition results into an equilibrium between CheR and CheB<sub>p</sub>, leading to the non observation of the methylation process. Since CheR and CheB<sub>p</sub> compete for a specific binding domain of CheA, one can therefore assume that autophosphorylation of CheA coupled with receptors methylation are the key processes to controlling flagella rotations, and hence the out-coming motion. In contradiction, adding a chemoattractant to receptors decreases the autophosphorylation rate of CheA, with two major consequences: the phosphotransfer to CheY does not occur, entailing a net decrease of CheY<sub>p</sub> in the cytoplasm. Therefore, as CheY concentrations are higher, their affinity with flagella triggers CCW rotations of the latter ones. The second effect of adding a chemoattractant is that CheB<sub>p</sub> concentrations decrease, and the receptors get methylated by the methyltransferase CheR. Consequently, an autophosphorylation of CheA occurs, hence returning the system to its unstimulated state. We display on the left panel of Fig. 1 brief details of the machinery described above, and on the right, the different associated displacement patterns.

When the extracellular medium (ECM) of the cell changes positively (presence of chemoattractant), chemoreceptors' activity drops hence phosphorylation rate of CheA decreases. Consequently, CheY<sub>p</sub> concentration reduces, causing counterclockwise rotations of flagella. In the same way, CheB<sub>p</sub> concentration decreases as well, increasing the methylation rate of receptors by CheR. As an outcome, their activity rises hence leading them to a pre-stimulated autophosphorylated state CheA, and the cycle starts all over again. Reversely, when negative variations occur, autophosphorylation rate of CheA increases, hence increasing CheY<sub>p</sub> and CheB<sub>p</sub> concentrations. Thus, clockwise rotations of flagella cause cells to tumble. Subsequently, the rise of CheB<sub>p</sub> favors receptors demethylation leading to

a return to the prestimulated phosphorylated state CheA, as well as the CheB<sub>p</sub> and CheY<sub>p</sub>. Though each species may present its own specific chemotaxis proteins due to physiological differences, the above-described machinery is similar in many species [35], hence letting us think that it might be a common feature in several biological entities. The underlying process may be summarized as

**Signal detection**  $\longrightarrow$  **Signal processing**  $\longrightarrow$  **Response to signal**  $\longrightarrow$  **Adaptation**.

The integration of the above linear chain over several units indicates a continuous bias of flagellar rotations, with a possible outcome of large scale motions as those observed in collective dynamics of swimming fishes, traffic jams, herd flocks, bird swirling, collective behavior of pedestrians in a busy street, just to name few. The overall process of bacterial motion starting from signal sensing to collective dynamic can be described by important intrinsic characteristics including sensitivity, adaptation, and robustness. In other words, the individual response of bacteria requires some changes in the signal processing networks that is further responsible for biasing flagella motors. This also implies that the above characteristics enable cells filter the signal being processed. Adaptation mediated the termination of the bacterial response, and it does not alter either signal processing or provokes spatial rearrangement. These observations enforce the understanding of principles prevailing at the cellular level. These ones presents several opportunities to design biotechnological setups for controlling the transport of higher densities and by ricochet the collective dynamic. Our point that those basic principles in fact might present some influences at the macroscale, in the sense that they may be applied to decipher structural changes such as the degradation of receptors.

### 1.3 From microscopic to emergence of a bulk collective motion

From the precedent section, chemotactic motion possesses complex molecular origins, hence the need for more accurate, in-depth qualitative and quantitative analyses. To this end, a significant and strategic body of works has emphasized on describing chemotaxis at single cell unit and the population level. Both lines of work started in the middle sixties with the pioneering experiments of Adler [11], and has since then been served as the basis for unraveling chemotactic systems, experimentally and theoretically. In occurrence, active convergence of cells towards attractive regions may be responsible for contamination due to higher densities biofilm formation on surfaces [39].

In his work, Adler studied *E. coli* migration in agar plates containing different chemoattractant substances. He observed the formation of circular bands of cells depending on the attractant consumed [11, 40]. Attractant consumption at the microscopic scale drives each constituent of the colony to exhibit an irreversible dynamic. The observations of these traveling bands sparked much interest in the modeling of population behavior at large scales. It is reasonable to think that self-propelled

biological entities may form coherent sub-class of active matter systems that can be theoretically assessed. It is a common feature when investigating collective dynamics to consider mathematical models emanating from microscopic interactions [11-14, 19-22, 37, 38, 40].

Several approaches have been adopted to analyze the collective motion of bacterial densities in their natural habitat. At a single cell level (left panel of Fig. 2), the canonical view of runs (quasi-straight distances covered at constant speed) punctuated by tumbles (angular deviation from the previous direction orientation occurs at a quasi-constant rate) leads over a high number of particle, to a diffusive like behavior (right panel of Fig. 1). However, observations of Fig. 2 facilitate the establishment of a

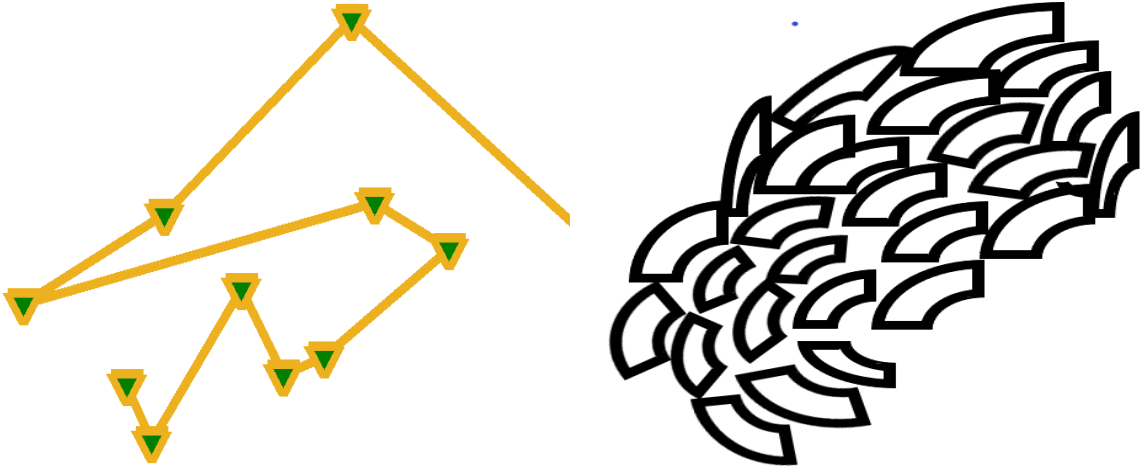


Figure 1.2: On the left, the simulated path of a single cell dynamics while the right displays the crystalline order of a bacterial flock.

connection between single-cell dynamics, and broad range phenomena existing in the subsequent high particles density systems derived after application of suitable coarse-grained analyses. In this view, the application of the latter requires considering the deterministic diffusion equation describing the probability distribution function coupled to a single particle evolution equation. These coarse-grained models are used to describe large space phenomena such as dense cluster formation often associated with down-regulation of bacterial swimming speed. This implies that chemical communication/sensing experienced by cells presents effects on each unit of the colony that in bulk, can be observed as density-dependent velocity. For instance, when the medium is quasi-dilute, the velocity smoothly decorrelates and bacteria asymmetrically catalyze chemoattractant conversion into a fuel following the biochemical cascades described in section 1.2, hence leading to a mechanical motion (flagella actions). Therefore, an acute tuning of sensing mechanisms of each cell may lead to a new state called Motility Induced Phase Separation (MIPS) [41, 42]. Though MIPS also occurs in many non-biochemical situations, it summarizes the fact that collective assemblies are the result of individuals particles coherently moving

accordingly with their neighbor for the realization of a common task. This also implies that particles' interactions with one another and with their environment give rise to highly correlated motion and mechanical events that cannot only be explained by the biochemical machinery involved. A clear distinctive feature associated with chemotactic collective behaviors in large spatial dimensions is that each particle consumes and produces a chemoattractant, and the chemoattractant is initially precisely located. This characteristic enables the system to avoid shear flows like behaviors that are literally due to energy sources localized at the boundaries in some systems [43].

Though the chemotaxis machinery of many species is well documented, a complete description of the phenomenon seems far to be attained due to complexity and the high number of variables to be handled. However, for a given population, quantifying key parameters of the dynamical behavior may provide an effective way improve our understanding of the generic process behind living matter motion. This is achievable by investigating global principles such as transport, conservation, and symmetry. Questioning some hypotheses accessible to theory as performed in the seminal work [44] may offer a suitable approach to this end.

Individual-based models have been applied to decipher the influences of single-cell behaviors on the cellular population. An example of this approach was performed by the authors of [45] while investigating the contribution of stochasticity in the chemotactic signaling network upon the bulk dynamic. Their analyses shed light on two majors problems: the incapacity of agents based models to probe the influences of variations of receptor sensitivity, adaptation, and motor response at the population level. Secondly, it is incapable of distinctively accounting for the relation between flagella rotation bias and  $CheY_p$  concentration. These issues have been circumvented by the authors of [46, 47] who built a detailed model consisting of approximately 90 ordinary differential equations (ODEs). Incorporating biophysical data, they produced a good approximation of swimming patterns of cells, hence bridging the gap between single cell and population-scale models. However, the number of equations involved in the model is relatively high, rendering tedious its complete analysis.

On the other side, the jet lag between excitation and adaptation allowed [48] to show that temporal cellular evolution can be coarse-grained. In the same way, the authors of [49] showed that the chemotactic response vanishes as the adaptation time tends to zero, hence paving the way toward simulations of chemotactic behaviors under reasonable time limits. Though this approach leads to interesting results, the common issue associated with this approach is that the application of coarse-grained methods shifts the system from discrete to continuous, hence the contribution of an individual cell on the global dynamic is significantly hidden.

Following [12, 50] it is clear that the chemotactic behavior also follows stochastic paths. Though this approach offers the possibility to understand the correlation between collective chemotactic motion

and random walks of a cell, it does not help to bridging intracellular biochemical cascades to the observed large-scale behaviors. However, considering the temporal change in receptor occupancy, the approach developed in [50], represents a starting point to explain how a single cell trait affects population behavior. All the above shreds of evidence suggest that chemotaxis can be primarily analyzed at a single cell level as well as at macroscale, and in some rare cases a bridge between both observations can be built. However, in nature, bacteria collectively travel as a bundle. This last observation paves the way towards unraveling collective chemotaxis behavior by measuring the average bacterial density. Such an exercise can be made possible in experimental settings or using direct numerical integrations of the models under consideration.

## 1.4 Propagation of weakly nonlinear excitations in active systems

Biological systems in occurrence, collections of chemotactic bacteria are excitable systems that are set into motion due to energy or metabolic supply high enough to internally trigger changes at the biochemical level. This means that understanding bacterial collective behaviors depends on the scale one attaches its attention to. However, whether one is interested in either macroscopic or microscopic description, the laws describing complex phenomena in biological systems are often empirically derived using simplistic ideas and hypotheses such as transport, symmetry, kinetics, linearization, and Taylor expansion. The latter approach has helped produce results with remarkable accuracy, yet extending its use to complex systems such as chemotaxis/haptotaxis has proven difficult since the biochemical structures induced by chemotaxis/haptotaxis have non-trivial consequences at the macroscopic scales. This difficulty resides in the fact that the approach becomes mathematically taxing, enforcing to consider different scales of the problem. The aim is to be able to reduce the complexity of a model and hence provide a description of the problem that shares the characteristics of the different scales initially considered. A systematical way of doing this consists of replacing a non-integrable nonlinear problems with their equivalent ones that are linear. A technically affordable method while proceeding so maybe through perturbation analysis which implies the use of slowly varying wave amplitudes often qualified as weakly nonlinear waves.

Although weakly nonlinear waves approximations may be used without the need to rely on a specific experimental situation, their related phenomena diverge from the results obtained through linear analysis. This is principally due to the fact that small displacement of a physical quantity in the equation may yield large deviations from its expected value. In this sense, the use of a multiscale



analysis may be convenient and has been used in spatially extended systems. Weakly nonlinear waves and their applications in complex extended systems range from biology, plasma physics water wave surfaces [51, 52, 53, 54, 55], just to name a few. In fact, when dealing with a system that is analytically difficult to analyze nonlinear waves offer a better alternative for probing mathematical models with remarkable accuracy. In this regard, the authors of [51] were able to provide explicit analytical solutions to a model describing the movement of charges in plasma. More recently in the same approach, nonlinear excitations were in a plasma system were used to generate soliton solutions of a plasma system in three dimensions [53]. In [54], nonlinear waves propagating in a viscoelastic tube were used to generate Mayer waves, which are well known for their applications in the study of cardiovascular problems. In their study of signal transmission in neural networks, the authors of [55] showed that weak nonlinear waves may be used as a key to generating stable and coherent modes as long as the bandwidth frequency remains within a predetermined interval. More recently, in our investigations of collective dynamics of chemotactic in fluid [56] and invasive processes induced by mesenchymal cells [57], we used weak nonlinear waves to prove that apparently complicated systems of partial differential equations may be solved by considering finite sums of modulated nonlinear solutions. Despite the possibilities generated by the application of multiscale methods, one can confidently affirm that it provides a compelling framework to describe mathematical models using a solid footing. Moreover, it offers a unified tool for modeling the different scales appearing in physical systems, in occurrence in biological models.

## **1.5 Experimental and theoretical evidences of chemotactic waves, the outline of the present work**

Besides the fact that bacteria are responsible for several pathological issues, they are also used in pharmaceutical and biotechnological industries for drug delivery and recycling purposes. When placed in a specific medium, they aggregate to form complex geometrical shapes with a remarkable speed, and the process may not only be explained through experimental observations. Starvation-induced aggregation of *Dictyostelium discoideum* into a multicellular has been observed, letting us wonder how and when short-range chemical gradients at a single cell level lead to emission of moving macroscopic structures akin to traveling waves. Answering this question implies considering how local interactions among cells, and between cells and their direct surrounding medium might contribute to enhance the formation and propagation of bands that, mathematically may be described using a traveling wave analysis. In this section, we provide the experimental context, the theoretical foundations for the

existence of traveling waves propagating within chemotactic systems, and highlight their roles at the physiological level.

### 1.5.1 Experimental and theoretical foundations of chemotactic traveling waves

Qualitative and quantitative analyses of bacterial collective motion have been carried in several experiment settings and theoretical frameworks [1-50]. The first demonstration of traveling bands of cells is imputed to Adler [11], who observed the behaviors of *E. coli* cells placed at one end of a one-dimensional racetrack setting. He found that when an attractive chemical is placed at the other end of the tube, several bands form and travel at different velocities. The bands were not formed instantaneously, and samples of bacteria taken in two distinct bands showed they present different velocities, leading to think that cells localization may be predicted with good accuracy. Starting from experimental observations of Adler, Keller and Segel derived a mathematical model for chemotaxis from whose solutions are traveling pulses [13]. Those solutions exist under the very problem of a singular chemotactic drift velocity. The latter implies that cells density might indefinitely grow and their velocity goes to infinity. Under these conditions, those solutions might not be physically relevant and call for advanced experimental investigations of traveling bands of chemotactic cells. The collective dynamic of cells happens as a transition from a single cell to multicellular network behavior, which the authors of [58] numerically and experimentally analyzed using cell-cell correlations. They were able to demonstrate that long-range communication is at the onset of aggregation. Experimental studies presented in [59, 60] revealed the formation of bands of cells. In so doing, the authors extend the results obtained by Adler and proved that The nature, the type, the number of bands, and their moving speed depend on the medium characteristics. While patterns formed in fluids are simple geometrical forms with a lifetime of about a few minutes, complex patterns were observed in semi-solid media and take several days to form [2, 59]. These observations imply that in the former case the cellular proliferation may not play an important role, in contradiction with the latter.

Combining experimental, computational, and theoretical analyses, the authors of [25] provide compelling evidence of bacterial bands displacement structures akin to traveling waves. The study shows that bacteria are principally carried through traveling pulse profiles, and, both the wave velocity and characteristic length were recovered from the model proposed. Following the same approach traveling bacterial pulses for two-chemotactic populations migrating with different speeds towards the same attractant source were analyzed in [19]. The authors prove the emergence of collective behavior that depends on the fraction of the fast population. Further theoretical studies of bacterial traveling

waves for two-species chemotactic models with Lotka-Volterra kinetics reveal that traveling waves connect two spatially homogeneous states and travel with a speed greater than a critical admissible value that does not depend on the chemotaxis strength [18]. In nutrient limiting cases, numerical simulations and experimental analyses figured out that the heterogeneity between two-chemotactic populations was found as a key to accelerating the progression of the population presenting chemotactic superiority characteristics [61]. On the other hand, in the flux limiting cases, it has been theoretically and numerically proving that the Keller-Segel approach to chemotaxis admits backward traveling waves. The latter was shown to be initially responsible for the population saturation in stable states and later engender cells transition towards unstable modes [62]. All the above-described observations reveal that chemotaxis promotes bacterial expansions towards unoccupied domains and that traveling wave analysis may be applied to assess the characteristics of such an invasive mechanism. Exact solutions methods may therefore be applied to propose analytical solutions to chemotaxis models, and use the latter to derive the spatiotemporal properties of these models. To the best of our knowledge, such an approach has not yet been done, hence our motivations.

## 1.5.2 Outline and the contribution of the present work

The above paragraph summarizes the fact that collective dynamics of cells may experimentally, numerically, and theoretically be described using traveling waves analyzes. Yet, in a reactive system where several aspects ranging from biochemical to mechanical events are at play, explicit analytical solutions have not yet been provided and discussed to a great extent. Pragmatically speaking, reaching out to biological problems is one of the main motivations for getting involved in this kind of research. This thesis derives and solves in one and two spatial dimensions chemotactic models appearing under several conditions, and the solutions constructed are used to power out some predictions.

### ♠ Chemotaxis in a fluid with uniform flow rate

In order to describe the contribution of the medium flow on the global dynamic of the bacteria, we introduce a mathematical model for chemotaxis that taken into consideration the medium flow rare, proliferation and chemoattractant consumption rate. Further, to elucidate the contribution of the average chemotactic flow emanating from bacterial motion, we construct a model that takes into consideration traction forces as well as long-range interactions. The resulting equations are sets of coupled reaction-linear and nonlinear cross-diffusion equations that are highly nonlinear. Under realistic boundary conditions, analytical solutions of these models are constructed, and their existence is discussed.

### ♠ Mechanical waves generation in chemotaxis

In this approach, we consider the mechanical properties cells might undergo in their respective media. Such a configuration requires considering the different physical mechanisms interfering in cells' motion, namely chemotaxis, haptotaxis, and advection. The resulting model is a set of four reaction-diffusion equations with nonlinear cross diffusive terms describing the dynamics of cellular density, chemical concentration, medium density, and the bulk orientation of cells. Furthermore, several other aspects such as medium compressibility properties, long-range diffusion, haptotaxis, and traction are also considered. As result, the models obtained are coupled nonlinear equations describing kinetic law, continuity, and momentum balanced. Under realistic boundary conditions, solutions are approximated using finite sums through which stability properties may be deduced at the linear orders. A further calculation may lead to model reduction and later to analytical solutions.

#### ♠ **Bacterial wave patterns in presence of non-uniform hydrodynamic interactions**

In their natural habitat, bacteria are capable of interacting directly with the neighborhood through friction, traction. Also, it is well known that bacteria present different swimming patterns depending on the medium within which they are immersed. Starting with these observations, it is amenable to think of bacteria as entities or particles capable of undergoing both steric and hydrodynamic interactions. Moreover, considering bacteria to be denser than the fluid medium within which they are immersed, they are more likely to exhibit a vertical motion when the density of their accumulation reaches an upper threshold or when they lose their sensitivity. Taking into consideration those aspects, applying force balance conditions and conservation laws leads to an extended chemotaxis-fluid model. The stability properties of such systems are of high importance to comprehend how coherent patterns emerge.

## 1.6 Conclusion

In summary, we exposed in this chapter the power points of bacterial and cellular collective motion, starting from microscopic observations. We emphasize on the chemotaxis-induced collective motion as a traveling wave, and we provided its theoretical as well as experimental foundations. We recall our aim that is to construct stable traveling bacterial waves, and their existence conditions.

---

# Chapter 2

## Model derivation and methodology

### 2.1 Introduction

The previous chapter showed that chemotaxis and haptotaxis may be at the onset of a wide range of phenomena such as collective motion, self-assemblies, patterns formation, and phase separation/transition just to name a few. Moreover, in their natural habitat, bacterial cells undergo inter and intra-species interactions and exhibit diverse swimming patterns. In that sense, a collection of cells may be considered as a highly interesting dynamical system whose properties may be used in applied biological sciences and biotechnology. In their study of chemotaxis, Keller and Segel started from microscopic observations and examined the motion of an amoeba. In doing so, they were able to build the first mathematical model mimicking with great accuracy their experimental observations. Since then, several other approaches have been proposed to derive models for chemotaxis. In this chapter, we present the general frameworks for deriving chemotaxis models under several circumstances, and we also present the tools used to analyze those models.

### 2.2 The Keller-Segel class models: Description, derivation

In their description of chemotaxis on slime molds [13, 63], Keller and Segel observed the formation of many species. By entirely examining the motion of a unit cell in a given population and standing from the macroscopic point of view, they derived a mathematical model that explains their experimental observations. In this paragraph, our aim is to recall the derivation of the Keller-Segel model for chemotaxis.

In reality, chemotaxis takes place in a medium containing bacterial cells, a nutrient, chemoattractant. Bacteria consume both nutrients and chemoattractants and they also produce an enzyme

---

responsible for chemoattractant depletion. As usually observed in a reactive system, the chemoattractant and the enzyme may combine to form a complex which is unstable and that decays quickly [13, 63]. Rather than studying biochemical processes, we are interested in understanding physics laws that apply to a collection of multicellular cells. Through this thesis, we denote by  $n(\mathbf{r}, t)$  the bacterial density and  $c(\mathbf{r}, t)$ , the chemoattractant concentration,  $t$  the time variable and  $\mathbf{r} = x, (x, y)^T, (x, y, z)^T$  is the position vector in one, two and three dimensions, respectively. In order to derive the equations describing both  $n(\mathbf{r}, t)$  and  $c(\mathbf{r}, t)$ , we assume that (a) bacteria may produce and consume chemoattractant, (b) bacteria and chemoattractant diffusions may be classified as Fickian processes, and the bacterial total flux should be modified to include chemotaxis effects, (c) time scales are long enough such that bacteria birth-death are not negligible, (d) variations of bacterial density happen as the combined effects of diffusion and that of the positive chemoattractant gradient that designs the swimming direction. Considering an arbitrary bounded regular domain  $\Omega_b$  in a two-dimensional frame, temporal variations of bacterial density (chemoattractant concentration) balances both the outwards diffusive fluxes and the kinetics terms, hence we write

$$\frac{d}{dt} \int_{\Omega_b} n dr = \int_{\Omega_b} F_n dr - \int \mathbf{J}_n \cdot \eta_s ds, \quad (2.1a)$$

$$\frac{d}{dt} \int_{\Omega} c dr = \int_{\Omega_b} F_c dr - \int \mathbf{J}_c \cdot \eta_s ds. \quad (2.1b)$$

$s$  represents the surface delimiting the boundaries of  $\Omega_b$ .  $\eta_s$  is an outward unit vector.  $F_n(n, c)$  is a kinetics term accounting for bacterial birth-death and  $F_c(n, c)$  describe chemoattractant production consumption.  $\mathbf{J}_n$  and  $\mathbf{J}_c$  are bacterial and chemoattractant fluxes, respectively. Using the hypothesis (b), we write  $\mathbf{J}_n = D_n \nabla n - \chi(n, c) \nabla c$ , and  $\mathbf{J}_c = D_c \nabla c$ .  $D_n$  and  $D_c$  are bacterial and chemoattractant diffusions, respectively.  $\chi$  is the chemotaxis strength which may also depend on  $n$  and  $c$ . Application of the divergence theorem on Eqs. (1) permits to write

$$\frac{\partial n}{\partial t} = D_n \nabla^2 n - \nabla \cdot (\chi(n, c) \nabla c) + F_n \quad (2.2a)$$

$$\frac{\partial c}{\partial t} = D_c \nabla^2 c + F_c. \quad (2.2b)$$

Eqs. (2) is Keller-Segel model for chemotaxis. Eq. (2a) describes a reaction-drift process while Eq. (2b) is a purely reaction-diffusion mechanism. With appropriate initial and boundary conditions, Eqs. (2) can be solved to determined  $n$  and  $c$  at any later time. Though the model Eqs. (2) is derived under realistic biological assumptions, it still presents some limitations, namely: (a) The Keller-Segel model does not show how the flow of the medium within cells are immersed may affect the collective motion of cells; (b) In a highly dense system, the motion of a unit cell may affect its neighbors, hence modifying the average flow in the medium; (c) the Keller-Segel model considers bacteria as

non-deformable particles, an assumption that only holds in relatively dilute systems. In other words, when the bacterial/cellular population is high, the incompressibility condition is not very consistent, hence the aim to revisit our description of chemotaxis. Furthermore, in their analyses of chemotaxis, Keller and Segel did not take into consideration the Function  $F_n$  accounting for intrinsic properties of cells such as proliferation. These enforces that cellular density remains constant, yet for timescales under consideration in experiments, it is well known that cells duplicate. These drawbacks encourage the derivation of more realistic models.

## 2.3 The models investigated in the present study

In this paragraph, we derive the models for chemotaxis investigated through our studies. In order to do that, we assume that (a) the medium within which cells are immersed has a dynamic of its own, (b) the motion of a cell may affect its neighborhood, meaning that traction forces and nonlocal responses of the cell to external stimuli may be at play.

### 2.3.1 The (2+1)-dimensional Keller-Segel model in a uniform flow

In this part of the work, we consider a bounded domain  $\Omega_b$  containing a density  $n(\mathbf{r}(t), t)$  and chemoattractant concentration  $c(\mathbf{r}(t), t)$ . The domain  $\Omega_b$  is considered deformable, and those deformations arise by the motion of cells in and out the domain  $\Omega_b$ . Therefore, it is amenable to think that local stresses on  $\Omega_b$  primarily depend on the bacterial density. The application of material derivative coupled with conservation law on  $\Omega_b$  may be written as

$$\frac{d}{dt} \int_{\Omega_b} n dr = \int_{\Omega_b} \left( \frac{\partial n}{\partial t} + \frac{d\mathbf{r}}{dt} \cdot \nabla n \right) dr = \int_{\Omega_b} F_n dr - \int \mathbf{J}_n \cdot \boldsymbol{\eta}_s ds \quad (2.3a)$$

$$\frac{d}{dt} \int_{\Omega_b} c dr = \int_{\Omega_b} \left( \frac{\partial c}{\partial t} + \frac{d\mathbf{r}}{dt} \cdot \nabla c \right) dr = \int_{\Omega_b} F_c dr - \int \mathbf{J}_c \cdot \boldsymbol{\eta}_s ds. \quad (2.3b)$$

$\frac{d\mathbf{r}}{dt} = \delta_0$  represents the velocity of a material point taken in  $\Omega_b$ . In this thesis, we assume a Fisher logistic growth term for bacterial density  $F_n(n, c) = rn(\sigma - n)$ , the chemoattractant kinetic of the form  $F_n(n, c) = -\beta nc$  and the chemotaxis strength of the form  $\chi(n, c) = \chi_0 n$ . The application of the divergence theorem on Eqs. (2.3) leads to advection-chemotaxis model

$$\frac{\partial n}{\partial t} + \delta_0 \cdot \nabla n = D_n \nabla^2 n - \chi_0 \nabla \cdot (n \nabla c) + rn(\sigma - n), \quad (2.4a)$$

$$\frac{\partial c}{\partial t} + \delta_0 \cdot \nabla c = D_c \nabla^2 c - \beta nc. \quad (2.4b)$$

Eqs. (2.4) is our chemotaxis model for particles placed in a fluid medium.  $\chi_0$  represents the chemotaxis strength and  $\delta_0 = (\delta_{0_x}, \delta_{0_y})^T$  the two dimensional flow rate which we assume uniform in each

spatial direction.  $r$  is the proliferation rate of cells and  $\sigma$  is the medium carrying capacity.  $\beta$  is the chemoattractant consumption rate. The model Eqs. (2.4) states that the collective motion of cells influences the medium dynamics with the consequence of creating short-range mechanical effects on cells. In [2, 13] simplest versions of Eqs. (2.4) have been investigated in one dimensional settings in absence of flow rate  $\delta_0 = (0, 0)^T$ . However sudden reversal of cells due to chemotaxis and random dispersal leads us to think that a better description of chemotaxis is well suited in two-dimensional frames. Analytical calculations to the best of our knowledge have not yet been done under such configuration for the model Eqs. (2.4). Furthermore, the bacterial logistic growth combined with a uniform advection may nucleate fluid mixing hence leading to instability. More recently, using a kinetic theory, the authors of [20] derived a modified chemotaxis model and used their model to predict the emergence of a traveling pulse that carries a limited amount of cells. Their model does not take into account growth either advection phenomena. From the above observations, it is amenable to think that the model Eqs. (2.4) is a better one to probe cellular collective motion only when the short-range response of cells to excitations is concerned. Hereafter, we circumvent this issue by introducing a model that takes into account cell-cell traction forces and long-range effects.

### 2.3.2 Chemotaxis, traction and long-range diffusion in fluids

As in the previous paragraph, we consider a bacterial density  $n(\mathbf{r}, t)$  and a chemoattractant concentration  $c(\mathbf{r}, t)$  in a bounded domain  $\Omega_b$ . In a situation where cells are highly packed, variations and deformations of a bacterium taken at the position  $\mathbf{r}$  have contributions emanating from its nearest and farthest neighbors situated at position  $\mathbf{r}'$ . We consider close neighbors effects dominate that of those placed at long distances, which implies that cells' response to stimuli located at relatively long distances must be averaged over the entire domain. Besides the advection and chemotactic fluxes, the conservation equation for bacterial density must include the contributions of all neighboring cells, a situation that is mathematically described by an integro-differential equation [2]. Incorporating neighbor effects in the model Eqs. (2.4) yields.

$$\frac{\partial n}{\partial t} + \nabla \cdot \mathbf{J}_n = F'_n(n, c) + \int_{-\infty}^{+\infty} w(|\mathbf{r} - \mathbf{r}'|)n(\mathbf{r}', t)d\mathbf{r}', \quad (2.5a)$$

$$\frac{\partial c}{\partial t} + \nabla \cdot \mathbf{J}_c = F_c(n, c). \quad (2.5b)$$

$w(|\mathbf{r} - \mathbf{r}'|)$  is a kernel quantifying the effects of cells located at  $\mathbf{r}$  have on their neighboring placed at  $\mathbf{r}'$ .  $w(|\mathbf{r} - \mathbf{r}'|)$  must be chosen to fit experimental realities such as the positivity and finiteness of the bacterial density. We assume a symmetric kernel hence  $w(|\mathbf{r} - \mathbf{r}'|) = w(\mathbf{r} - \mathbf{r}') = w(\mathbf{r}' - \mathbf{r})$ . If  $F'_n(n, c) \rightarrow 0$ , the bacterial rate of change positivity is ensured as soon as  $\int_{\Omega_b} w(|\mathbf{r} - \mathbf{r}'|)n(\mathbf{r}', t)d\mathbf{r}' > 0$ .



The condition  $\lim_{|\mathbf{r}-\mathbf{r}'|\rightarrow\infty} w(|\mathbf{r}-\mathbf{r}'|) \rightarrow 0$  ensures bounded bacterial densities. Let introduce a new variable  $\mathbf{z} = \mathbf{r} - \mathbf{r}'$ . In the case of a narrowing kernel,  $\mathbf{z} \rightarrow \mathbf{0}$  and Eq. (2.5a) becomes

$$\frac{\partial n}{\partial t} + \nabla \cdot \mathbf{J}_{\mathbf{n}} = F'_n(n, c) + \int_{-\infty}^{+\infty} w(z)n(\mathbf{z} + \mathbf{r}', t)dz, \quad (2.6)$$

Taylor expansion around  $z = 0$  yields

$$\begin{aligned} \frac{\partial n}{\partial t} + \nabla \cdot \mathbf{J}_{\mathbf{n}} = & F'_n(n, c) + n \int_{-\infty}^{+\infty} w(z)dz + \nabla n \cdot \int_{-\infty}^{+\infty} \mathbf{z}w(z)dz \\ & + \frac{\nabla^2 n}{2} \int_{-\infty}^{+\infty} z^2 w(z)dz + \frac{\nabla^3 n}{6} \int_{-\infty}^{+\infty} z^3 w(z)dz + \frac{\nabla^4 n}{24} \int_{-\infty}^{+\infty} z^4 w(z)dz + \dots \end{aligned} \quad (2.7)$$

The symmetry hypothesis of  $w(|\mathbf{r}-\mathbf{r}'|)$  permits

$$\int_{-\infty}^{+\infty} z^{2m+1}w(z)dz = 0, \quad D'_{2m} = \frac{1}{(2m)!} \int_{-\infty}^{+\infty} z^{2m}w(z)dz \neq 0, \quad m \in \mathbb{N}. \quad (2.8)$$

Further, diffusive fluxes are chosen as  $\mathbf{J}_{\mathbf{n}} = \delta n + \chi_0 n \nabla c - D_n \nabla n$ ,  $\mathbf{J}_{\mathbf{c}} = \delta c - D_3 \nabla c$ . Eqs. (2.5) therefore take the form

$$\frac{\partial n}{\partial t} + \nabla \cdot (n\delta) = D_0 n + D_1 \nabla^2 n + D_2 \nabla^4 n - \chi_0 \nabla \cdot (n \nabla c) + F_n(n, c), \quad (2.9a)$$

$$\frac{\partial c}{\partial t} + \nabla \cdot (c\delta) = D_3 \nabla^2 c + F_c(n, c). \quad (2.9b)$$

In Eqs. (2.9),  $F_n(n, c) = D_0 n + F'_n(n, c)$ ,  $D_1 = D_n + D'_2$ ,  $D_2 = D'_4$ . To complete the model construction, we evaluate the velocity of a point material taken in the domain  $\Omega_b$ . Recent studies of bacterial migration in a confined one-dimensional racetrack showed nucleation of strong flows emanating from cells closed to channel boundaries [64]. These flows are capable of swerving the bulk dynamic of cells placed far from channel walls. In other words, the bulk velocity field in the system comprises an active part generated by the collective motion of cells and a passive part emanating from the perturbations of the medium within which cells are immersed, hence we write

$$\delta = \delta_0 + \nabla H(n, c), \quad \text{where} \quad H(n, c) = \frac{\tau_0 n}{1 + \lambda n}. \quad (2.10)$$

In this definition of the bulk velocity in the medium, the function  $H$  permits to account for traction forces cells exert upon each other. This function may be used to measure medium deformations due to cells activity.  $\tau_0$ , the maximum traction force ensures that the velocity remains finite when the population increases in a quasi-dilute medium.  $\lambda$  measures the velocity reduction due to a higher density of cellular aggregation. In the thermodynamic limit, this choice of  $H$  ensures that the velocity remains finite both at low and high densities. In this thesis, we have considered quasi dilute systems which implies that  $\lambda \rightarrow 0$ , a situation corresponding to weak hydrodynamic properties of bacteria.

Furthermore, we choose  $F_n(n, c) = rn(\sigma - n)$  and  $F_c(n, c) = \frac{k_0 n}{k_1 + k_2 n^2} - \beta nc$ .  $r$ ,  $\sigma$ , and  $\beta$  are the proliferation rate, the medium carrying capacity, and the chemoattractant consumption rate, respectively. The first term in  $F_c$  describes chemoattractant production, and numerical values of  $k_0, k_1, k_2$  are not known to the best of our knowledge. This choice of chemoattractant production is motivated by experimental pieces of evidence which suggest that chemoattractant production is linked to a saturating cellular density [2]. This in other words also means that only a small number of particles is expected to be involved in chemoattractant production. It is therefore safe to consider  $\frac{k_2 n^2}{k_1} \ll 1$ . Using Taylor expansions,  $F_c(n, c) = \beta_1 n - \beta_3 n^3 - \beta nc$ .  $\beta_1 = \frac{k_0}{k_1}, \beta_3 = \frac{k_0 k_2}{k_1^2}$  arbitrary unknown real constants. Finally the system Eqs. (2.9) become

$$\frac{\partial n}{\partial t} + \nabla \cdot (n\delta_0) = D_1 \nabla^2 n - D_2 \nabla^4 n - \tau_0 \nabla \cdot (n \nabla n) - \chi_0 \nabla \cdot (n \nabla c) + rn(\sigma - n), \quad (2.11a)$$

$$\frac{\partial c}{\partial t} + \nabla \cdot (c\delta_0) = D_3 \nabla^2 c - \tau_0 \nabla \cdot (c \nabla n) + \beta_1 n - \beta_3 n^3 - \beta nc. \quad (2.11b)$$

More than a simple reaction-diffusion-advection process, the system of Eqs. (2.11) is dynamically interesting. It takes into consideration simple and nonlinear cross diffusions, in addition to incorporating two active transport mechanisms, namely chemotaxis and traction. Traction has been the subject of intensive experimental studies [22, 65] and to the best of our knowledge, its contribution has not yet been mathematically formulated in a chemotactic system. The model Eqs. (2.11) indicates that taking into account traction forces enhances both cellular and chemical displacement towards one another. In this sense, Eqs. (2.11) can be used to explain a broad range of phenomena in systems made of composite materials. For example, it may describe the spreading behavior of two chemotactic subpopulations of bacteria moving toward each other with different velocities. Such a differential velocity may lead to rich phenomena like instabilities and new patterns formation just to name a few. We propose Eqs. (2.11) as a viable generalized chemotaxis model that incorporates several aspects of bacterial collective motion not discussed in previous models presented in [2, 13, 18, 19, 20, 22, 25, 63]

### 2.3.3 The coupled haptotaxis-chemotaxis model

In this part of our work, we are interested in pathological tissues such as invasion, tumor development, and metastasis where chemotaxis may play a key role. In fact, tumor development starts with normal cells being transmuted negatively. Such a transmutation allows them to escape the homeostatic mechanisms accompanied by proliferation and spatial spread as the result of the diffusion. Through metastasis, cells may also come close to chemical and substrate factors with the potential of modifying their migration [4, 15, 16]. On the other hand, they also chemotactically respond to the extracellular matrix (ECM) when proteolytic degradations solubilize the ECM and release chemicals

that were attached to the ECM. The release of those chemicals is responsible for a chemical-based cellular reorientation [15, 16], enforcing the conclusion that the medium density has the potential to influence cells' motion. The latter phenomenon is known as haptotaxis. It rises to improve the ability of invasive cells to optimally detect and respond to positive external gradients, a situation that helps to recruit neighboring cells. The latter contributes to building networks through which the tumor's food transits. These observations demonstrate that besides advection, diffusion, and chemotaxis, other factors including adhesion-mediated migration, and haptotaxis largely contribute to cellular motion. Therefore, chemotaxis and haptotaxis are two distinct active mechanisms through which invasion happens in soft tissues. From the physical perspective, this implies modifying the fluxes in such a way as to consider all the above cite phenomena. In our mathematical description, we assume a continuum approach where the variables of interest are cellular density  $n(\mathbf{r}, t)$ , the chemoattractant concentration  $c(\mathbf{r}, t)$ , the medium density  $\rho(\mathbf{r}, t)$  and cellular orientation  $\mathbf{u}(\mathbf{r}, t)$ . Applying force-balanced condition and conservation laws result in the chemotaxis-haptotaxis model for cellular invasion [2, 4, 15, 16]

$$\frac{\partial n}{\partial t} + \nabla \cdot \left( n \frac{\partial \mathbf{u}}{\partial t} \right) = D'_n \nabla^2 n - \nabla \cdot [n (\chi \nabla c + a_1 \nabla \rho)], \quad (2.12a)$$

$$\frac{\partial c}{\partial t} + \nabla \cdot \left( c \frac{\partial \mathbf{u}}{\partial t} \right) = D'_c \nabla^2 c - \beta_0 n c + \alpha_0 c, \quad (2.12b)$$

$$\frac{\partial \rho}{\partial t} + \nabla \cdot \left( \rho \frac{\partial \mathbf{u}}{\partial t} \right) = 0, \quad (2.12c)$$

$$\nabla \cdot \left[ \left( \mu_1 \frac{\partial \varepsilon}{\partial t} + \mu_2 \frac{\partial \theta}{\partial t} \mathbf{I}_d \right) + \varepsilon + \nu' \theta \mathbf{I}_d + \frac{\tau' n}{1 + \lambda_0 n^2} (\rho + \gamma_0 \nabla^2 \rho) \mathbf{I}_d \right] = s_0 \rho \mathbf{u}. \quad (2.12d)$$

In the system Eqs. (2.12),  $D_n$  and  $D_c$  are the cellular and chemoattractant diffusions, respectively.  $\chi$  and  $a_1$  are respectively the chemotactic and the haptotactic functions which we hereafter consider constants.  $\beta_0$  is the chemoattractant consumption's rate while  $\alpha_0$  is the chemoattractant production rate.  $\rho$  is the ECM density,  $\mathbf{u}$  being displacement vector of a material point of the ECM, and  $\frac{\partial \mathbf{u}}{\partial t}$  the associated velocity.  $\varepsilon = \frac{1}{2} (\nabla \mathbf{u} + \nabla \mathbf{u}^T)$  is the strain tensor, and  $\theta = \nabla \cdot \mathbf{u}$  is the dilatation rate of the extracellular matrix.  $\mu_1$  and  $\mu_2$  are the shear and bulk viscosities.  $\nu'$  is the Poisson ratio,  $\tau'$  is a measure of the traction force generated by a cell,  $\lambda_0$  is the force reduction in presence of other cells. In the force/momentum Eq. (2.12d), the term  $\frac{\tau' n}{1 + \lambda_0 n^2} (\rho + \gamma_0 \nabla^2 \rho)$  describes tractions forces cells exert upon the ECM, and hence accounts for cell-ECM interactions.  $\tau' > 0$  measures the maximal intensity of the traction forces.  $\lambda_0 > 0$  ensures that traction forces go to zero at higher cellular density as experimentally suggested [2], and  $\gamma_0 > 0$  measures the nonlocal long range of cell-ECM interactions. In fact, experimental shreds of evidence suggest that filopodia which allow cells to attach to ECM may extend far beyond the direct neighborhood of those cells. Therefore, it appears reasonable to take into consideration long-range effects in the traction forces. In the right-hand side of Eq. (2.12d),

$s_0\rho\mathbf{u}$  represents the body force that counterbalances traction and viscous forces. In that term,  $s_0$  is a parameter measuring intensity with which a point material in the ECM is moved towards a restraining position along the  $\mathbf{u}$  direction. It may be taken as an adhesion or attachment parameter.

We introduce the dimensionless variables

$$\begin{aligned} t' &= \frac{t}{T}, & \nabla' &= \frac{\nabla}{L}, & n' &= \frac{n}{N}, & c' &= \frac{c}{c_r}, & \rho' &= \frac{\rho}{\rho_r}, & \mathbf{u}' &= \frac{\mathbf{u}}{L}, & \lambda &= \lambda_0 N^2, & \chi_0 &= \frac{\chi c_r T}{L^2}, \\ D_n &= \frac{D'_n T}{L^2}, & \alpha_1 &= \frac{a_1 \rho_r T}{L^2}, & D_c &= \frac{D'_c T}{L^2}, & \beta &= \frac{\beta_0 T}{N c_r^2}, & \alpha &= \frac{\alpha_0 T}{c_r^2}, & \mu &= \frac{\mu_1 + \mu_2}{1 + \nu'}, \\ \tau_0 &= \frac{\tau'}{1 + \nu'}, & s &= \frac{s_0}{1 + \nu'}. \end{aligned} \quad (2.13)$$

Furthermore, at the early stage of invasion, the maximum distance covered by cancer cells is  $L \sim 0.1 - 1\text{cm}$  [15]. Parameter values for the model Eqs. (2.12) may be taken as in [2]. However cellular diffusion is known to be of magnitude  $D'_{n,c} \sim 10^{-6}\text{cm}^2/\text{s}$  [2, 15, 16]. With this choice, the dimensional values of diffusion  $D_{n,c} \sim 10^{-3}$  given in [2] allows to deduce the reference time scale  $T \sim 10$  s. This value is relatively small compared to the time scales required for cellular proliferation to occur. Cellular proliferation may be responsible for the co-existence of multiple cell clones. Its effects during invasion are beyond the scope of this work and will be analyzed in future investigations. In the present model, we limit ourselves to the cases of a zero proliferation rate, an assumption that applies to experimental situations where the number of cells remains constant. This also means that we are interested in migration mechanisms where the effects of the existence of multiple cell clones are not considered. By omitting the prime, Eqs. (2.12) become

$$\frac{\partial n}{\partial t} + \frac{\partial}{\partial x} \left( \frac{\partial u}{\partial t} n \right) = D_n \frac{\partial^2 n}{\partial x^2} - \frac{\partial}{\partial x} \left[ n \left( \chi_0 \frac{\partial c}{\partial x} + \alpha_1 \frac{\partial \rho}{\partial x} \right) \right], \quad (2.14a)$$

$$\frac{\partial c}{\partial t} + \frac{\partial}{\partial x} \left( \frac{\partial u}{\partial t} c \right) = D_c \frac{\partial^2 c}{\partial x^2} - \beta n c + \alpha c, \quad (2.14b)$$

$$\frac{\partial \rho}{\partial t} + \frac{\partial}{\partial x} \left( \frac{\partial u}{\partial t} \rho \right) = 0, \quad (2.14c)$$

$$\mu \frac{\partial^3 u}{\partial x^2 \partial t} + \frac{\partial^2 u}{\partial x^2} + \tau_0 \frac{\partial}{\partial x} \left[ \frac{n}{1 + \lambda n^2} \left( \rho + \gamma \frac{\partial^2 \rho}{\partial x^2} \right) \right] = s \rho u. \quad (2.14d)$$

Initially, cellular/ECM densities, chemoattractant concentration, and position of a material point in the ECM are considered non-null and can be chosen arbitrarily to match an experimental situation of interest. Further, considering the case invasion takes place in a confined domain (quasi-isolated system), we assume zero flux boundary conditions which can be experimentally realized. Let  $\Omega_b$  the bounded domain within which the invasion takes place, and  $\frac{\partial}{\partial \nu}$  the outward normal derivative on  $\partial\Omega_b$ . Then the initial value problem and the zero-flux boundary condition described above are situations

that mathematically, are respectively translated by [15, 16]

$$n(x, 0) = n_0(x), \quad c(x, 0) = c_0(x), \quad \rho(x, 0) = \rho_0(x), \quad \text{and} \quad u(x, 0) = u_0(x), \quad \forall x \in \Omega_b.$$

$$D_n \frac{\partial n}{\partial \nu} - \chi_0 n \frac{\partial c}{\partial \nu} - \alpha_1 n \frac{\partial \rho}{\partial \nu} = \frac{\partial c}{\partial \nu} = \frac{\partial \rho}{\partial \nu} = \frac{\partial u}{\partial \nu} = 0, \quad \forall x \in \partial\Omega_b.$$

What is interesting with Eqs. (2.14) is that cells and the ECM are actively convected by the matrix, and the convection is amongst the primary transport mechanism in the medium. Moreover, it accounts for viscous and traction forces in addition to the fact that it also considers spatiotemporal dynamics of the ECM coupled with variations of the chemoattractant concentrations. These aspects were not taken into consideration in the seminal models discussed in [15, 16, 66]. Therefore, Eqs. (2.14) sets a stepping stone to evaluating the geometrical deformations a delimited volume element, taken in the system might experience. Mathematical models for chemotaxis-haptotaxis have been proposed and analyzed [4, 15, 16, 67] set into evidence competitive interactions between haptotaxis and chemotaxis though they do not consider viscous and traction forces. In addition, chemoattractant degradation/production mechanisms were taken as a linear function of the bacterial density and the chemoattractant concentration, yet experimental shreds of evidence suggest that it may be nonlinear [2]. The insightful work of Lolas and Chaplain [16] did not take into consideration ECM density variations and cell orientations. This says they exclude the possibility of ECM displacement and/or the differential transport of cells locally entailed as advection. Generally, the ECM is constituted of composite materials such as macromolecules, ions, enzymes [15, 16, 66] which makes us think that collective motion of cells may induce mechanical actions on the ECM and further contribute to carrying the elements present in the ECM. In that sense, the models discussed by the authors of [2, 4, 15, 16, 17, 66] present some limitations that the model Eqs. (2.14) is expected to cover. Besides, in his seminal book [2], Murray proposed models that described cellular invasion mechanisms where mechanical forces were accounted for. He did not take into consideration the contribution of chemoattractant concentration variations, meaning that he cancel out the possibility of cells to undergo chemotaxis, and he used a linear theory to derive his models. However, a simple observation of Eqs. (2.14) tells that the active transport of cells in the medium may be highly nonlinear. The latter property may render the search for analytical solutions of Eqs. (2.14) a tough exercise. Also, the existence of several transport strategies underlines the existence of parameter regions within which each of them dominantly drives the cellular transport in the medium. In fluids, for example, recent works suggest the existence of a critical Rayleigh number separating stable from unstable modes that depend on chemotaxis strength [68]. In other words, chemotaxis has stabilizing/destabilizing effects, and we suspect haptotaxis to have similar characteristics on the system when acting alone. From this description, it is clear that the model Eqs. (2.14) represents a viable  $(1 + 1)$ -dimensional extension of

the models analyzed in [2, 4, 15, 16, 67]. We suspect it describes intriguing spatiotemporal dynamical behaviors that to the best of our knowledge have not yet received complete attention.

### 2.3.4 The hydrodynamic description of chemotactic suspensions

Up until now the models introduced considered the fluid velocity uniform. Yet, experimental investigations suggest that when active particles are placed in a medium, their motion produces fluctuations from which force balance and moment conservations are shifted. In this conception of chemotactic suspensions, we consider systems constituted of fore-aft asymmetric particles (particles presenting different physical characteristics at both ends). Those types of particles are well described by ciliated or flagellated entities such as molecular swimmers (bacteria, sperm cells just to name a few). We assume distributions within which volume elements contain several cells so that it may be reasonable to analyze the variables of interest such as population density, chemical concentrations, and velocities by their averages over a volume element, as functions of time and space variables. Such approach enforces to consider the bulk velocity of the system has a contribution emanating from the average chemotactic flow of cells, and a drag flow induced by the stress gradients in the medium [69, 70, 71, 72]. The other contribution comes from the velocity fields of the medium within which cells are immersed. The medium flow rate accounts for advective transport as well as frontal collisions amongst cells in a two-dimensional framework. The physics of such a configuration is well suited for higher space dimensions analyses. Regardless of the geometrical configurations and orientations of bacteria, the parameters of interest obey the continuity and the conservation equations:

$$\frac{\partial n}{\partial t} + \nabla \cdot (\mathbf{U}n) = D_n \nabla^2 n - \nabla \cdot (\chi n \nabla c) + \nabla \cdot (n \nabla \phi_0) \quad (2.15a)$$

$$\frac{\partial c}{\partial t} + \nabla \cdot (\mathbf{U}c) = D_c \nabla^2 c - \beta_0 n c. \quad (2.15b)$$

In the system Eqs. (2.15),  $\nabla = (\frac{\partial}{\partial x}, \frac{\partial}{\partial y})^T$ , and  $\nabla^2 = \frac{\partial^2}{\partial x^2} + \frac{\partial^2}{\partial y^2}$  are respectively the gradient and the Laplacian operators in two dimensions.  $n$  and  $c$  respectively represent the bacterial distribution and the chemoattractant concentration, and,  $D_n$  and  $D_c$  their respective diffusion constant.  $\chi$  is the chemotactic strength of bacteria, and  $\phi_0$  is the gravitational potential that accounts for gravitational forces when the number of cells vertically increases. This situation happens when cells lose their active properties, hence leading to sedimentation. Recent investigations on active suspensions rule out this term since the sedimentation's speed can be neglected when compared to instability timescale [73, 74, 75, 76, 77]. However, the authors in [74] hypothesized the existence of a critical vertical gradient density above which instability occurs. This implies that not all the cells in the medium are involved in the rise of bioconvective instability. Thus, we introduce  $\phi_0 = \mu_0 V_n g (\rho_n - \rho) y$ .  $\mu_0$

is a scaling parameter that we introduce to measure the proportion of cells carried vertically in the system as the direct result of gravity effects. If  $\mu_0 \ll 1$  very few cells are directly under gravity forces influence, and a majority of bacteria is directly subject to gravity forces when  $\mu_0 \sim 1$ . The idea of introducing a parameter that controls the number of cells subject to gravity is a completely new one. Though this parameter is directly linked to the Rayleigh number, we suspect it to be the seat of dynamical behaviors that are systematically different from those observed in [74, 75, 76, 77] where only the Rayleigh number was under consideration.  $V_n$  is the volume occupied by bacteria,  $g$  the gravity constant,  $\rho_n$  the bacterial density, and  $\rho$  the fluid density. In Eq. (2.15b),  $\beta_0$  is the rate consumption of chemoattractant by cells.  $\mathbf{U} = (u, v)^T$  is the two-dimensional velocity field. Eq. (2.15a) indicates that chemotaxis induces a motion with a local average velocity that is proportional to the chemoattractant gradient. This drag flow induced by the chemotactic activity superimposes itself to the free velocity field and drives a net local deformation of the fluid streamlines. Thus, the local velocity reads  $\mathbf{U}_{loc} = \mathbf{U} + \chi \nabla c$ . This proposed relation indicates the existence of flow regimes either dominated by fluid or chemotaxis. These possibilities may be observed in experimental settings where the chemoattractant is non-uniformly distributed in such a way acceleration/deceleration areas of active particles rise. However, the fact that higher density aggregation is characterized by a decreasing velocity stems that flow rate reduces considerably at the core of the distribution. It is thus reasonable to think that in the Stokes regime, frictions act on the local velocity  $\mathbf{U}_{loc}$ . For higher bacterial density in shallow water, friction and body forces counterbalance viscous effects, hence the force-balance condition in thin fluid [69, 72] is modified to yield

$$\nabla \cdot \Sigma = \gamma \mathbf{U}_{loc} + n \nabla \phi_0. \quad (2.16)$$

In Eq. (2.16),  $\gamma$  is the dynamic viscosity, and can also be understood as the parameter that measures cellular attachment at a particular position. Eq. (2.16) indicates that the superimposition of adhesives and body forces is counterbalanced by viscous forces emanating from background flow and the flow induced by the collective cellular displacement.  $\Sigma$  is the stress tensor that we consider to be composed of an active part  $\Sigma_a$  (that depends on the diffusive components  $n$  and  $c$ ), and a passive part  $\Sigma_p$  [70] emanating from fluids dynamics properties

$$\begin{aligned} \Sigma &= \Sigma_a(n, c) I_d + \Sigma_p, \\ \Sigma_p &= \eta_0 \left[ \nabla \mathbf{U} + (\nabla \mathbf{U})^T - \frac{2}{d} (\nabla \cdot \mathbf{U}) I_d \right] + \eta_v (\nabla \cdot \mathbf{U}) I_d. \end{aligned} \quad (2.17)$$

$d$  is the dimension of the space,  $I_d$  is the unit tensor of dimension  $d$ ,  $\eta_0$  and  $\eta_v$  are the shear and bulk viscosities respectively [70]. The introduction of the active part of the stress tensor as the function of the diffusive components is motivated by the fact that at the leading order of linearity, the velocity

is a function of diffusive components [69]. This means that the gradient of the active part of the stress tensor acts as external leading forces on fluid and drives local flows within which the quantity of the particles carried decreases, hence creating a net decay in the velocity field over a distance equal to the hydrodynamic length scale [71]. We consider bacteria as hard-rod particles of average dimensions smaller than the hydrodynamic length scale that interacts attractively in both short and long ranges as the consequence of auto-chemotaxis [6, 22, 65]. Since bacterial reproduction is ruled out of consideration, the number of bacteria is quasi constant, and, at high-density distribution, bacteria can be considered as particles obeying thermodynamic laws. Under these considerations, we propose the active part of the stress tensor  $\Sigma_a = \frac{p_0 n}{n+n_r}$  with  $n_r$  being the reference concentration of cells. In the limits of a dilute system ( $n \rightarrow 0$ ),  $\Sigma_a \propto n$  which is reminiscent of the equation of state expressing the pressure in ideal gases. After introducing the dimensionless variables,

$$\begin{aligned} \nabla' &= \frac{\nabla}{L_0}, \quad t' = \frac{t D_n}{L_0^2}, \quad L_0^2 = \frac{\eta_0}{\gamma}, \quad n' = \frac{n}{n_r}, \quad c' = \frac{c}{c_r}, \quad \mathbf{u}' = \frac{L_0}{D_n} \mathbf{U}, \quad \nu = 1 + \frac{\eta_v}{\eta_0}, \quad \alpha = \frac{D_c}{D_n}, \\ \gamma_0 &= \frac{n_r g V_n (\rho_n - \rho) L_0^3}{\eta_0 D_n}, \quad \chi_0 = \frac{\chi c_r}{D_n}, \quad \chi_1 = \gamma \chi_0, \quad P_e = \frac{p_0}{\gamma D_n}, \quad \beta = \frac{\beta_0 n_r L_0^2}{D_n c_r}, \end{aligned} \quad (2.18)$$

keeping the (2 + 1)–spatial dimensions formulation of the problem, and omitting the prime for sake of simplicity, Eqs. (1)-(3) are transformed as

$$\frac{\partial n}{\partial t} + \nabla \cdot (\mathbf{u}n) = \nabla^2 n - \mu_0 \gamma_0 \gamma \nabla \cdot (n \mathbf{e}_y) - \chi_0 \nabla \cdot (n \nabla c), \quad (2.19a)$$

$$\frac{\partial c}{\partial t} + \nabla \cdot (\mathbf{u}c) = \alpha \nabla^2 c - \beta n c, \quad (2.19b)$$

$$\nu \frac{\partial^2 u}{\partial x^2} + \frac{\partial^2 u}{\partial y^2} + (\nu - 1) \frac{\partial^2 v}{\partial x \partial y} - u + \chi_1 \frac{\partial c}{\partial x} - \frac{P_e}{(1+n)^2} \frac{\partial n}{\partial x} = 0, \quad (2.19c)$$

$$(\nu - 1) \frac{\partial^2 u}{\partial x \partial y} + \nu \frac{\partial^2 v}{\partial y^2} + \frac{\partial^2 v}{\partial x^2} - v + \chi_1 \frac{\partial c}{\partial y} - \frac{P_e}{(1+n)^2} \frac{\partial n}{\partial y} - \mu_0 \gamma_0 n = 0. \quad (2.19d)$$

In Eqs. (2.18),  $D_n \sim 10^{-6} \text{cm}^2/\text{s}$  is the bacterial diffusivity and  $L_0 \sim 1 \text{cm}$  is the average running length of bacteria. Under the latter configurations, a real-time  $t = 2 \cdot 10^4 \text{s}$  corresponds to a dimensional time  $t' = 2 \cdot 10^{-2}$ . This time is sufficiently long for cellular proliferation to be observed. Proliferation may be responsible for the rise and the co-existence of multiple clones in the medium. However, we do not take into consideration the latter, meaning that we limit our analyses to situations the number of cells in the medium remains constant during the experiment.  $P_e$  is a parameter measuring traction cells exert on the fluid and  $\gamma_0$ , the analogous Rayleigh number in thermal convection for our system [73]. We consider the case bacteria are about 10 percent denser than fluid particles (here water). They move chemotactically and experience gravitational forces responsible for the sedimentation of cells. Gravity thus appears to increase the number of bacteria carried along the y-line. Bacteria and chemoattractant are transported by the fluid, and bacteria diffuse proportionally to chemoattractant



diffusion's rate. Such a differential diffusivity amongst components of a system may either drives the latter one out of stability or may be used to predict with quite a good accuracy the type of patterns that might emerge.  $\chi_1 \propto \gamma$  implies that frictions hamper or leverage the contribution of the average flow emanating from the chemotactic activity of cells. Depending on the strength of the interplay between frictions, gravity, and viscosities, local distortions of the flow streamlines may be observed. In absence of viscosities ( $\eta_0 = 0$  and  $\eta_v = 0$ ), gravitation forces, ( $\phi_0 \sim 0$ ) and contribution of chemotactic motion of cells on the fluid, Eq. (2.19c) and Eq. (2.19d) indicate a down bacterial migration to density gradient through an exclusion weighted by the factor  $P_e/(1+n)^2$ . This factor goes to zero at high cell density and presents a maximum value equal to  $P_e$  when  $n \rightarrow 0$ . This causes bacteria to move faster at low density and slower at high density, stemming that the velocity field within the system is not infinite in both spatial directions. Therefore, the superimposition of the active stress gradient and the chemotactic activity of cells induces another nonlinearity in the system. In their study of active fluids, the authors of [69, 70, 71, 72] introduced a simplified model of Eqs. (2.19), yet they did not consider one of the diffusive species to be presenting chemotactic activity. Moreover, these works did not investigate the contribution of gravity effects on cells. The latter insufficiency was circumvented by the papers [68, 71, 74, 75, 76, 77]. In addition to the fact that these works did not point out the local aspects such as friction, tractions cells might experience in the fluids, they also neglected the contribution of the average flow generated by cells on the fluids. Nevertheless, the authors proved that chemotaxis-fluid systems are highly interesting dynamical systems. In the sense that the model Eqs. (2.19) considered here that takes into account the combined effects of gravity, traction, friction, chemotaxis, and kinetics, we can afford to assume that it describes an active fluid that to the best of our knowledge has not yet been fully investigated. We henceforth aim at deciphering some facets of its dynamical behaviors.

## 2.4 Theoretical calculations methods

### 2.4.1 The Extended F-expansion method

The F-expansion method [78, 79] is a powerful technique used to construct analytical solutions of nonlinear partial differential equations. In this paragraph we provide a brief outline of the method. Let consider a  $(1 + 1)$ -dimensional partial differential equation of the form

$$G \left( U, \frac{\partial U}{\partial t}, \frac{\partial U}{\partial x}, \frac{\partial^2 U}{\partial x \partial t}, \frac{\partial^2 U}{\partial t^2}, \frac{\partial^2 U}{\partial x^2}, \frac{\partial^3 U}{\partial t^2 \partial x}, \frac{\partial^3 U}{\partial t \partial x^2} \dots \right) = 0, \quad (2.20)$$

where  $U(x, t)$  is the dependent variable to be found. The application of the method requires the introduction of the traveling wave variable  $\xi = kx - \omega t$ , where  $\frac{1}{k}$  is the wave width and  $\omega$  the wave

velocity. Then, Eq. (2.20) becomes

$$G\left(U, \frac{dU}{d\xi}, \frac{d^2U}{d\xi^2}, \frac{d^3U}{d\xi^3} \dots\right) = 0. \quad (2.21)$$

Solutions of Eq. (2.21) may be sought as a polynomial expansion

$$U(\xi) = \sum_{i=0}^l a_i F^i(\xi). \quad (2.22)$$

In Eq. (2.21),  $l$  is calculated by balancing the higher order derivative term with the higher order nonlinearity. The  $a_i$ 's are coefficients to be determined and  $F(\xi)$  is an auxiliary function that is solution to the equation

$$\left(\frac{dF(\xi)}{d\xi}\right)^2 = P_4 F(\xi)^4 + P_3 F(\xi)^3 + P_2 F(\xi)^2 + P_1 F(\xi) + P_0. \quad (2.23)$$

$P_4, P_3, P_2, P_1, P_0$  are real constants conditioning the form of  $F(\xi)$ . Solutions of Eq. (2.23) may be found in [78, 79, 80]. Eq. (2.22) is plugged into Eqs. (2.21) using Eq. (2.23). Then, assembling all the terms with the same  $F^j(\xi)$  together leads to a set of algebraic equations that is solved for the variables  $a_i, k, \omega$ .

## 2.4.2 The reductive perturbation method and its applications

Analytical solutions of systems of partial differential equations are important in the sense they may be used to make long time predictions. Hence the need to develop consistent methods to extract them from the models being considered. However, when these solutions are not directly accessible through classical techniques, they may still be approximated by considering weak fluctuations of the variables to be determined. Such consideration requires redefining the spatiotemporal variables within which those small fluctuations may be significantly perceived. Besides shifting the reference, dependent variables may be expanded using convergent power series. Let us assume that the models to be solved are given by Eq. (2.20). Then the application of the methods requires the introduction of slow spatiotemporal variables  $\xi = \epsilon(x - V_g t)$ , and  $\tau = \epsilon^2 t$ .  $\epsilon$  measures nonlinearity order,  $V_g$  being the group velocity. Furthermore, we expand for solutions of Eq. (2.20) around a reference state  $U_0$ , hence the consideration of the finite sum [51]

$$U = u_0 + \sum_{j=1}^{\infty} \epsilon^j \sum_{l=-j}^j U_l^{(j)}(\xi, \tau) A^l(x, t), \quad (2.24)$$

The series Eqs. (2.24) contains all the overtones  $A^l(x, t) = \exp[i l(kx - \omega t)]$  up to order  $j$ . We also consider the relations  $U_{-l}^{(j)} = (U_l^{(j)})^*$ , where  $()^*$  denotes the complex conjugate of the quantity in between parentheses. The solutions Eq. (2.24) is inserted in Eq. (20). The resolution is made at each

order of  $\varepsilon$  to determine the harmonics  $U_l^{(j)}$ . In this study, we apply this method to determine how the first-order harmonics propagate in the models (2.14) and (2.19). Full and detailed applications of the method on one and two-spatial dimensions models are described in appendices A and B.

### 2.4.3 The Hirota Bilinear Method (HBM)

The HBM offers a compelling framework to determine localized structures propagating in nonlinear systems. Its principle lies on the fact any nonlinear system may be written in a simple form, provided that the suitable transformation is used. Let us consider Eq. (2.20) as the model to be solved. The bilinearization of Eq. (2.20) requires to consider  $U(x, t)$  in a specific form that in reality depends on how the equation is built. For example, if Eq. (2.15) is the nonlinear Schrödinger equation, then we must set  $U(x, t) = \frac{H(x, t)}{F(x, t)}$ , and if Eq. (2.20) is the cubic complex Ginzburg-Landau equation, then  $U(x, t) = \frac{H(x, t)}{F^{1+i\delta_i}(x, t)}$ . If Eq. (2.20) is of KdV class, then  $U(x, t) = \frac{\partial^2 F}{\partial x^2}$ . In all these cases,  $H(x, t)$  is complex,  $F(x, t)$  is as well as  $\delta_i$  are real. The reader is referred to [81, 82] for more details. Once the right form of  $U(x, t)$  is determined and inserted into Eq. (2.20), the bilinear operators

$$D_{x, \alpha}^m F(x) \cdot H(x) = \left( \frac{\partial}{\partial x_1} - \alpha \frac{\partial}{\partial x_2} \right)^m F(x_1) G(x_2) |_{x_1=x_2=x}, \quad m \in \mathbb{N}, \quad (2.25)$$

are considered. Then, Eq. (2.20) is factorized in a polynomial form hence:

$$P(D_t, D_x, D_x \cdot D_t, D_{xx} \dots) F \cdot F = 0. \quad (2.26)$$

Eq. (2.26) is the generic class of bilinear equations resulting from Eq. (2.20). Solutions of Eq. (2.26) are determined by expanding the function  $F(x, t)$  as

$$F(x, t) = f_0 + \epsilon f_1(x, t) + \epsilon^2 f_2(x, t) + \epsilon^3 f_3(x, t) + \epsilon^4 f_4(x, t) + \dots \quad f_0 = c^{nst}. \quad (2.27)$$

The first order solution of Eq. (2.26) is obtained by truncating the expansion Eq. (2.27) at the first order, hence Eq. (2.26) becomes

$$P(D_x, D_t, D_x \cdot D_t, D_{xx} \dots) [f_0 \cdot f_0 + \epsilon (f_0 \cdot f_1 + f_1 \cdot f_0) + \epsilon^2 (f_1 \cdot f_1)] = 0 \quad (2.28)$$

Eq. (28) is solved recursively at each order of  $\epsilon$ . The first and second order of  $\epsilon$  yield

$$\epsilon : P \left( \frac{\partial}{\partial t}, \frac{\partial}{\partial x}, \frac{\partial^2}{\partial x \partial t}, \frac{\partial^2}{\partial x^2} \dots \right) f_1(x, t) = 0, \quad (2.29a)$$

$$\epsilon^2 : P(D_x, D_t, D_x \cdot D_t, D_{xx} \dots) f_1 \cdot f_1 = 0. \quad (2.29b)$$

Eq. (2.29a) is linear hence its solutions may be taken as

$$f_1(x, t) = e^{px+qt+po}. \quad (2.30)$$

$p$ ,  $q$ , and  $p_0$  are constants that may be determined by inserting the solution Eq. (2.30) into Eq. (2.29b), hence are constructed analytical solutions of Eq. (2.20).

## 2.5 Numerical methods

Analytical techniques used to solve our models Eqs. (2.4), (2.11) and (2.14) are based on approximation methods, which means that the corresponding solutions present some imperfections that shall inhibit their propagation for long time in large spatial domains. In reality, solutions expected must present good stability properties, hence the motivation of comparing analytical with numerical solutions. In this section, we display techniques applied to numerically solve Eqs. (2.4), (2.11), (2.14) and (2.19).

### 2.5.1 The fourth order Runge-Kutta method (RK4)

The RK4 is an integration technique used to numerically approximate solutions of ordinary (linear and nonlinear) differential equations. Assuming that the equation to solve takes the form of Eq. (2.20), the first step to apply the RK4 methods consists of writing Eq. (2.20) in the form of an ordinary differential equation. One way of doing that consists of discretizing all the spatial derivatives embedded in Eq. (2.120) using a centered finite difference. At a precise point of the gridsapce, Eq. (2.20) becomes

$$\frac{du_j}{dt} = F(t, u_j(t)), \quad u_j(t=0) = u_{j0}, \quad t > 0, \quad \text{where} \quad u_j(t) = u(x = j \cdot dx, t) \quad (2.31)$$

Then integrating Eq. (2.31) using the RK4 scheme requires to calculate the intermediary variables and used the latter ones to extract the values of  $u(x,t)$ . The algorithm reads

$$\begin{aligned} K1_j &= F(t, u_j(t)) \\ K2_j &= F(t + dt/2, u_j(t) + K1_j/2) \\ K3_j &= F(t + dt/2, u_j(t) + K2_j/2) \\ K4_j &= F(t + dt, u_j(t) + K3_j) \\ u_j(t + dt) &= \frac{1}{6} (K1_j + 2 \cdot K2_j + 2 \cdot K3_j + K4_j). \end{aligned} \quad (2.32)$$

### 2.5.2 The Fourier Pseudo-spectral

In order to apply the RK4 method to solve Eq. (2.20), the previous paragraph suggest to discretize spatial derivatives. Another way of dealing with the latter ones consists of changing the reference frame within which Eq. (2.20) is solved. In that end, the Fourier transform is a better candidate and provide the advantage to ease the implementation of periodic boundary conditions. Following the

Fourier transform rules, Eq. (2.20) may be written in the form

$$\frac{d\hat{u}(k, t)}{dt} = F(k, t, \hat{u}(k, t)), \quad \hat{u}(k, t = 0) = \hat{u}(k, 0), \quad t > 0, \quad \text{where} \quad (2.33a)$$

$$\hat{u}(k, t) = \frac{1}{2\pi} \int_{-\infty}^{+\infty} u(x, t) e^{-2\pi i k x} dx. \quad (2.33b)$$

Then using Eqs. (2.32), Eq. (2.33) is solved in the Fourier space. Once that is done, the inverse Fourier transform is applied to recover the corresponding data in the real domains.

## 2.6 Conclusion

In summary, using mass conservation and force balanced conditions, extended chemotaxis models have been constructed. In their natural habitat for instance, bacteria are subject to several mechanical events, which makes us think that those models taking into consideration several effects including traction, adhesion, chemotaxis, haptotaxis, long-range diffusion, advection, chemoattractant consumption rate and gravity are very realistic. Further, mathematical and the numerical tools used to probe the models constructed are presented. The F-expansion and the Hirota Bilinear methods are used to construct analytical solutions of the equations under consideration, while the reductive perturbation method is used to reduce highly stiff set of coupled nonlinear partial differential equations. In order to test the numerical stability of the solutions constructed, numerical integration methods applied include the fourth-order Runge-Kutta scheme and the Fourier pseudo-spectral method.

---

# Chapter 3

## Results and Discussion

### 3.1 Introduction

Experimental observations of bacteria collectively traveling by forming bands of matter moving at finite speed suggest that those bands may be mathematically described using the traveling analysis methods. In this chapter, we use the latter approaches to investigate chemotactic models derived in the previous. We principally apply the F-expansion and the Hirota bilinear methods to integrate the equations under consideration. Also, finite sums of modulated nonlinear excitations are applied to reduce the models when they are not directly integrable. Both approaches allow us to construct analytical solutions, discuss their existence. Those solutions are later used probe the inherent dynamics of the system considered. In each of these cases numerical simulations are performed to ascertain that our solutions are analytically and numerically stable.

### 3.2 (2+1)-Traveling chemotactic waves in fluid

#### 3.2.1 Exact solutions of Eqs. (2.4) through the F-expansion method

The models Eqs. (2.4) and (2.11) describe two-dimensional spatiotemporal evolutions of bacteria and chemoattractants under very different circumstances, although happening in fluid media with a uniform flow rate. Solutions of those systems have not been derived before, to the best of our knowledge. In this section, we fill the gap by deriving a few solutions and discussing their existing conditions. To determine analytical solutions of Eqs. (2.4), the traveling wave variable  $\xi = kx + ly - \omega t$  is assumed.  $\frac{1}{k}$  and  $\frac{1}{l}$  are the wave widths in  $x$ - and  $y$ - directions, respectively, while,  $\omega$  is the wave

---

pulsation. Combination of Eqs. (2.4) leads to the ordinary differential equation

$$\begin{aligned} D_n (k^2 + l^2) \frac{d^2 n}{d\xi^2} - \chi_0 (k^2 + l^2) \frac{dn}{d\xi} \frac{dc}{d\xi} - \frac{\beta\chi_0}{D_c} n^2 c + rn(\sigma - n) &= 0, \\ \omega &= k\delta_{0_x} + l\delta_{0_y}. \end{aligned} \quad (3.1)$$

On the other side and without loss of generality, the positive sign of  $\omega$  implies a forward wave propagation or a collective motion of cells towards the energy source. However, If  $\delta_{0_x} = \delta_{0_{xcrit}} = -\frac{l\delta_{0_y}}{k}$ , ( $\delta_{0_y} > 0$ ),  $\omega = 0$ , there is no longer any chemoattractant-induced collective displacement. This corresponds to a stationary motion of cells. For values of  $\delta_{0_x} < \delta_{0_{xcrit}}$  and for  $\delta_{0_y}$  fixed, the medium constrains the cells to follow its motion. Since the flow rate is externally imposed by the experimenter, the above result indicates that in confined domains the fluid flow rate may be chosen so that the wave propagates without interacting with the boundaries neither create any reflexive patterns. Solutions of Eq. (3.1) are sought by assuming the expansions

$$\begin{aligned} n &= a_{-2}F(\xi)^{-2} + a_{-1}F(\xi)^{-1} + a_0 + a_1F(\xi) + a_2F(\xi)^2, \\ c &= b_{-1}F(\xi)^{-1} + b_0 + b_1F(\xi). \end{aligned} \quad (3.2)$$

$a_{-2}, a_{-1}, a_0, a_1, a_2$  and  $b_{-1}, b_0, b_1$  are real constants to be determined later. The auxiliary function  $F(\xi)$  is solution to the equation [78, 79]

$$\left( \frac{dF(\xi)}{d\xi} \right)^2 = d_4 F(\xi)^4 + d_2 F(\xi)^2 + d_0. \quad (3.3)$$

$d_4, d_2, d_0$  are real constants that define the form of  $F(\xi)$ . Exact solutions of Eq. (3.4) may be found in the existent literature [78, 79]. Inserting Eq. (3.2) into Eq. (3.1) using Eq. (3.3), collecting all coefficients of powers  $F(\xi)^m$ , then setting each coefficient to zero yields a set of over-determined algebraic equations for the unknown  $a_j$  ( $j = -2, -1, 0, 1, 2$ ) and  $b_i$  ( $i = -1, 0, 1$ ). We solve the over-determined set equations and extract only those which are physically relevant objects and obtain

$$\begin{aligned} a_{-2} = a_{-1} = b_{-1} = 0, \quad a_2 &= -\frac{2d_4\nu}{\beta\chi}, \quad b_0 = -\frac{r}{\beta\chi} + \frac{r\sigma a_0 - \frac{8\nu d_0 d_4}{\beta\chi}}{\beta\chi a_0^2 + \frac{4\nu^2 d_0 d_4}{3\beta\chi}} \\ a_1^2 &= \frac{4d_4}{3\beta\chi} \frac{[3\mu + \nu(b_0 + \frac{r}{\beta\chi})](\beta\chi a_0^2 - \frac{4\nu^2 d_0 d_4}{\beta\chi})}{\mu d_2 + r\sigma - 2\beta\chi a_0(b_0 + \frac{r}{\beta\chi})}, \quad b_1 = \frac{4d_4}{3a_1\beta\chi} [3\mu + \nu(b_0 + \frac{r}{\beta\chi})], \\ a_1^2 &= \frac{4\nu d_4 a_0(b_0 + \frac{r}{\beta\chi}) - \frac{2\nu d_4}{\beta\chi}(r\sigma + 4\mu d_2)}{\beta\chi(b_0 + \frac{r}{\beta\chi})} - \frac{\frac{4d_2}{3\beta\chi}(\nu d_2 + 2\beta\chi a_0)[3\mu + \nu(b_0 + \frac{r}{\beta\chi})]}{\beta\chi(b_0 + \frac{r}{\beta\chi})}, \\ b_1 &= \frac{4d_4}{3a_1\beta\chi} [3\mu + \nu(b_0 + \frac{r}{\beta\chi})], \\ a_1^2 &= \frac{16d_4\nu}{\beta\chi} \frac{(a_0 + \frac{\nu d_2}{\beta\chi})[3\mu + \nu(b_0 + \frac{r}{\beta\chi})]}{6\mu - 8\nu(b_0 + \frac{r}{\beta\chi})}, \quad b_1 = \frac{4d_4}{3a_1\beta\chi} [3\mu + \nu(b_0 + \frac{r}{\beta\chi})]. \end{aligned} \quad (3.4)$$

In these solutions,  $a_0$  is an arbitrary real constant and we set  $\mu = D_n(k^2 + l^2)$ ,  $\nu = \chi_0(k^2 + l^2)$  and  $\chi = \frac{\chi_0}{D_c}$ . The set of parameters Eqs. (3.4) are obtained for the auxiliary functions

$$F(\xi) = \sqrt{\frac{-d_2}{d_4}} \cosh\left(\sqrt{d_2}\xi\right)^{-1}, \quad d_4 = -1, \quad d_2 = 1, \quad d_0 = 0 \quad (3.5a)$$

$$F(\xi) = \sqrt{\frac{-d_2}{2d_4}} \tanh\left(\sqrt{\frac{-d_2}{2}}\xi\right), \quad d_4 = 1, \quad d_2 = -1, \quad d_0 = \frac{d_2^2}{4d_4}. \quad (3.5b)$$

### 3.2.2 Existence, dynamical behavior of solutions of Eqs. (2.4)

Using Eqs. (3.4) and (3.5), we construct bacterial and chemoattractant waves

$$n(\xi) = a_0 + \sqrt{\frac{4}{3\beta\chi} \frac{3\mu + r\sigma a_0}{r\sigma - \mu} \frac{1}{\cosh(\xi)} + \frac{2\nu}{\beta\chi} \left(\frac{1}{\cosh(\xi)}\right)^2}, \quad (3.6a)$$

$$c(\xi) = \frac{r(\sigma - 1)}{\beta\chi} - \frac{4(r\sigma\nu + 3\mu\beta\chi a_0)}{3a_0(\beta\chi)^2} \sqrt{\frac{3\beta\chi(r\sigma - \mu)}{4(3\mu + r\sigma a_0)} \frac{1}{\cosh(\xi)}}, \quad (3.6b)$$

$$\text{provided that } r\sigma > D_n(k^2 + l^2), \quad \text{and } a_0 \neq -\frac{3D_n}{r\sigma\chi_0} = a_{0crit}. \quad (3.6c)$$

Eqs. (3.6a) and (3.6b) stand for traveling pulse which have been demonstrated to be excellent candidate to mimicking experimental results [19, 20, 25]. Eq. (3.6c) is the global existence condition within traveling pulse may be observed, enforcing that the wave widths  $\frac{1}{k}, \frac{1}{l}$  must fall within the circle of radius  $\frac{r\sigma}{D_n}$ . Further, Eq. (3.5b), one recovers the bacterial and the chemoattractant step waves

$$n(\xi) = a_0 + \sqrt{-\frac{2\mu(\nu^2 + \beta^2\chi^2 a_0^2)}{\beta^2\chi^2(\mu + r\sigma)} \frac{(a_0 - a_{01})(a_0 - a_{02})}{(a_0 - a_{03})(a_0 - a_{04})} \tanh\left(\sqrt{\frac{1}{2}}\xi\right) - \frac{\nu}{\beta\chi} \left(\tanh\left(\sqrt{\frac{1}{2}}\xi\right)\right)^2},$$

$$c(\xi) = \frac{-3\beta^2\chi^2 r a_0(\sigma - a_0) - \nu(\nu r + 6\beta\chi\mu)}{\beta\chi(\nu^2 + 3\beta^2\chi^2 a_0^2)} + b_1 \tanh\left(\sqrt{\frac{1}{2}}\xi\right). \quad (3.7)$$

$$a_{01} = -\frac{r\sigma\nu}{6\beta\chi\mu} \left[1 + \sqrt{1 + \frac{12}{r^2\sigma^2}}\right], \quad a_{02} = -\frac{r\sigma\nu}{6\beta\chi\mu} \left[1 - \sqrt{1 + \frac{12}{r^2\sigma^2}}\right],$$

$$a_{03} = \frac{\mu\nu}{\beta\chi(\mu + r\sigma)} \left[2 - \sqrt{\frac{11}{3} + \frac{r^2\sigma^2}{3\mu^2}}\right], \quad a_{04} = \frac{\mu\nu}{\beta\chi(\mu + r\sigma)} \left[2 + \sqrt{\frac{11}{3} + \frac{r^2\sigma^2}{3\mu^2}}\right].$$

Solutions Eqs. (3.7) exist for  $a_0 \in ]a_{01}, a_{02}[ \cup ]a_{03}, a_{04}[$ . It is clear from Eqs. (3.6a-b), and Eqs. (3.7a-b) that the densities are proportional to the system parameters, hence providing the experimenter with the framework to control the number of particles carried by each of these waves. Solutions Eqs. (3.6) and (3.7) are bell-shaped and step traveling waves, respectively. Specifically, the bell-shaped profile Eqs. (3.6) is a  $(2 + 1)$ -dimensional extension of the one dimensional counterpart obtained in [13, 19, 20, 25, 63] without any medium flow rate nor cellular proliferation. On the other hand, the step wave profile solutions Eqs. (3.7) are striking ones and their occurrence indicates a bacterial distribution as



well as chemoattractant concentration shift over time at a precise location. The asymmetry associated with this wave profile can be seen as the result of a chemoattractant concentration gradient that triggers a slower than expected cellular response to signal detection amongst units of a given population. These solutions are matter carriers and their occurrence reveals the excitable nature of the system and its subsequent associated transport strategies. These ones connect stable spatially homogeneous states and ensure cellular survival as well as long-distance communication.

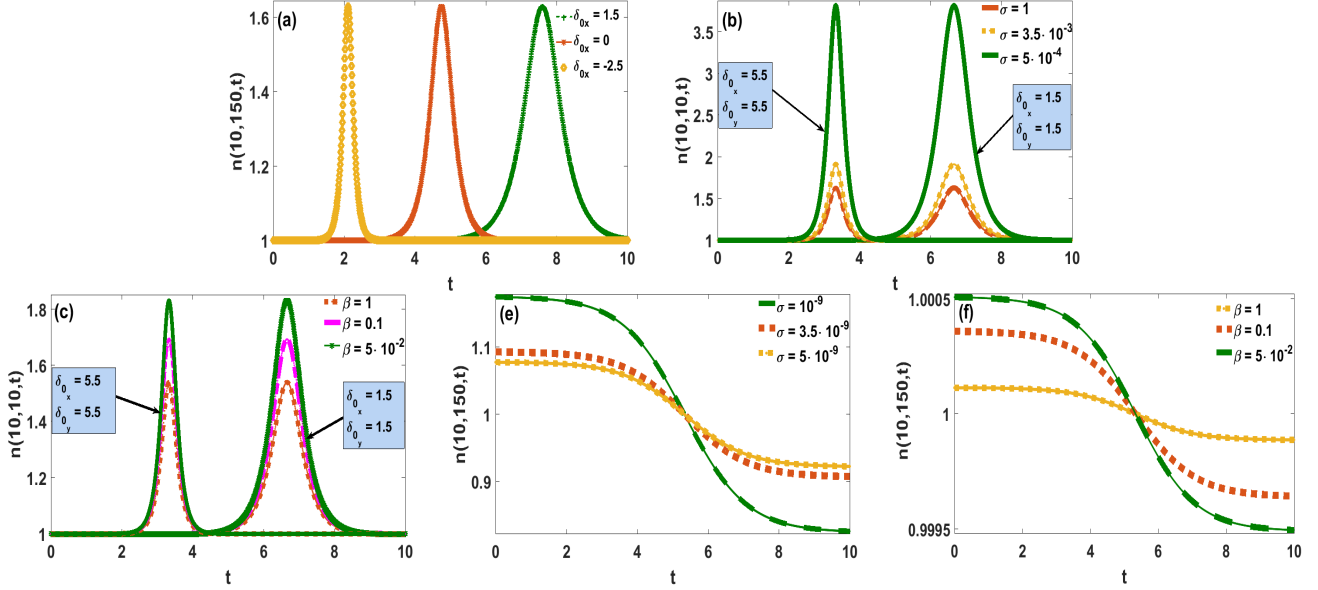


Figure 3.1: The temporal evolution of bacterial waves shows that wave thickness and velocity vary as fluid flow (a). Reduction of the carrying capacity increases amplitude and wave thickness. The same observations hold when the chemoattractant consumption's rate decreases as displayed on panels (c), (f). Parameters  $D_n = 4 \cdot 10^{-6}$ ,  $D_c = 8.9 \cdot 10^{-6}$ ,  $\chi_0 = 3.9 \cdot 10^{-9}$ ,  $r = 2 \cdot 10^{-4}$ ,  $\sigma = 3.5$ ,  $\beta = 1$ ,  $k = 0.9$ ,  $l = 0.9$ ,  $\delta_{0x} = 1.5 \cdot 10^{-6}$ ,  $\delta_{0y} = 1.5 \cdot 10^{-6}$

Investigating the effects of the carrying capacity of the medium as well as chemoattractant consumption rate on the two different solutions Eqs. (3.6) and Eqs. (3.7) reveal interesting dynamical features. In Fig. 3.1(a) where the advection  $\delta_{0x}$  is gradually reduced, the traveling wave has a smaller velocity yet it propagates at quasi-constant amplitude. It is also observed that the wave thickness reduces when the advection decreases, implying that the flow does not affect the number of cells carried, but rather their spatial distribution. As consequence, the number of collisions of cells per unit volume is modified, hence leading to a spatial homogeneity in which the frequency bandwidth of the communication mechanisms amongst units becomes tighter, an observation consistent with experimental observations in [6] and numerical simulations in [20]. Further, increasing values of the carrying capacity  $\sigma$  as per panel (b) of Fig. 3.1, it is observed that the wave velocity reduces at high flow

rates. Yet the wave is detected at the same time, and it experiences amplitude and width increase. Intriguingly, optimal cellular transport corresponding to higher wave amplitude is observed when the carrying capacity takes small values. Such an outcome is appealing since it indicates a departure shift between the number of cells the traveling wave can sustain and the number of cells the medium can support without undergoing saturation. In this way, the response of the number of cells the wave carries is measured by the excitation (here the exposure to chemoattractant) from which local dynamic is subtracted. Under this configuration, cells can detect and amplify signals irrespectively to their direct surrounding medium. Interestingly on the other side, increasing the chemoattractant consumption's rate as on panel (c) of Fig. 3.1 leads to the conclusion that both parameters have the same effects on the traveling bacterial pulse. One can thus afford to assume that a faster bacterial progression is expected to be observed when a small number of cells possess a high food consumption rate or when the fraction area containing cells is accordingly reduced. This set into evidence the complementary roles played by these two parameters for the sake of cell development and survival. This study, therefore, suggests that in order to avoid cannibalism or competition among units of the same population, these parameters may be tuned accordingly, an issue manageable and that must be initially addressed by the experimenter. The traveling dip step profile as depicted in panels (e), (f) of Fig. 3.1 shows that the transition from higher to lower values is softened when the carrying capacity reduces or the chemoattractant consumption's rate increases. The occurrence of this wave profile in reactive systems sets into evidence the existence of differential cellular density across the medium. Thus panels (e) – (f) of Fig. 3.1 indicate that in order to stabilize the number of particles carried by this wave profile when time increases, either the carrying capacity of the medium or the chemoattractant consumption rate should be increased. Under the action of these parameters, the traveling dip step profiles tend to adopt a quasi-linear (uniform) feature, meaning that the number of particles carried from the initial till the final time does not vary much. Therefore, these parameters may offer a better option to counterbalance the dissipative nature of reactive systems which are often responsible for non-conservativeness effects during cellular transport in soft tissues. In this way, cells can travel for a long time without being absorbed or attenuated. Such an outcome is significant for technological and medicinal applications, in the sense it indicates that cells may take more time to cover a distance when their food consumption rate or the carrying capacity, or the medium within which they are immersed independently increase.

### 3.2.3 Numerical confirmation through the Fourier pseudo-spectral method

In this part of the work, we numerically test the robustness of the solutions constructed. Eqs. (3.6) and Eqs. (3.7) are used as initial conditions to numerically integrate the original model Eqs. (2.4). Our numerical simulations run up to  $t_{final} = 10$  with the time step  $dt = 10^{-4}$ . The Fourier pseudo-spectral method is used to integrate Eq. (2.4). We have considered 1024 points in each direction of a squared integration domain of dimensions  $x, y \in [-10, 10]$ . For all numerical simulations, analytical solutions injected at the initial time were randomly perturbed by a noise of strength one percent of the maximum magnitude of the analytical solutions, and results are depicted in Fig. 3.2 and Fig. 3.3. To be precise, top panels (a), (b), (c) of Fig. 3.2 (resp. bottom panels (d), (e), (f) of Fig. 3.2) display snapshots of the bacterial density (resp. chemoattractant concentration) at  $t = 0, 5, 10$  respectively, obtained with the analytical solution Eqs. (3.6) (resp. Eqs. (3.7)) as the initial condition. In Figs. 3.2(a), (b), (c), the initial solution for bacterial density evolves without disintegration and remains very close to the analytical one, though the insertion of a random perturbation at the initial time. Hence, the analytical solution presented in Figs. 3.2(a), (b), (c) is stable. This implies that our two-dimensional model that takes into account advection and proliferation may be used as a predictive tool for the investigation of the bacterial collective motion. In general, bacterial cells are immersed in a medium with a nonvanishing velocity field, our numerical results confirm the existence of bands of collective motion of bacteria. Results not found in previous works to the best of our knowledge. We expect that families of solutions presented in this work may motivate two-dimensional experiments as only one-dimensional experiments had been carried in the absence of the velocity field of the medium [19, 25]. Now with two-dimensional experiments available, [83], we do believe that tests of our results on the two-dimensional model Eqs. (2.4) may be carried in the near future. Conversely, the chemoattractant concentration decreases with time (see panels (d), (e), (f) of Fig. 3.2), a situation rather different from the prediction provided by the analytical calculations presented above (Eqs. (3.6)). The origin of the discrepancy between analytical and numerical results is due to the large difference amongst the magnitude of the diffusion, the advection rate against the chemoattractant consumption rate. This calls to a proper definition of  $\beta$  unlike the one used here taken from [2]. This work would be carried elsewhere. We now consider the analytical solutions Eqs. (3.7) for the bacterial density and the chemoattractant concentration, respectively. Once again, numerical results in Figs. 3.3(a), (b), and (c) for the density recover the analytical predictions with a pretty much good accuracy while, due to a large value of  $\beta$  the numerical results differ from the analytical prediction for the chemoattractant concentration displayed in Fig. 4(d), (e), (f).

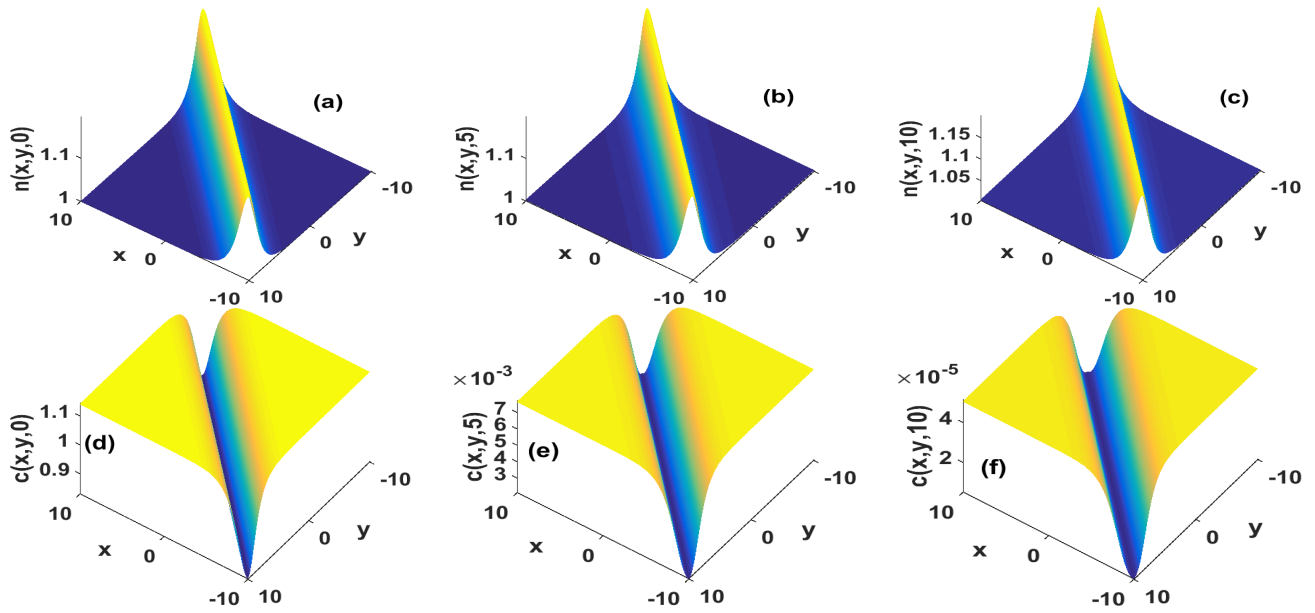


Figure 3.2: Stable evolution of traveling bacterial (top) and chemoattractant concentrations (bottom) waves. Parameters are taken as on Fig. 3.1(a), (b). The thickness of chemoattractant waves slightly increases and its amplitude decreases as time evolves.

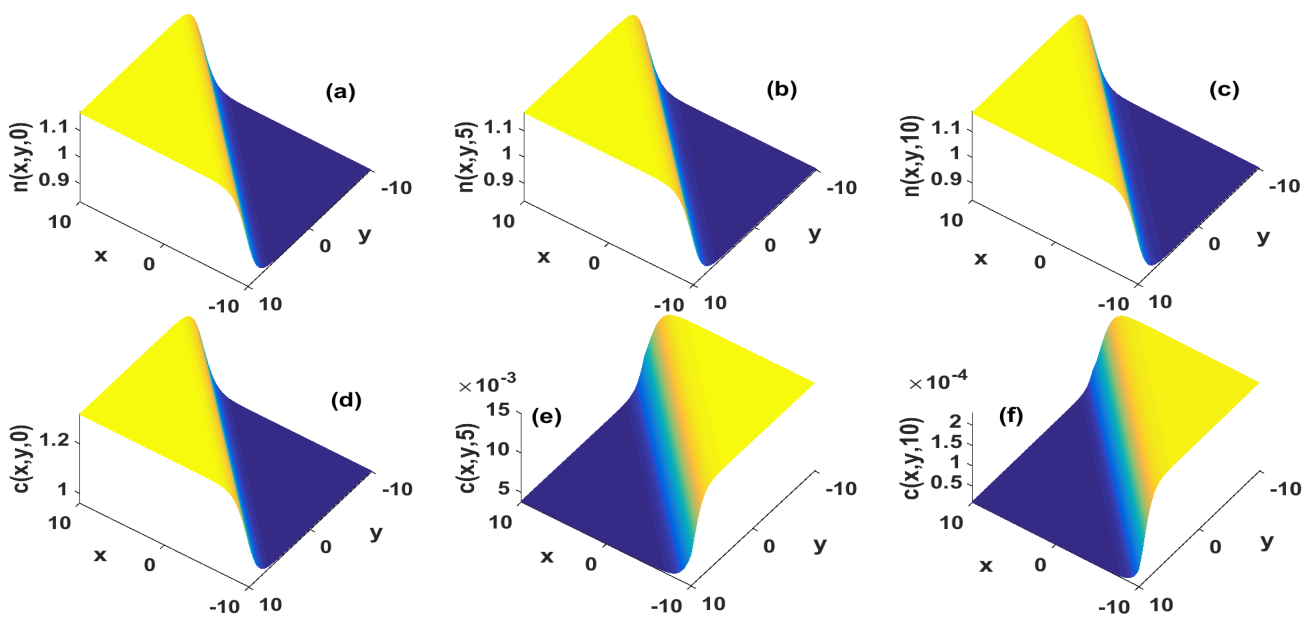


Figure 3.3: Propagation of traveling bacterial-step (top panels), and chemoattractant (bottom panels) waves. Parameters are taken as on Figs. 3.1(c), (d). Chemical wave shifts from step to down-step profile.

### 3.3 Bacterial and chemical waves in chemotactic system with long-range diffusion, traction and kinetics

#### 3.3.1 Analytical solutions of Eqs. (2.11) through an extended F-expansion method

The models Eqs. (2.11) indicate that due to inherent nature of the medium within which cells might be placed, nonlocal responses of the latter to external stimuli leads to spatiotemporal behaviors worth revisiting using exact solutions methods. As in the previous section, we introduce the traveling wave variable  $\xi = kx + ly - \omega t$ , and reduce the model Eqs. (2.11)

$$D_2 K^2 \frac{d^4 n}{d\xi^4} + \chi_0 \left( \frac{\Omega_0}{\chi_0 - \tau_0} \right)^2 + \left[ \frac{\beta \chi_0 \Omega_0 \xi}{K(\chi_0 - \tau_0)^2} + \frac{\beta}{\tau_0} \frac{D_1(\chi_0 - \tau_0) + \tau_0 D_3}{\chi_0 - \tau_0} - r\sigma + \beta_1 \right] n + \left( r + \frac{\beta \tau_0}{\chi_0 - \tau_0} \right) n^2 - \beta_3 n^3 = 0, \quad (3.9)$$

provided that

$$c(\xi) = -\frac{\tau_0 n(\xi) + D_3}{\chi_0 - \tau_0} - \frac{\Omega_0 \chi_0 \xi}{K(\chi_0 - \tau_0)^2} - \frac{D_1}{\tau_0}. \quad (3.10)$$

$K = k^2 + l^2$ ,  $\Omega_0 = \delta_{0_x} k + \delta_{0_y} l - \omega$ . We restrict ourselves to the case where  $\omega = k\delta_{0_x} + l\delta_{0_y}$  to avoid nonphysical solutions that diverge at infinity. Such a choice is also consistent with recent numerical and theoretical results presented in [83, 84, 85] where the authors proved that the wave velocity in the Martiel-Golbeter chemotaxis model (for *Dictyostelium discoideum* dynamics) varies linearly with the imposed flow. On the other hand, Eq. (3.10) tells that variations of chemoattractant and bacterial waves are directly linked, hence corroborating results obtained in the analysis of chemotactic *Dictyostelium* colonies [84]. The same study showed that by increasing background level, the directed propagation can be suppressed, due to memory inactivation. In other words, cells can be swept or their direction propagation swerved, enforcing the conclusion that medium flow rate has the potential of favoring the rise of progressive or regressive waves. In the present study, the transition from forwards to backward propagation is attained when parameters are chosen such that the critical line  $\frac{\delta_{0_x}}{\delta_{0_y}} = \frac{-l}{\sqrt{K-l^2}}$  corresponding to stationary patterns is violated. In the latter configuration, our solutions may be either progressive ( $\omega > 0$ ) or regressive ( $\omega < 0$ ). The former is responsible for faster bacterial colonization of unoccupied regions, while the latter may be the signature of backward waves. In the flux limiting cases, the backward waves in a chemotactic system were shown to be responsible for a population saturation in a stable state accompanied by a transition toward unstable modes [62].

Physical acceptable solutions of Eqs. (2.11) correspond to positive bacterial and chemoattractant wave amplitudes. In addition, both bacterial densities and chemoattractant concentrations must re-

main finite, hence using Eq. (3.10) and assuming that  $n(\xi) \geq 0$ , the finiteness of the chemoattractant concentration implies the following restrictions

$$\tau_0 > \chi_0, \quad \tau_0 \neq 0, \quad c(\xi) \geq \frac{D_3}{\tau_0 - \chi_0} - \frac{D_1}{\tau_0} = c_{min}, \quad D_1 \leq \frac{D_3 \tau_0}{\tau_0 - \chi_0}. \quad (3.11)$$

Before proceeding further, Eqs. (3.11) provide important characteristics about the solutions to be found below. The traction forces must be non-null and greater than the chemotaxis strength implying that the experimenter must choose an appropriate chemoattractant substance that is consistent with Eqs. (3.11). Moreover, there exists a critical chemoattractant concentration that completely depends on system parameters  $(\tau_0, \chi_0, D_1, D_3)$ , below which the corresponding solutions are unphysical. The solutions will be viable only if the chemoattractant concentration is at least equal to  $c_{min}$ , a situation which means that chemoattractant diffusion rate is always greater or equal than a minimal value  $D_3 \geq D_1 \left(1 - \frac{\chi_0}{\tau_0}\right) = D_{3min}$ . The fact that  $D_1 > D_{3min}$  implies  $D_1 > D_3$ . The latter inequality is a situation rather different from experimental values reported in [2, 19, 20, 25, 45, 59]. Therefore, traction forces substantially modify the behaviors of chemotactic systems.

Balancing higher-order derivative with the higher-order nonlinear terms in Eq. (3.9) permits the polynomial expansion

$$n = a_0 + a_1 F(\xi) + a_2 F(\xi)^2, \quad (3.12)$$

where  $a_0, a_1, a_2$  are real constants to be determined later. The function  $F(\xi)$  is a solution of the auxiliary equation

$$\left(\frac{dF(\xi)}{d\xi}\right)^2 = P_4 F(\xi)^4 + P_3 F(\xi)^3 + P_2 F(\xi)^2 + P_1 F(\xi) + P_0. \quad (3.13)$$

$P_4, P_3, P_2, P_1, P_0$  are real constants. Solutions of Eq. (3.13) may be found in [79, 78, 80]. Plugging Eq. (3.12) into Eq. (3.9) and using Eq. (3.13) yields a set of algebraic equations that we solve for the variables  $a_0, a_1, a_2, K, \beta_3$  and obtain different families of solutions

**Family A:**  $P_0 = P_1 = P_3 = 0, P_2 > 0, P_4 < 0, F(\xi) = \sqrt{-\frac{P_2}{P_4}} \cosh^{-1}(\sqrt{P_2} \xi)$

$$a_0 = 0, \quad a_1 = 0, \quad a_2 = \frac{15\sigma_1 P_4}{2\sigma_2 P_2}, \quad K = \frac{1}{4P_2} \sqrt{-\frac{\sigma_1}{D_2}}, \quad \beta_3 = -\frac{2\sigma_2^2}{15\sigma_1}, \quad (3.14)$$

**Family B:**  $P_0 = \frac{P_2^2}{4P_4}, P_1 = P_3 = 0, P_2 < 0, P_4 > 0, F(\xi) = \sqrt{-\frac{P_2}{2P_4}} \tanh\left(\sqrt{-\frac{P_2}{2}} \xi\right)$

$$a_0 = -\frac{15\sigma_1}{2\sigma_2}, \quad a_1 = 0, \quad a_2 = \frac{15\sigma_1 P_4}{2\sigma_2 P_2}, \quad K = -\frac{1}{2P_2} \sqrt{-\frac{\sigma_1}{D_2}}, \quad \beta_3 = -\frac{2\sigma_2^2}{15\sigma_1}. \quad (3.15)$$

**Family C:**  $P_0 = P_1 = 0, P_2 > 0, P_3 = 2\epsilon\sqrt{P_2P_4}, P_4 > 0, F(\xi) = \frac{\epsilon}{2}\sqrt{\frac{P_2}{P_4}}\frac{\cosh(\frac{\sqrt{P_2}}{2}\xi)^{-2}}{\epsilon\tanh(\frac{\sqrt{P_2}}{2}\xi)-1}$

$$\begin{aligned} a_0 &= -\frac{\sigma_1(\sqrt{105} + 21)}{14\sigma_2}, & a_1 &= \epsilon\sqrt{\frac{P_4}{P_2}}\frac{3\sigma_1(35 - \sqrt{105})}{7\sigma_2}, & a_2 &= -\frac{3\sigma_1P_4(35 - \sqrt{105})}{7P_2\sigma_2} \\ \beta_3 &= -\frac{28\sigma_2^2}{3\sigma_1(7 + 3\sqrt{105})} & K &= \frac{1}{P_2}\sqrt{-\frac{\sigma_1(\sqrt{105} - 7)}{14D_2}}. \end{aligned} \quad (3.16)$$

### 3.3.2 Existence, dynamical behavior of solutions Eqs. (3.14)-(3.16)

For analytical conveniences in Eqs. (3.14)-(3.16), we set

$$\sigma_1 = \beta_1 - r\sigma - \beta c_{min} \neq 0, \quad \sigma_2 = r + \frac{\beta\tau_0}{\chi_0 - \tau_0} \neq 0, \quad \tau_0 \neq \chi_0 \quad \text{and} \quad \epsilon = \pm 1.$$

A straightforward analysis of Eqs. (3.14)-(3.16) shows that bacterial and chemoattractant solutions exist if  $D_2 \neq 0, \sigma_1 < 0, \sigma_2 > 0$  which lead to the constraints

$$\beta_1 < r\sigma + \beta c_{min} = \beta_{1_{crit}}, \quad \text{and} \quad r > \frac{\beta\tau_0}{\tau_0 - \chi_0} = r_{min}. \quad (3.17)$$

The first inequality of Eq. (3.17) proves that the linear chemoattractant production rate  $\beta_1$  possesses a minimum value  $r\sigma$ , and linearly increases with chemoattractant consumption rate  $\beta$ . The second inequality shows that our system admits a proliferation rate always greater than the threshold value  $r_{min}$ . Eqs. (3.11) and Eqs. (3.17) describe the general conditions on the existence of bacterial and chemoattractant concentration but, do not provide any details on dynamical properties. We discuss below some dynamical properties of both bacterial and chemoattractant waves such as their profiles, velocities, amplitudes, thicknesses, and we analyze effects of  $\tau_0, \chi_0, D_2, D_1$ , and  $\beta$ . To this end, we take  $\beta_1 = \frac{\beta_{1_{crit}}}{10}, r = r_{min} + r_0, r_0 = 1.69 \cdot 10^{-9}$  being the proliferation rate given in [2].

Using Eqs. (3.14), one recovers the bell-shape traveling wave

$$n(x, y, t) = -\frac{15\sigma_1}{2\sigma_2} \left( \frac{1}{\cosh[\sqrt{P_2}(kx + ly - \omega t)]} \right)^2, \quad (3.18a)$$

$$c(x, y, t) = -\frac{15\sigma_1\tau_0}{2\sigma_2(\chi_0 - \tau_0)} \left( \frac{1}{\cosh[\sqrt{P_2}(kx + ly - \omega t)]} \right)^2 + c_{min}, \quad (3.18b)$$

where the associated velocity reads:

$$\omega = \delta_{0_x} \sqrt{\frac{1}{4P_2} \sqrt{\frac{1}{D_2} [r\sigma - \beta_1 + \beta c_{min}] - l^2}} + \delta_{0_y} l = \omega_{bs}. \quad (3.19)$$

From Eq. (3.19), one deduces the existence of minimal/maximal wave velocities

$$\omega_{min} = 0 \leq \omega \leq \omega_{max} = \sqrt{\frac{\delta_{0x}^2 + \delta_{0y}^2}{4P_2}} \sqrt{\frac{1}{D_2} [r\sigma - \beta_1 + \beta c_{min}]},$$

where  $\omega_{min} = \omega(l = l_{crit})$  and  $\omega_{max} = \omega(l = l_0)$ .  $l_{crit}$  is recovered by solving  $\omega|_{l=l_{crit}} = 0$ , and the maximum velocity  $\omega_{max}$  is reached at  $l_0$ . The latter is determined by solving  $\frac{d\omega}{dl}|_{l=l_0}$ , hence we have

$$l_{crit} = \delta_{0x} \sqrt{\frac{\omega_0}{\delta_{0x}^2}}, \quad l_0 = \delta_{0y} \sqrt{\frac{\omega_0}{\delta_{0y}^2}}, \quad \delta_0^2 = \delta_{0x}^2 + \delta_{0y}^2, \quad \omega_0 = \frac{1}{4P_2} \sqrt{\frac{1}{D_2} [r\sigma - \beta_1 + \beta c_{min}]}.$$

$l_0$  and  $l_{crit}$  depend on the system parameters, which means the experimenter has the potential of controlling fast or slow wave propagation if he accurately tunes the experimental setups. From Eqs. (18)  $n_{\infty bs} = \lim_{\xi \rightarrow \infty} n(x, y, t) \rightarrow 0$  and  $c_{\infty bs} = \lim_{\xi \rightarrow \infty} c(x, y, t) \rightarrow \frac{D_3}{\tau_0 - \chi_0} - \frac{D_1}{\tau_0}$ , which mean that bacterial and chemoattractant wave amplitudes are finite as their associated velocity. This confirms that bell-shape solutions Eqs. (18) are physical ones. The bell-shape profile Eqs. (18) is displayed in Fig. 3.4 at the time  $t = 100$ . Traveling waves in reactive systems are either matter carriers or

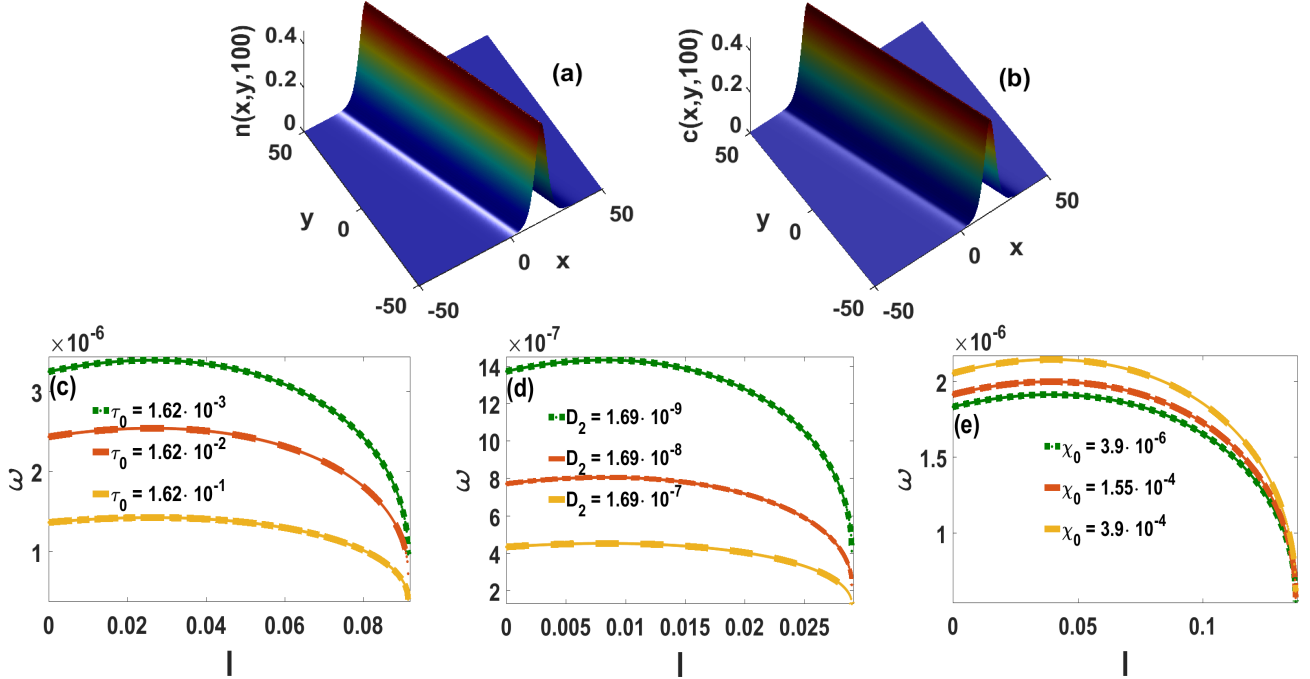


Figure 3.4: Bell-shape solutions Eqs. (3.18) for density (a) and chemoattractant concentration (b). Wave velocity increase with traction (c), chemotaxis (e), or as long-range diffusion (d) decreases. Parameters are  $D_1 = 8.9 \cdot 10^{-6}$ ,  $D_2 = 1.69 \cdot 10^{-9}$ ,  $D_3 = 4 \cdot 10^{-6}$ ,  $\chi_0 = 6.49 \cdot 10^{-5}$ ,  $\tau_0 = 1.62 \cdot 10^{-3}$ ,  $\sigma = 2.4231 \cdot 10^8$ ,  $\beta = 3.5 \cdot 10^{-8}$ ,  $\delta_{0x} = 1.5 \cdot 10^{-5}$ ,  $\delta_{0y} = 4.5 \cdot 10^{-4}$ ,  $P_2 = 4$ .

information conveyors, the bell-shaped profile obtained here may explain collective bands of bacteria



usually observed in reactive systems. Its velocity is depicted in panels (c)-(e) of Fig. 3.4. It is seen that the amplitude of  $\omega_{bs}$  decreases with increasing values of traction and long-range diffusion, respectively [see Figs. 3.4(c)-(d)], meaning that the traction and the long-range diffusion slow down the waves. Conversely, the amplitude of  $\omega_{bs}$  increases with increasing values of  $\chi_0$  implying that the chemotaxis strength accelerates the wave propagation.  $\tau_0$ ,  $D_2$ , and  $\chi_0$  have competing effects on the velocity of the wave. This property may be used in experiments to detect or characterize the waves. In all the cases, the velocity reduces with increasing values of  $l$ , thus thinner waves move faster than wider ones.

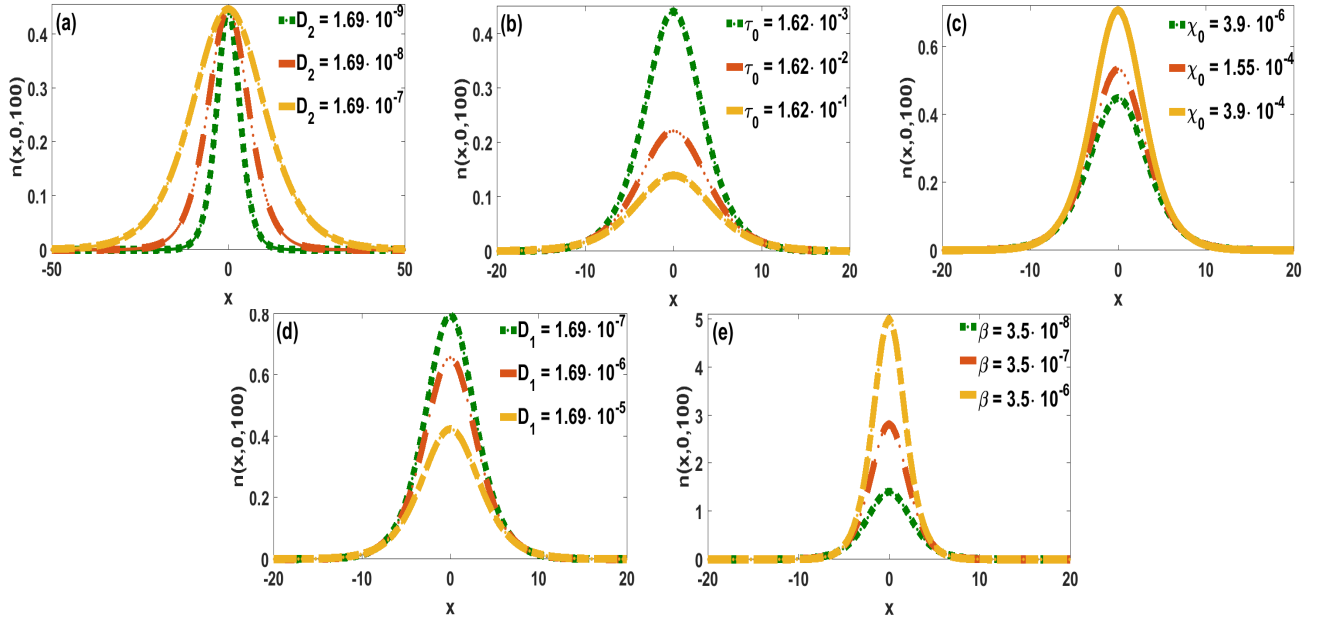


Figure 3.5: Influence of long-range diffusion (a), traction (b), chemotaxis (c), short-range diffusion (d) and chemoattractant consumption rate (e) upon the bell-shape bacterial wave at  $y = 0$  and time  $t = 100$  s. Except where mentioned, parameters are taken as in Fig. 3.4.

Considering the influences of system parameters on the bell-shaped wave, one observes that when long-range diffusion increases [Fig. 3.5(a)], the wave thickness widens, hence the cellular distribution occupies a larger spatial domain. At high values of long-range diffusion  $D_2$ , the coordination degree amongst units of the bacterial population decreases, resulting in a diminution of the global velocity of the aggregation. Such a result is in accordance with the idea that diffusion of particles should break up coordination and communication degree amongst particles. Wave thickness variations are a common feature in reactive systems as extensively discussed in [83, 85] and its occurrence in the present study signifies that cells do not lose their active properties, but rather rearrange themselves to accommodate chemoattractant concentrations across the medium. In panels (b)-(e) of Fig. 3.5, wave

thickness variations are accompanied by an amplitude variation. Amplitude and thickness increase is observed when traction Fig. 3.5(b) and short range-diffusion Fig. 3.5(d) increase, while chemotaxis Fig. 3.5(c) as well as the chemoattractant consumption rate Fig. 3.5(e) decrease. Wave thickness reduction or increase coupled with amplitude variations in systems with uniform flows have also been reported in autocatalytic fronts [86], the Fitz-Hugh-Nagumo model [87], and the Belousov-Zhabotinsky reaction [88, 89]. We propose such a coupled dynamic between wave thickness and amplitude as a tool to slice spatial domains in intervals within which cells activity remains optimized, and above which cellular density drastically reduces.

Using the parameters given in Eq. (3.15) leads the dip traveling wave solutions

$$n(x, y, t) = -\frac{15\sigma_1}{4\sigma_2} \left[ 2 + \tanh \left( \sqrt{-\frac{P_2}{2}}(kx + ly - \omega t) \right)^2 \right], \quad (3.20a)$$

$$c(x, y, t) = c_{min} + \frac{15\tau_0\sigma_1}{4\sigma_2(\chi_0 - \tau_0)} \left[ 2 + \tanh \left( \sqrt{-\frac{P_2}{2}}(kx + ly - \omega t) \right)^2 \right]. \quad (3.20b)$$

In the long time/large space limits,  $n_{\infty dw} = \lim_{\xi \rightarrow \infty} n(x, y, t) \rightarrow -\frac{45\sigma_1}{4\sigma_2} > 0$  and  $c_{\infty dw} = \lim_{\xi \rightarrow \infty} c(x, y, t) \rightarrow \frac{1}{\tau_0 - \chi_0} \left[ D_3 - \frac{45\sigma_1\tau_0}{4\sigma_2} \right] - \frac{D_1}{\tau_0} > 0$ . The velocity associated with solutions Eqs. (22) reads

$$\omega = \delta_{0,x} \sqrt{-\frac{1}{2P_2} \sqrt{\frac{1}{D_2} [r\sigma - \beta_1 + \beta c_{min}] - l^2} + \delta_{0,y} l = \omega_{dw}. \quad (3.21)$$

Figs. 3.6(a), and 3.6(b) show the snapshots at time  $t = 100$  of bacterial density (Eq. (3.20a)) and chemoattractant concentration (Eq. (3.20b)). The dip waves travel faster than the bell-shape waves since  $\omega_{dw} > \omega_{bs}$ . A straightforward comparison of Eqs. (3.20) and Eqs. (3.18) allows to figure out that the model parameters have similar effects on dip waves and their velocity  $\omega_{dw}$  as on the bell-shape wave presented above.

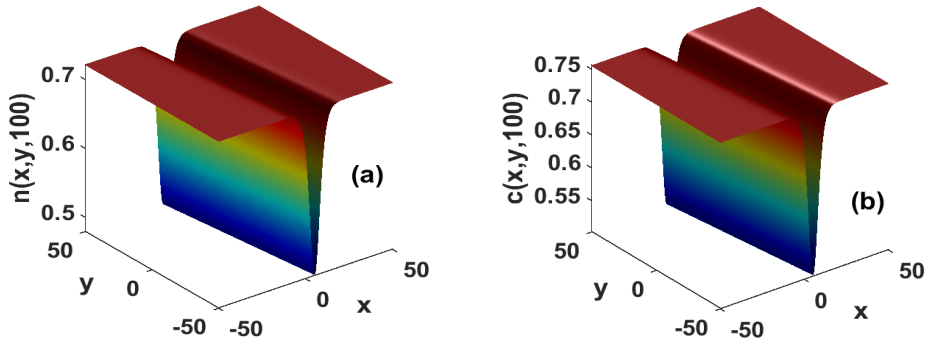


Figure 3.6: Dip traveling waves for bacterial density (a) and chemoattractant concentration (b) given by Eqs. (3.20). Same parameters as in Fig. 1 except for  $P_2 = -2$ .

Plugging the parameters set Eq. (3.15) into Eq. (3.12) and Eq. (3.10) allows us to construct step traveling waves whose analytical formula are

$$\begin{aligned}
n(x, y, t) &= -\frac{\sigma_1(21 + \sqrt{105})}{14\sigma_2} - \frac{3\sigma_1(35 - \sqrt{105})}{28\sigma_2} \frac{\cosh\left(\sqrt{\frac{P_2}{4}}(kx + ly - \omega t)\right)^{-2}}{\tanh\left(\sqrt{\frac{P_2}{4}}(kx + ly - \omega t)\right) - 1} \times \\
&\quad \left[ -2 + \frac{\cosh\left(\sqrt{\frac{P_2}{4}}(kx + ly - \omega t)\right)^{-2}}{\tanh\left(\sqrt{\frac{P_2}{4}}(kx + ly - \omega t)\right) - 1} \right], \tag{3.22} \\
c(x, y, t) &= -\frac{D_1}{\tau_0} - \frac{1}{\chi_0 - \tau_0} \left[ D_3 - \frac{\tau_0\sigma_1(21 + \sqrt{105})}{14\sigma_2} \right] + \\
&\quad \frac{3\sigma_1\tau_0(35 - \sqrt{105})}{28\sigma_2(\chi_0 - \tau_0)} \frac{\cosh\left(\sqrt{\frac{P_2}{4}}(kx + ly - \omega t)\right)^{-2}}{\tanh\left(\sqrt{\frac{P_2}{4}}(kx + ly - \omega t)\right) - 1} \left[ -2 + \frac{\cosh\left(\sqrt{\frac{P_2}{4}}(kx + ly - \omega t)\right)^{-2}}{\tanh\left(\sqrt{\frac{P_2}{4}}(kx + ly - \omega t)\right) - 1} \right].
\end{aligned}$$

The velocity associated with solutions Eqs. (3.22) is

$$\omega = \delta_{0x} \sqrt{\frac{1}{P_2} \sqrt{\frac{\sqrt{105} - 7}{14D_2}} [r\sigma - \beta_1 + \beta c_{min}] - l^2} + \delta_{0y} l = \omega_{sw}. \tag{3.23}$$

Furthermore,  $n_{-\infty_{sw}} = \lim_{\xi \rightarrow -\infty} n(x, y, t) \rightarrow -\frac{\sigma_1(21 + \sqrt{105})}{14\sigma_2}$ ,  $c_{-\infty_{sw}} = \lim_{\xi \rightarrow -\infty} c(x, y, t) \rightarrow \frac{D_3}{\tau_0 - \chi_0} - \frac{D_1}{\tau_0} - \frac{\sigma_1\tau_0(21 + \sqrt{105})}{14\sigma_2(\tau_0 - \chi_0)}$ , and  $n_{+\infty_{sw}} = \lim_{\xi \rightarrow +\infty} n(x, y, t) \rightarrow -\frac{\sigma_1(420 - 11\sqrt{105})}{14\sigma_2}$ ,  $c_{+\infty_{sw}} = \lim_{\xi \rightarrow +\infty} c(x, y, t) \rightarrow \frac{D_3}{\tau_0 - \chi_0} - \frac{D_1}{\tau_0} - \frac{\sigma_1\tau_0(420 - 11\sqrt{105})}{14\sigma_2(\tau_0 - \chi_0)}$ . Step waves obtained here translate the transition process happening between two different levels of bacteria as well as chemoattractant distribution. The gap between the levels depends on system parameters, which means that the experimenter has the potential of choosing how and the position at which the transition happens. Figs. 3.7 display bacterial and chemoattractant step waves Eqs. (3.22) in panels (a), (b), respectively.

Numerical values of short-range diffusions  $D_1, D_3$ , chemotaxis strength  $\chi_0$ , chemoattractant consumption rate  $\beta$ , and medium carrying capacity  $\sigma$  were chosen as in [2, 20, 19, 83]. The fluids flow rate was taken according to experimental studies [83, 19]. The other parameters  $\tau_0, D_2, \beta_1, \beta_3$  to the best of our knowledge are not yet available. While the analytical formalism used allows to determine  $\beta_3$ , and the existence of solutions discussed yields a minimum value of  $\beta_1$ . Though traction forces dominate the chemotaxis strength, the latter is shown to still have strong effects on wave characteristics namely the velocity, amplitude, and thickness. These observations are consistent with conclusions reported in [19, 25]. More importantly, for the same set of parameter values, comparison of Eqs. (3.19), Eqs. (3.21) and Eqs. (3.23) yields  $\omega_{dw} > \omega_{sw} > \omega_{bs}$ : the dip waves travel faster than the step and the bell-shaped waves. In other words, dip waves are better candidates to achieve fast coordination of

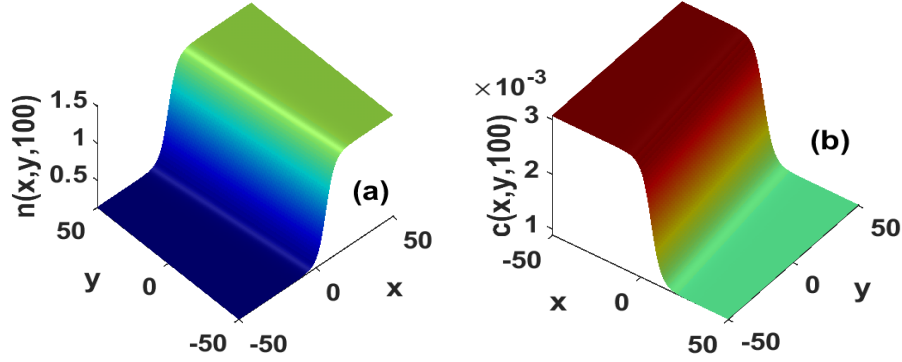


Figure 3.7: Step traveling waves for bacterial density (a) and chemoattractant concentration (b) (Eqs. (3.22)).  $P_2 = 4$ , other parameters taken as in Fig. 1.

cells or to quickly convey a piece of information within a bacterial population. From Eqs. (3.18), Eqs. (3.20) and Eqs. (3.22), one derives the inequalities  $n_{sw} > n_{dw} > n_{bs}$ . Step waves carry a higher amount of particles compared to dip and bell-shaped waves. Generally speaking, an optimal transport is expected for higher velocities and wave amplitudes, but the results obtained here draw the roadmap to characterizing an optimal transport as follows: while step waves ensure the transport of a higher number of particles, a faster transport is guaranteed through dip wave structures. In reactive systems without traction and long-range diffusion, it has been shown that optimal transport necessitates the coupled dynamic between short-range diffusion and feedback [90]. However, the present study stresses that traction and long-range diffusion deeply alter the optimal transport of waves, hence must be taken into account for a better description of waves propagation.

### 3.3.3 Numerical experiments with the bell-shape traveling wave

In this section, we ascertain the ability of waves discussed above to propagate in a stable fashion way in model Eqs. (2.11). To this end, direct numerical integrations of Eqs. (2.11) on a square spatial domain of length  $L = 100$  are performed. We take  $N = 1024$  points along each spatial direction with a time step is  $dt = 10^{-3}$ . Integrations are performed through the pseudo-spectral method. We initially launched the simulations by introducing perturbed analytical solutions with a noise strength of ten percent of the initial amplitude of the wave. Simulations are ran over a final time  $t_{fin} = 200$  s and results are displayed in Figs. 3.8. To be precise, panels (a), (b), (c) of Figs. 3.8 (resp. panels (d), (e), (f)) display snapshots of the bacterial density (resp. chemoattractant concentration) at  $t = 0$  s, 100 s, 200 s respectively, obtained with the analytical solutions Eqs. (3.18), (3.20), and (3.22) as initial conditions. Though we inserted a random perturbation at the initial time, results are depicted in Figs. 3.8 show that initial solutions evolve without undergoing any collapses nor explosions. Our solutions

are numerically stable ones. In addition, from Eqs. (3.18), (3.20), and (3.22), the analytical solutions found above predict waves whose profiles, widths, amplitudes, and velocities remain unchanged during their evolutions, but slightly displaced due to small velocities of magnitude about  $10^{-5}$ . Snapshots of waves displayed in Figs. 3.8 are in good agreement with analytical predictions. Our solutions are therefore stable ones, such that they are likely to be observed in experiments. Our results are new ones and we do believe this work may motivate further two-dimensional experimental investigations in chemotaxis systems where traction forces, advection, and long-range diffusion are at play. To the best of our knowledge, such experimental investigations that take into account the latter effects are still missing.

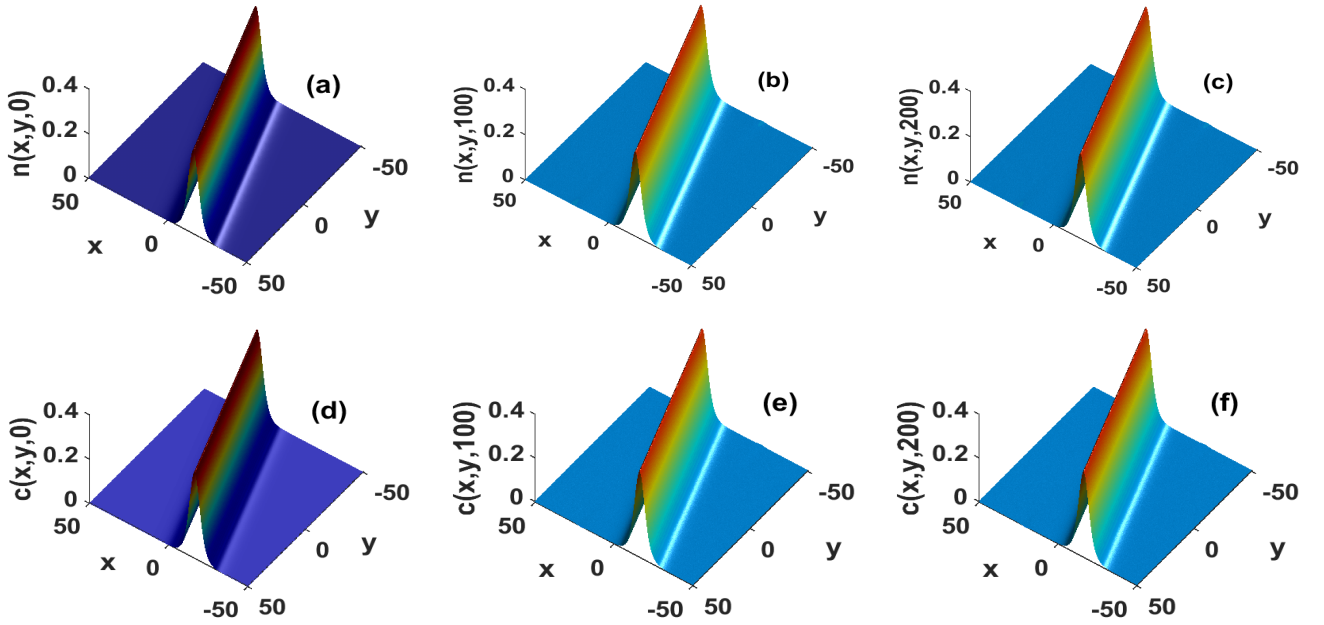


Figure 3.8: Snapshots of stable numerical bell-shape solutions for bacterial (chemoattractant) wave  $att = 0$  s (a) [(d)],  $t = 100$  s (b) [(e)], and  $t = 200$  s (c) [(f)]. Parameters as in Figs. 3.4.

## 3.4 Dynamic of nonlinear excitations in coupled haptotaxis-chemotaxis systems

### 3.4.1 Results of the application of the reductive perturbation method: The wave frequency, group velocity, and the reduced model

In order to apply the reductive perturbation method, we consider slow spatiotemporal variables  $\xi = \epsilon(x - V_g t)$ , and  $\tau = \epsilon^2 t$ .  $\epsilon$  measures nonlinearity order,  $V_g$  being the group velocity. We Look for

solutions of dependent variables  $n$ ,  $c$ ,  $\rho$ ,  $u$ , as expansions around the reference quantities  $(n_0, c_0, \rho_0, u_0)$

$$\begin{aligned} n &= n_0 + \sum_{j=1}^{\infty} \epsilon^j \sum_{l=-j}^j n_l^{(j)}(\xi, \tau) A^l(x, t), & c &= c_0 + \sum_{j=1}^{\infty} \epsilon^j \sum_{l=-j}^j C_l^{(j)}(\xi, \tau) A^l(x, t), \\ \rho &= \rho_0 + \sum_{j=1}^{\infty} \epsilon^j \sum_{l=-j}^j \rho_l^{(j)}(\xi, \tau) A^l(x, t), & u &= \sum_{j=1}^{\infty} \epsilon^j \sum_{l=-j}^j u_l^{(j)}(\xi, \tau) A^l(x, t) \end{aligned} \quad (3.24)$$

are introduced into Eqs. (2.14). Hereafter, we assume  $(n_0, c_0, \rho_0) = (1, 1, 1)$ . Inserting the nonlinear excitations Eqs. (3.24) into the model Eqs. (2.14) permits the extraction of the wave frequency and the group velocity, respectively given by Eqs. (A.3) and Eq. (A.8) in Appendix A. We display in Fig. 3.9 the variations of these quantities as a function of the modulation wave  $k$ , for a different set of parameter values. We assume the wave pulsation given by Eq. (A.8) writes  $\omega = \omega_r + i\omega_i$ .  $\omega_r$  represents the angular frequency and  $\omega_i$  is the factor that represents the growth rate of the expansion Eq. (2.24) while propagating in the model Eq. (2.14). The sign of  $\omega_i$  reveals whether the excitations die ( $\omega_i < 0$ ) or grow ( $\omega_i > 0$ ) exponentially as time increases. In the present study, the fact that  $\omega$  is complex reveals viscoelastic properties, translating the inability of the medium to effectively convey information without modifying it. In fact, when space parameters converge toward  $\omega_i > 0$ , nonlinear excitations Eqs. (3.24) get amplified, a situation that may be nonrelevant for biological applications. Yet the situation  $\omega_i < 0$  describes amplitude decay with time. We infer the above-stated behaviors as the consequences of localized inhomogeneities, that in the latter case, cause some waves to continuously lose their energy and decay via radiation to infinity. This is also observed in bounded domains where interactions of forward waves with boundaries nucleate backward propagations or compressive waves. This implicitly says that perturbations steadily cancel out when  $\omega_i < 0$ . Moreover, the angular

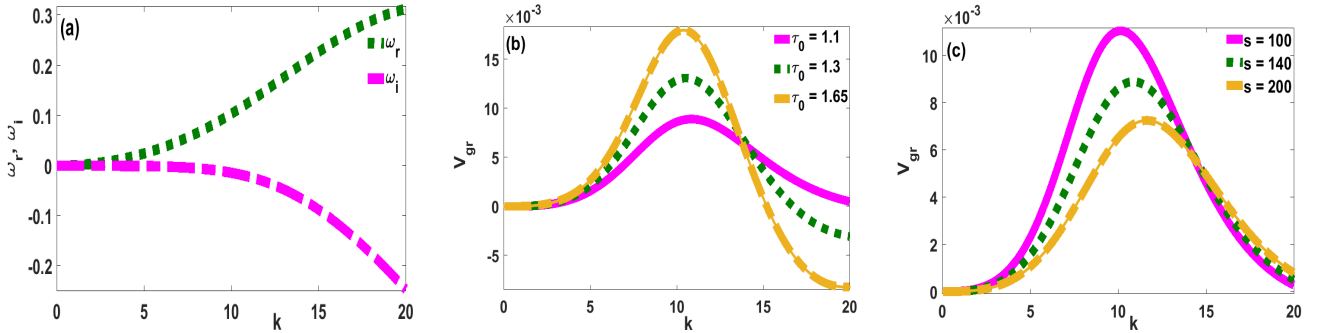


Figure 3.9: The wave frequency, the growth rate and the group velocity as functions of the wave vector. The parameters taken as in [2] are:  $D_n = D_c = \alpha_1 = \gamma = \chi_0 = 10^{-3}$ ,  $\mu = 1$ ,  $\lambda = 0.12$ ,  $\beta = 0.05$ ,  $\alpha = 1$ ,  $\tau_0 = 1.1$ ,  $s = 140$ . Panel (a) shows not significant influences on wave frequency, while panel (b), the group velocity switches sign as traction increases, showing an expansive/compressive wave transition point. In panel (c), the group velocity remains positive as adhesion increases.

frequency depiction Fig. 3.9(a) reveals the existence of a lower and an upper cutoff mode. Invasion mechanisms of cells within biological tissues require some degree of coherence or synchronization of the population, though each individual might be undergoing specific and spontaneous activity with a specific associated frequency. Fig. 3.9(a) indicates the existence of bands frequencies within which each individual should tune in, in order to coherently move accordingly with others. And more interestingly, both traction and substrate attachment do not significantly modify the admitted gap frequency, stemming that they might be more sensitive to intrinsic properties of cells such as chemoattractant consumption's rate. In the present paper, we assume that each individual of the population has its frequency comprised in between the lower and the upper frequencies as depicted in Fig. 3.9(a).

Panels Fig. 3.9(b), Fig. 3.9(c) show the influences of traction and adhesion on the group velocity, plotted as a function of the wave vector  $k$ . The observed concavity and sign change of the group velocity shows that the wave is either expansive  $V_{gr} > 0$  or compressive  $V_{gr} < 0$  as in Fig. 3.9(b). The sign change of  $V_{gr}$  is observed for increasing values of traction  $\tau_0$ , meaning that cell-ECM interactions may generate backward propagations. In other words,  $\tau_0$  may be used to control the transition between forwards and backward propagations. On the other side, increasing cell attachment leads to a net reduction of  $V_{gr}$ , but this last one remains positive and therefore only forward propagating waves would be observed. In addition, variations of  $V_{gr}$  with adhesion and traction imply that they may be used to control the number of particles carried by the waves, and probe with good accuracy the biological tissues being invaded.

### 3.4.2 Analytical solutions of the reduced model: The bilinear approach

Further, following the RPM technique, we establish in Appendix A that weak nonlinear excitations propagating in Eqs. (2.14) may be governed by the cubic complex Ginzburg-Landau equation

$$i \frac{\partial \psi}{\partial \tau} + P \frac{\partial^2 \psi}{\partial \xi^2} + i R_{11} \frac{\partial \psi}{\partial \xi} + Q |\psi|^2 \psi + i \varphi(\tau) \psi = 0 \quad (3.25)$$

In order to specify spatiotemporal evolutions of weak order bacterial densities, solutions of Eq. (3.25) should be constructed. For sake of simplicity, we focus our analytical treatment on the cases  $\varphi(\tau) = c^{nst}$ , and apply the transformation

$$\psi(\xi, \tau) = \Phi(\xi, \tau) e^{-\varphi \tau}, \quad (3.26)$$

into Eq. (3.25) to obtain

$$i \frac{\partial \Phi}{\partial \tau} + P \frac{\partial^2 \Phi}{\partial \xi^2} + i R_{11} \frac{\partial \Phi}{\partial \xi} + Q e^{-2\varphi \tau} |\Phi|^2 \Phi = 0. \quad (3.27)$$

The application of the Hirota bilinear method requires to consider the Hirota's operators [57, 82]

$$D_{\delta,\tau}^{m_0} D_{\delta,\xi}^{m_1} F(\xi, \tau) \cdot G(\xi, \tau) = \left( \frac{\partial}{\partial \tau} - \delta \frac{\partial}{\partial \tau'} \right)^{m_0} \left( \frac{\partial}{\partial \xi} - \delta \frac{\partial}{\partial \xi'} \right)^{m_1} F(\xi, \tau) G(\xi', \tau') \Big|_{\xi=\xi', \tau=\tau'}, \quad (3.28)$$

where  $m_0$ , and  $m_1$  are positive integers. Further, we look forwards solutions of Eq. (3.27) in the form

$$\Phi(\xi, \tau) = \frac{G(\xi, \tau)}{F^\delta(\xi, \tau)}, \quad (3.29)$$

$G(\xi, \tau)$  and  $F(\xi, \tau)$  being complex and real functions respectively, and  $\delta = \delta_r + i\delta_i$ , a complex constant to be determined. Plugging Eq. (3.29) into Eq. (3.27) and using Eq. (3.28) leads to the bilinear system:

$$(iD_{\delta,\tau} + PD_{\delta,\xi}^2 + iR_1 D_{\delta,\xi}) G \cdot F = 0, \quad (3.30a)$$

$$D_\xi^2 F \cdot F = \frac{2(P_r Q_i - P_i Q_r) e^{-2\varphi\tau}}{3\delta_i |P|^2} |G|^2, \quad (3.30b)$$

provided that

$$\delta_i^2 (P_r Q_i - P_i Q_r) + \delta_i (1 + 2\delta_r) (P_r Q_r + P_i Q_i) - \delta_r (1 + \delta_r) (P_r Q_i - P_i Q_r) = 0. \quad (3.31)$$

Solutions of Eqs. (3.30) can be investigated as wave traveling in polynomial forms. Thus, following methodology outlined by the authors of [82, 57]

$$G(\xi, \tau) = e^{\theta_1}, \quad F(\xi, \tau) = 1 + b_1(\tau) e^{\theta_1 + \theta_1^*} \quad \text{where} \quad \theta_1(\xi, \tau) = \xi k_1 + h_0(\tau), \quad k_1 = k_{1r} + i k_{1i}. \quad (3.32)$$

Functions  $h_0, b_1$ , are time-dependent complex and real functions, respectively. Inserting Eq. (3.32) into Eqs. (3.30) yields

$$\frac{dh_0}{d\tau} + k_1 (R_{11} - i P k_1) = 0, \quad (3.33a)$$

$$\frac{1}{b_1(\tau)} \frac{db_1}{d\tau} - \frac{dh_0}{d\tau} - \frac{dh_0^*}{d\tau} - 2R_1 k_{1r} = 0, \quad (3.33b)$$

$$k_{1i} = k_{1r} \delta_i, \quad (3.33c)$$

$$b_1(\tau) = \frac{P_r Q_i - P_i Q_r}{12 k_{1i} k_{1r} |P|^2} e^{-2\varphi\tau}. \quad (3.33d)$$

From Eq. (3.33c), we set  $\delta_i = \frac{k_{1i}}{k_{1r}}$ , and solve Eq. (3.31) for the new variable  $\frac{k_{1i}}{k_{1r}}$

$$\left( \frac{k_{1i}}{k_{1r}} \right)_\pm = \frac{-3(P_r Q_r + P_i Q_i) \pm \sqrt{9(P_r Q_r + P_i Q_i)^2 + 8(P_r Q_i - P_i Q_r)^2}}{2(P_r Q_i - P_i Q_r)}. \quad (3.34)$$

After integration of Eq. (3.33a) and Eq. (3.33b), we have

$$h_0(\tau) = -k_1 \tau (R_{11} - i k_1 P), \quad (3.35a)$$

$$b_1(\tau) = b_{00} \exp \left[ 2\tau k_{1r} \left( P_i + P_r \frac{k_{1i}}{k_{1r}} \right) \right]. \quad (3.35b)$$



$b_{00}$  is a real integration constant. Using Eq. (3.26), and inserting Eq. (3.35b) into Eq. (3.33d) enforces

$$\varphi = -k_{1r} \left( P_i + P_r \frac{k_{1i}}{k_{1r}} \right) \quad \text{and} \quad b_{00} = \frac{P_r Q_i - P_i Q_r}{12 k_{1i} k_{1r} |P|^2} \quad (3.36)$$

Making use of all the transformations applied until now, the one soliton solution of Eq. (3.25) is recovered

$$\psi(\xi, \tau) = \frac{\exp \left[ k_{1i} \xi - k_{1r} \tau (R_{11} - iP k_{1i}) + \tau k_{1r} \left( P_i + P_r \frac{k_{1i}}{k_{1r}} \right) \right]}{\{1 + b_{00} \exp[2k_{1r}(\xi - R_{11}\tau)]\}^{1+i \frac{k_{1i}}{k_{1r}}}}. \quad (3.37)$$

### 3.4.3 Existence and dynamical behaviors of soliton solutions Eq. (3.37)

Using Eq. (3.34), we write  $k_{1i}$  as a function of  $k_{1r}$ , and the solution Eq. (3.37) admits only  $k_{1r}$  as the free parameter, for a given modulation wave vector  $\mathbf{k}$ . With the known parameters of the original model Eq. (2.14), analytical solutions are well defined, and, they are physically and experimentally more likely to be observed when  $b_{00} > 0$ . Thus following Eqs. (3.34) and the second expression of Eq. (3.36),

$$b_{00} = \frac{(P_r Q_i - P_i Q_r)^2}{6 k_{1r}^2 |P|^2 \left[ 3 (P_r Q_r + P_i Q_i) \pm \sqrt{9 (P_r Q_r + P_i Q_i)^2 + 8 (P_r Q_i - P_i Q_r)^2} \right]} > 0. \quad (3.38)$$

The above condition is therefore satisfied only for the positive sign "+" corresponding to  $\left( \frac{k_{1i}}{k_{1r}} \right)_+$  of Eq. (3.34). In that sense, Eq. (3.38) stands for the existence condition of the soliton solution Eq. (3.37).

The one soliton solution we derived in the present study shows quasi constant wave amplitude at very small time scales. Broadly, a wave flattening feature when either traction  $\tau_0$  or chemoattractant consumption increase Fig. 3.10(b)/Fig. 3.10(d) or when the cell attachment  $s$  decreases Fig. 3.10(c) is reported. As the substrate attachment increases Fig. 3.10(c), the solitary pulse gets higher and wider, stemming that the number of cells involved in mechanical motion is continually increased, and their spatial repartition is continuously reorganized. Under the same configuration as depicted in Fig. 3.10(e), the corresponding group velocity decreases, a situation reminiscent of the striking phenomenon of motility induced phase separation (MIPS), responsible for local recruitment of cells as their velocity decreases. On the other hand, an amplitude decrease characterizing the reduction of the number of particles transported is observed when traction  $\tau_0$  and chemoattractant consumption  $\beta$  increase (panels 3.10(b) and 3.10(d) resp.). In fact, we earlier showed that increasing  $\tau_0$  generates backward or compressive waves. We argue that those counter-propagating waves may swerve the initial direction of transport of a proportion of the population, hence the amplitude decrease. The fact that the latter result may also be obtained by increasing chemoattractant consumption rate Fig. 3.10(d)

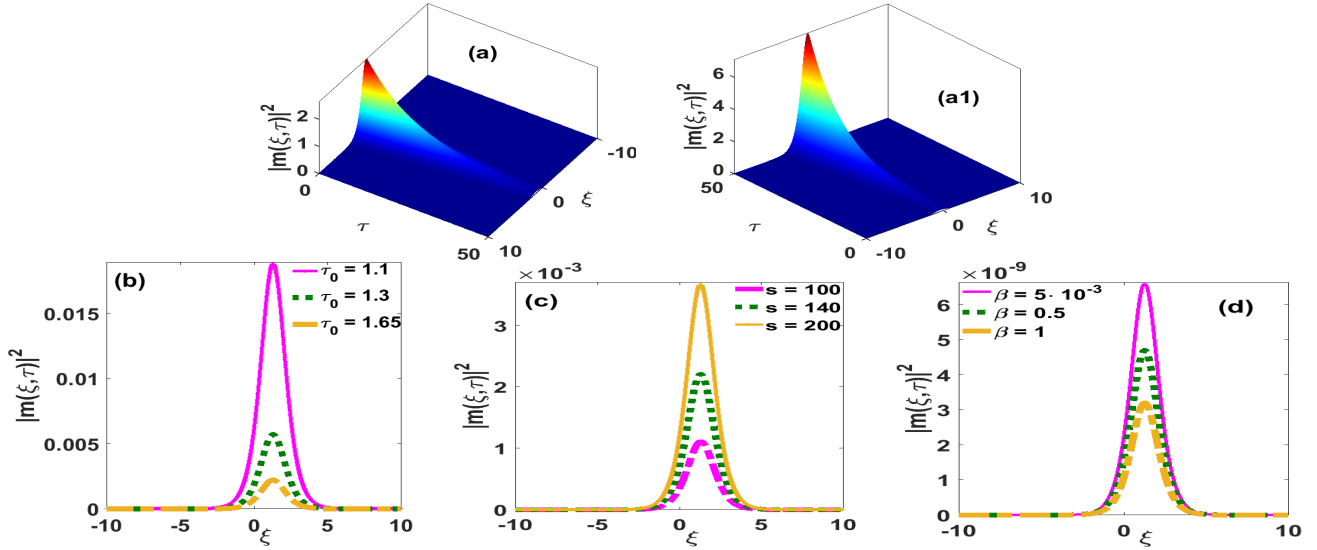


Figure 3.10: Solutions of Eq. (2.14) generated through Eq. (3.37) in the  $(\xi, \tau)$ -frame. Top row, in panel (a), solitary pulse experiences amplitude reduction for  $k = 1$  while (a1) displays and amplitude increase for  $k = 5$ . The bottom row panels show that the wave undergoes flattening and amplitude decrease when traction (b), chemoattractant consumption (d) rate increase, while substrate attachment decreases (c).  $k_{1r} = 0.9$ . Parameters as in Fig. 3.9

reveals an interplay between mechanical and biochemical properties of cells, that to the best of our knowledge have not yet been pointed out. Furthermore, in order to increase the mechanical activity in the medium (increase the number of cells carried by the soliton solution Eq. (3.37)), our results indicate that traction should be reduced or the adhesion parameter increased. Such an antagonistic behavior between traction and attachment indicates their pivoting role in designing dispersive and nonlinear properties of the medium, and hence its carrying capacity. Moreover, comparing top row panels (a) and (a1) of Fig. 3.10 reveals that though the energy consumption per capita might be high, the population still undergoes extinction Fig. 3.10(a) or a slow population increase Fig. 3.10(a1), and the propagation direction is conserved. The above analysis suggests that attachment, traction, consumption rate, and envelope wave vector have specific outcomes on the number of cells involved in the invasion. Therefore, experimenters how to tune their settings for the sake of their interests.

### 3.4.4 Numerical experiments

In this section, we ascertain the ability of the model Eqs. (2.14) to support the propagation of mechanical waves generated through nonlinear analysis performed so far. Taking into consideration all the transformations applied up until now, solutions of Eq. (A.17) for  $m(\xi, \tau)$  in the  $(\xi, \tau)$  frame

take the form

$$m(\xi, \tau) = \frac{\exp \left[ \xi \left( k_1 + \frac{iR_r}{2P_i} \right) - k_1 \tau (R_{11} - iP k_1) + \tau k_{1r} \left( P_i + P_r \frac{k_{1i}}{k_{1r}} \right) - \frac{iR_r \tau}{2P_i} \left( R_i + \frac{P_r R_r}{2P_i} \right) \right]}{\{1 + b_{00} \exp [2k_{1r}(\xi - R_{11}\tau)]\}^{1+i\frac{k_{1i}}{k_{1r}}}}, \quad (3.39)$$

and using Eq. (2.24) along with the transformations  $\xi = \epsilon(x - V_g t)$ ,  $\tau = \epsilon^2 t$ , we recover the solutions in the  $(x, t)$ -space for cellular density as

$$n(x, t) = n_0 + \epsilon \text{Real} [M(x, t)e^{i(kx - \omega t)}] \quad \text{where} \quad M(x, t) = m(\epsilon(x - V_g t), \epsilon^2 t). \quad (3.40)$$

Accordingly, Eq. (3.40) tells that in the  $(x, t)$ -frame,  $\epsilon$  appears to impact not only wave amplitude, but also other characteristics including wave velocity and width. Therefore its values must be chosen acutely. Numerical integrations of Eqs. (2.14) are performed through fourth-order Runge-Kutta scheme on a spatial domain of length  $L = 20$ . The final time of simulations is  $t_{fin} = 10^{-2}$  and the time step is  $dt = 10^{-7}$ . Initial conditions (ICs) generated by the solutions Eq. (3.40) (taken at  $t = 0$ ), are randomly perturbed at the initial time, with a noise of a strength one percent of the initial amplitude. The results are displayed in Fig. 3.11, analytical and numerical results taken at specific

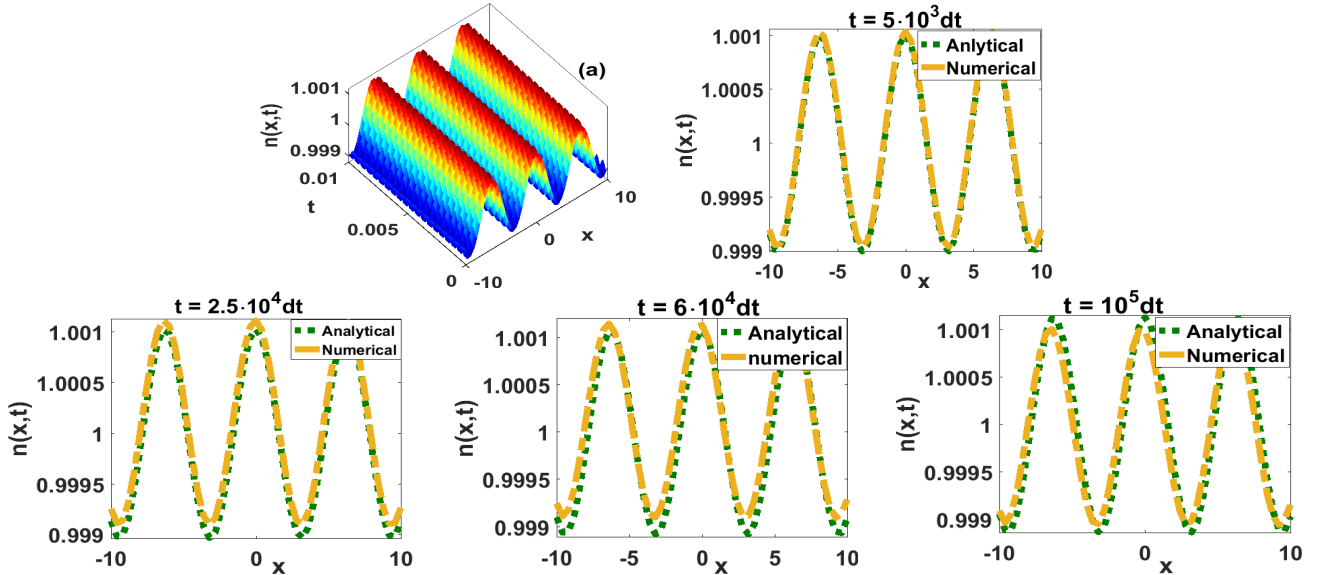


Figure 3.11: Numerical solutions of Eq. (2.14) generated through Eq. (3.40) as initial conditions in the  $(x, t)$ -plane. Parameters are taken as in Fig. 3.9. Panel (a) depict spatiotemporal evolution of the numerical solution. The other panels compare with great agreement numerical and analytical solutions at different times.

times are recorded. The initial condition for cellular density propagates in a stable fashion way without experiencing disintegration and remains very close to its analytical counterpart taken at the precise

time. Therefore, the model Eqs. (2.14) describing cellular invasion and that takes into consideration mechanical events like traction, adhesion, and viscous forces may be used as a predictive tool to deeply assess the evolution of waves rising during invasion within biological tissues. Though the reference state remains the dominant position, cells are constantly subject to small and non-null external factors that may contribute to their transport during the invasion. Generally speaking, cells placed in soft biological tissues are submitted to non vanishing physical factors such as viscous, convective, traction and attachment forces that have great impacts upon their displacement. Numerical simulations carried here to confirm that in a system where these parameters are accounted for, one may still observe small fluctuations around the reference accompanied by collections of cells moving towards a targeted domain. To the best of our knowledge, those results have not yet been found in previous theoretical or experimental works. We expect our results may trigger future experimental researches.

## 3.5 Nonlinear breathing chemotactic patterns in fluids

### 3.5.1 The linear analysis revisited

We perform the linear stability analysis of Eqs. (2.19). Initially, we consider homogeneous distributions of bacteria and chemoattractant about the reference quantities  $n_0$  and  $c_0$  in a medium undergoing a uniform flow at speed  $\mathbf{u}_0$ .  $n(\mathbf{r}, t) = n_0 + \varepsilon n_1(\mathbf{r}, t)$ ,  $c(\mathbf{r}, t) = c_0 + \varepsilon c_1(\mathbf{r}, t)$  and  $\mathbf{u}(\mathbf{r}, t) = \mathbf{u}_0 + \varepsilon \mathbf{u}_1(\mathbf{r}, t)$ , with  $\mathbf{r} = (x, y)^T$ . The uniform velocity  $\mathbf{u}_0$  is generated by the proportion  $\mu_0$  of cells under the direct influence of the gravitational forces, hence  $\mathbf{u}_0 = -\mu_0 \gamma_0 n_0 \mathbf{e}_y$ . We perform linear stability of the model Eqs. (2.19) in response to a perturbation of the form  $(n_1, c_1, \mathbf{u}_1) \propto e^{i\mathbf{k}\cdot\mathbf{r} - \lambda t} + c.c$  with  $\mathbf{k} = (k_x, k_y)^T$  the 2D wave vector and *c.c* stands for the complex conjugate.  $\lambda = \lambda_r + i\lambda_i$  is a complex parameter whose imaginary part  $\lambda_i$  stands for the wave frequency and its real part  $\lambda_r$  represents the growth rate from which stability properties must be deduced. Accordingly, if  $\lambda_r < 0$  the plane wave amplitude experiences an exponential growth as time evolves and may lead to unbounded solutions as instability signature. The other case of interest which happens when  $\lambda_r > 0$  indicates an amplitude decay, hence stable patterns. In the  $(k_x, k_y)$ -plane, the above ansatz leads to the hydrodynamic velocity

$$\mathbf{u}_1(\mathbf{k}, t) = \frac{i\mathbf{k}}{1+\nu k^2} \left[ \chi_0 n_0 \chi_1 c_1 - n_1 \left( \frac{P_e}{(1+n_0)^2} + \frac{i\gamma_0(\nu-1)\mathbf{k}\cdot\mathbf{e}_y}{1+k^2} \right) \right] - \frac{\mu_0 \gamma_0 n_1}{1+k^2} \mathbf{e}_y, \quad (3.41)$$

which extends the one previously derived by Vijay [70]. The last term of Eq. (3.41) indicates that the proportion of cells carried through gravity produces a velocity field of its own that superimposes itself to the flow created by diffusing and non-diffusing species of the medium. Eq. (3.41) is inserted into the linearized form of Eq. (2.19a) and Eq. (2.19b), hence the linear dispersion relation

$$\left[ \lambda - \alpha k^2 - \beta n_0 - \frac{\chi_1 c_0 k^2}{1 + \nu k^2} + i \mu_0 \gamma_0 n_0 \mathbf{k} \cdot \mathbf{e}_y \right] \left[ \lambda - k^2 - \frac{k^2 n_0 P_e}{(1 + n_0)^2 (1 + \nu k^2)} + i \mu_0 \gamma_0 \left( n_0 - \gamma + \frac{n_0}{1 + \nu k^2} \right) \mathbf{k} \cdot \mathbf{e}_y \right] - n_0 c_0 k^2 \left( \chi_0 + \frac{\chi_1}{1 + \nu k^2} \right) \left( \beta + \frac{P_e k^2}{(1 + \nu k^2)(1 + n_0)^2} - \frac{i \mu_0 \gamma_0 \mathbf{k} \cdot \mathbf{e}_y}{1 + \nu k^2} \right) = 0. \quad (3.42)$$

Using the dot product in the Cartesian coordinates system,  $\mathbf{k} \cdot \mathbf{e}_y = k_y$  and  $|\mathbf{k}| = k$ . Eq. (3.42) gives the possibility to investigate many situations amongst which the prevailing include transversal  $\mathbf{k} \cdot \mathbf{e}_y = 0$  and longitudinal  $\mathbf{k} \cdot \mathbf{e}_y \neq 0$  perturbations with respect to the y-axis. The former case is of least interest since it reduces Eq. (3.42) to an equation from which  $\lambda$  is found to possess real values only. Such an outcome enforces wave frequency to zero and the system admits a finite range of wave vectors. Under these configurations, using wave modulation in any spatial direction in Eqs. (2.19) cancels out automatically. Therefore, spatial perturbations must not deviate far from the y-axis or at least be contained in a plane within which the y-axis lies. In the case  $\mathbf{k} \cdot \mathbf{e}_y \neq 0$ , solutions of Eq. (3.42) are complex and may be written as  $\lambda = \lambda_r + i \lambda_i$ . Instability occurs by setting  $\lambda_r < 0$ , which leads to the following inequality

$$2\mu_0^2 \gamma_0^2 n_0 k_y \left( \frac{2 + \nu k^2}{1 + \nu k^2} - \frac{\gamma}{n_0} \right) + 2n_0 c_0 k^2 \left( \chi_0 + \frac{\chi_1}{1 + \nu k^2} \right) \left( \beta + \frac{P_e k^2}{(1 + n_0)^2 (1 + \nu k^2)} \right) - k^2 \left( 1 + \frac{P_e n_0}{(1 + n_0)^2 (1 + \nu k^2)} \right) \left( \beta n_0 + \alpha k^2 + \frac{\chi_1 c_0 k^2}{1 + \nu k^2} \right) > 0 \quad (3.43)$$

that stands for the condition at the onset of the emergence of unstable patterns. Figs. 3.12 display the growth rate  $\lambda_r$  in the  $(k_x, k_y)$ -plane. Different configurations determined by frictions, the number of cells vertically transported, and cellular density reference are considered. As observed, the instability presents different patterns and magnitudes, letting us think that the latter deeply affects the bulk system. The right and left panels show that for sufficiently high values of  $k_x$ , the instability domain is localized along the y-axis, while the middle panels reveal that instability is localized along both axes of the frame. In experimental situations, this also means that the experimenter has the potential of controlling how and the direction of any instability that might arise in the system. Moreover, Eq. (2.19) indicates that chemotaxis, viscosity, traction, friction, and the proportion of cells vertically transported have a great impact on the stability of plane wave solutions of Eqs. (2.19). In this sense, Eq. (3.43) extends the stability criterium derived and discussed in [75]. We can therefore afford to assume that each of the above mentioned parameters may be a source of instability in Eqs. (2.19). We display in Fig. 3.13 the effects of friction, the proportion of cells vertically transported and the traction force forces on the stability/instability domains. Investigating the effects of parameters of interest namely, friction (left panels of Fig. 3.13), gravity (middle panels of Fig. 3.13), and traction (right panels of Fig. 3.13) reveals how the instability domains vary. In the first step, the observations are quite similar in either the x- or the y-direction. It is broadly observed that instability domains

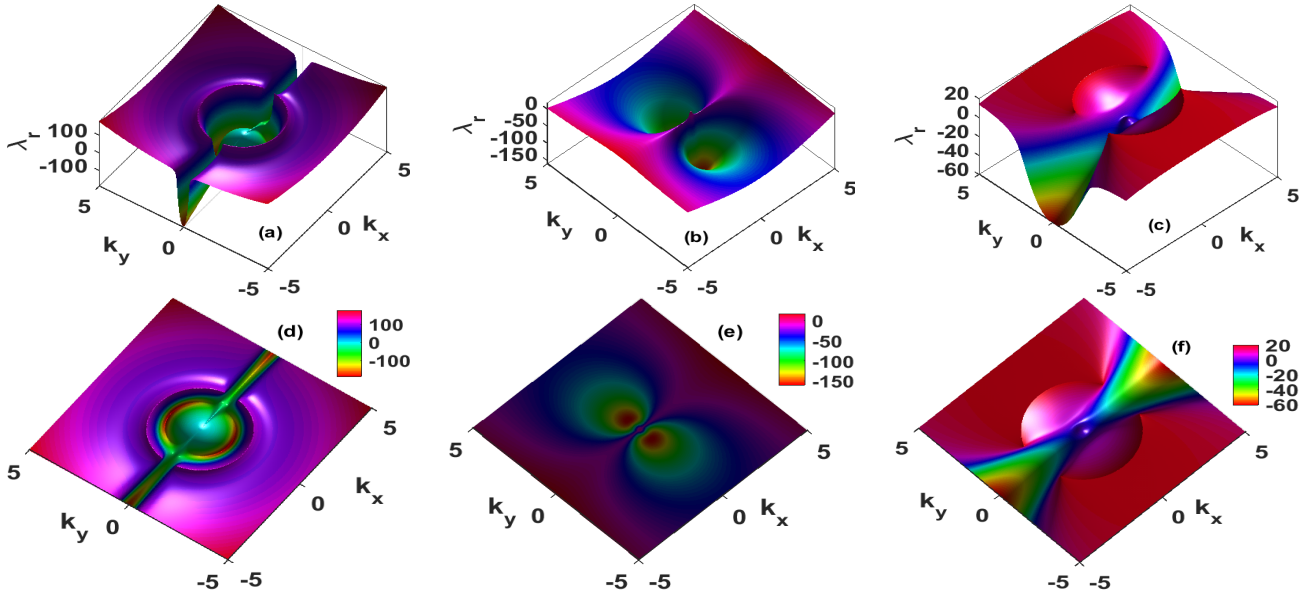


Figure 3.12: Growth rate of the linear stability for parameters  $\alpha = 1, \beta = 10, \gamma_0 = 10^3, \chi_0 = 10, \nu = 4, P_e = 1, c_0 = 1$ . Left panels,  $\gamma = 1, \mu_0 = 1, n_0 = 10$ . Middle panels  $\gamma = 10^{-2}, \mu_0 = 1, n_0 = 1$  and right panels  $\gamma = 1, \mu_0 = 5 \cdot 10^{-2}, n_0 = 1$ .

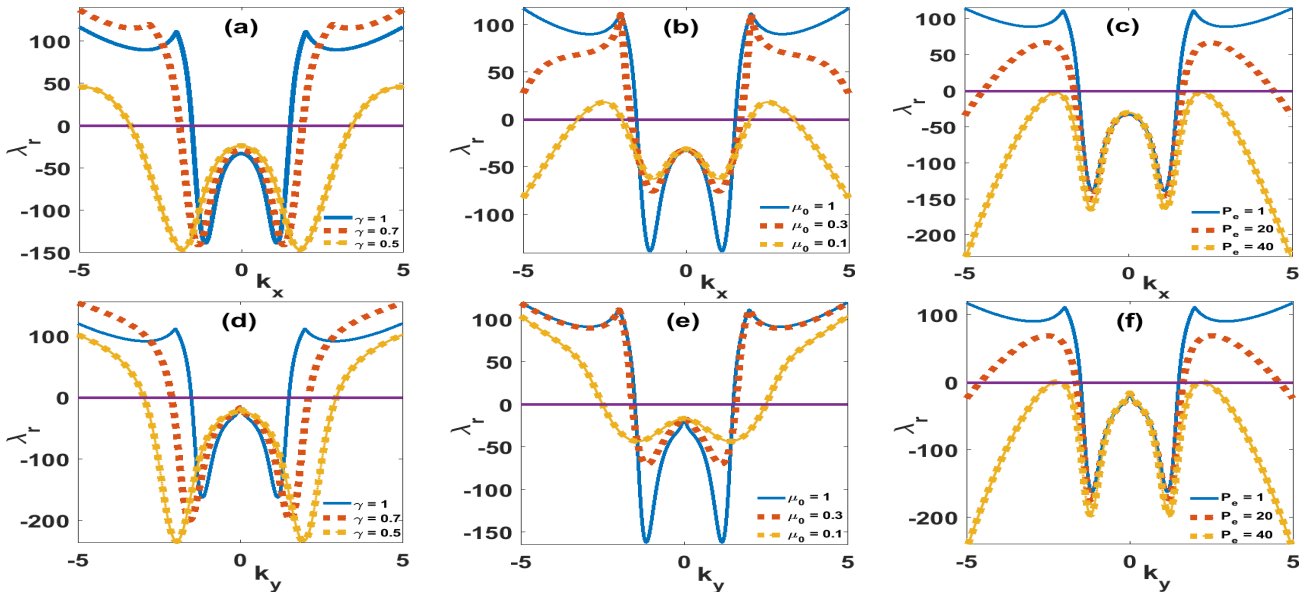


Figure 3.13: Influence of friction (left), gravity (middle) and traction (right) on stability domains. The magnitudes and the length of the instability domain increase when friction (a), gravity effects (b) decrease, while traction increases (c). Parameters taken as in Fig. 3.12

increase when friction and the number of cells vertically carried decrease, while the traction increases. This implies that for our system to generate stable and coherent patterns traction forces must be able to compensate the effects of friction and gravity forces, hence setting into evidence competitive dynamics in our system. As friction, traction, and proportion vertically carried depend on the medium properties, unstable patterns rise due to an energy imbalance, implying that the energy carried by the propagating plane wave may dissipate and entail some changes in the spatial reorganization of cells.

### 3.5.2 Model reduction through the application the reductive perturbation method

The above performed linear theory presents some limitations when it comes to fully investigate some physical aspects, in the sense the nonlinearity embedded in those systems is not qualitatively and quantitatively assessed. Eq. (2.19) in counterpart is the seat of highly dispersive and nonlinear diffusive events, that the dispersion relation Eq. (3.42) may not be sufficient to characterize the whole dynamic of the system. The fact that solutions of Eq. (3.42) reveal that the model Eqs. (2.19) is characteristic of absorbing hence the need to figure out the contribution of nonlinearity in the model Eqs. (2.19). Assuming that wave packets change slowly in the laboratory frame, it is amenable to think that their effects might become more vivid in the wave packets frame. Thus the introduction of slow spatiotemporal variables  $\xi = \epsilon(x - V_x t)$ ,  $\eta = \epsilon(y - V_y t)$ ,  $\tau = \epsilon^2 t$ . The dependent variables  $n$ ,  $c$ ,  $u$ , and  $v$  are expanded around their respective reference states as

$$\begin{aligned} n &= n_0 + \sum_{j=1}^{\infty} \epsilon^j \sum_{l=-j}^j n_l^{(j)}(\xi, \eta, \tau) A^l(x, y, t), \\ c &= c_0 + \sum_{j=1}^{\infty} \epsilon^j \sum_{l=-j}^j C_l^{(j)}(\xi, \eta, \tau) A^l(x, y, t), \\ \mathbf{u} &= \mathbf{u}_0 + \sum_{j=1}^{\infty} \epsilon^j \sum_{l=-j}^j \mathbf{u}_l^{(j)}(\xi, \eta, \tau) A^l(x, y, t). \end{aligned} \quad (3.44)$$

The finite sums Eq. (3.46) contain all the overtones  $A^l(x, y, t) = \exp[i l(k_x x + k_y y - \omega t)]$  up to order  $j$ .  $k_x$  and  $k_y$  are the wave vectors of the modulation along the respective x and y-directions.  $\omega = \omega_r + i\omega_i$  where the real part  $\omega_r$  stands for the wave frequency, while the imaginary part,  $\omega_i$  can be understood as the growth factor as discussed in the linear stability section. Thus the parameters  $V_x = V_{x_r} + iV_{x_i}$  and  $V_y = V_{y_r} + iV_{y_i}$  are the complex components of group velocities along the x- and y-axes, respectively. Eqs. (2.19) are recursively solved at each order of  $\epsilon$  by the injection of solutions Eqs. (3.46). The existence of nontrivial solutions at the first and the second orders of  $\epsilon$  leads to the dispersion relation Eq. (B.2) and the group velocities  $V_x, V_y$  Eqs. (B.5), respectively.

Limiting ourselves to wave vector ranges where  $\omega_r > 0$ , group velocities  $V_{x_r}$  and  $V_{y_r}$  in x, y-axes are presented in Fig. 3.14 Along the x-axis (top panels),  $V_{x_r}$  changes sign several times, meaning that

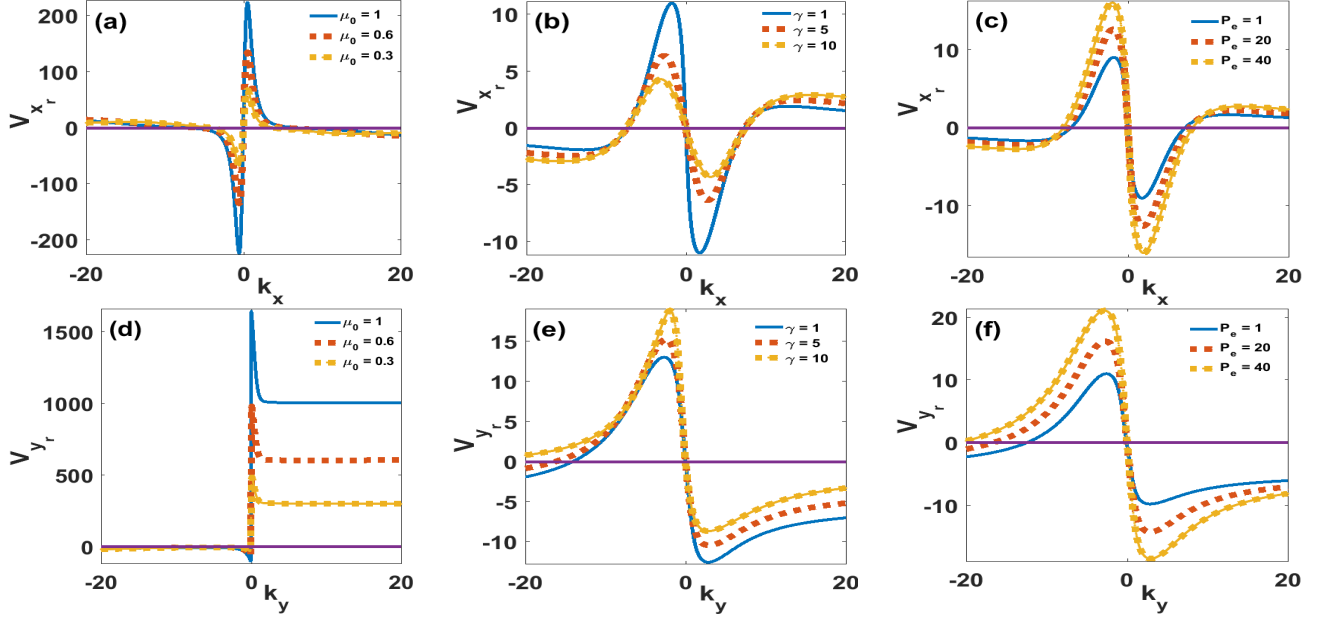


Figure 3.14: Influences of traction, friction and amount of cells carried vertically on group velocities  $V_{x_r}$  and  $V_{y_r}$ .  $k_y = 0.9$  (Top panels),  $k_x = 0.9$  (bottom panels), parameters taken as in Fig. 1(a).

the nonlinear excitation propagation direction changes as well. The asymmetry of the profiles permits us to limit our observations on the positive side of the frames. As the number of cells transported in the y-axis increases (a), the magnitude as well as the wave vector domains within which  $V_{x_r}$  is positive increase. In other words, the higher the effects of gravity, the more energetic the wave becomes, and its direction propagation is expected not to be reversed or shifted. Panels (b) and (c), show that the magnitude of  $V_{x_r}$  decreases when friction increases (b) or when traction decreases (c). However the  $V_{x_r} < 0$  at relatively long wave vector  $k_x$ , a situation that is in contradiction with observations of panel (a). The situation described along the x-axis is quite very different from the results derived by analyzing the situation along the y-axis. It globally comes out that the group velocity  $V_{y_r}$  along the y-axis does not change sign much. In panel (d) for example, increasing gravity effects increases the peak of  $V_{y_r}$ , and the latter becomes quasi constant. The panels (e) and (f) on the other hand show that  $V_{y_r} < 0$ . The above-described observations may be summarized as follows: the wave vector ranges within which the group velocity carries higher energy are localized. This in other words means the energy our nonlinear excitations may dissipate in each spatial direction may be quantified with precision. In fluids, for example, this result is of high importance in the sense it translates the fact that nonlinear excitations may be used to strengthen the emergence and propagation of coherent patterns even when the fluid is the seat of an unstable dynamic.

Then, continuing the resolution under the conditions Eq. (B.2) and Eqs. (B.5), the third order of



$\varepsilon$  yields the reduced model (The reader is referred to Appendix B for the full derivation)

$$i \frac{\partial n_1^{(1)}}{\partial \tau} + P_\xi \frac{\partial^2 n_1^{(1)}}{\partial \xi^2} + P_\eta \frac{\partial^2 n_1^{(1)}}{\partial \eta^2} + P_{\xi\eta} \frac{\partial^2 n_1^{(1)}}{\partial \xi \partial \eta} + Q_1 |n_1^{(1)}|^2 n_1^{(1)} + Q_0 n_1^{(1)} n_0^{(2)} = 0, \quad (3.45a)$$

$$\sigma_1 \frac{\partial^2 n_0^{(2)}}{\partial \xi^2} + \sigma_2 \frac{\partial^2 n_0^{(2)}}{\partial \eta^2} = \sigma_3 \frac{\partial^2 |n_1^{(1)}|^2}{\partial \xi^2} + \sigma_2 \frac{\partial^2 |n_1^{(1)}|^2}{\partial \eta^2}, \quad (3.45b)$$

which stands for a modified the Davey-Stewartson equation with complex coefficients. Eqs. (3.45) describes the spatiotemporal transport of active particles in fluids by weakly perturbed modulated wave packets propagating in a two-dimensional setting.  $P_\xi, P_\eta$  are the dispersion coefficients along the  $\xi$  and  $\eta$  axes respectively and  $P_{\xi\eta}$  emanates from the contribution of the cross-dispersion along  $\xi$  and  $\eta$  directions.  $Q_0$  and  $Q_1$  measure the nonlinear response of the medium to modulated envelope excitations. Eqs. (3.45) were initially derived to study the stability of surface waves in fluid systems with finite depth [52]. Though it is usually regarded as the  $(2 + 1)$ -dimensional Schroedinger equation, it has been associated with the propagation of stable coherent modes in plasma, photonics, and water waves systems [51, 52, 91, 92, 53]. In a  $(1 + 1)$ -dimensional setting, the Davey-Stewartson model given by Eqs. (3.45) reduces the cubic complex Ginzburg-Landau equation which is an integrable equation. We, therefore, suspect the above-presented  $(2 + 1)$ -dimensional model to be the seat of interesting dynamical behaviors that we intend to investigate through analytical techniques. For sake of simplicity, all the complex parameters in Eqs. (3.45) to be in the form  $\zeta = \zeta_r + i\zeta_i$ .

### 3.5.3 Analytical solutions and dynamical behaviors of bacterial densities in the chemotaxis-fluidss model Eqs. (5)

We introduce new variables  $Z = \frac{K\xi + L\eta}{z_0}, T = \frac{P\tau}{\epsilon_0 z_0^2}, n_1^{(1)}(\xi, \eta, \tau) = \sqrt{\frac{\epsilon_1 P}{Q z_0^2 \epsilon_0}} \psi(Z, T)$ .  $L, z_0, \epsilon_0$  and  $\epsilon_1$  are arbitrary real constants. Parameters  $L, P$ , and  $Q$  are given by

$$Q = Q_{1r} - \frac{Q_{0r} Q_{1i}}{Q_{0i}}, \quad K^2 = -\frac{\sigma_2 Q_{1i} + \sigma_4 Q_{0i}}{\sigma_1 Q_{1i} + \sigma_3 Q_{0i}} L^2,$$

$$P = \left[ P_{\eta r} - P_{\xi r} \frac{\sigma_2 Q_{1i} + \sigma_4 Q_{0i}}{\sigma_1 Q_{1i} + \sigma_3 Q_{0i}} + P_{\xi \eta r} \sqrt{-\frac{\sigma_2 Q_{1i} + \sigma_4 Q_{0i}}{\sigma_1 Q_{1i} + \sigma_3 Q_{0i}}} \right] L^2.$$

Then, Eqs. (3.47) are reduced to the traditional nonlinear Schroedinger equation

$$i \frac{\partial \psi}{\partial T} + \epsilon_0 \frac{\partial^2 \psi}{\partial Z^2} + \epsilon_1 \psi |\psi|^2 = 0. \quad (3.46)$$

For  $\epsilon_0 = \frac{1}{2}, \epsilon_1 = 1$  and following [93, 94, 95, 96], Eq. (3.46) admits first and second order rational solutions, respectively given by

$$\psi(Z, T) = \left[ 1 - \frac{4(1 + 2iT)}{1 + 4T^2 + 2Z^2} \right] e^{iT} = \psi_1(Z, T), \quad (3.47)$$

$$\begin{aligned} \psi(Z, T) &= \left[ 1 + \frac{(Z^2 + T^2 + \frac{3}{4})(Z^2 + 5T^2 + \frac{3}{4}) - \frac{3}{4} + iT \left[ T^2 - 3Z^2 + 2(Z^2 + T^2)^2 - \frac{15}{8} \right]}{\frac{1}{3}(Z^2 + T^2)^3 + \frac{1}{4}(Z^2 - 3T^2)^2 + \frac{3}{64}(1 + 12Z^2 + 44T^2)} \right] e^{iT} \\ &= \psi_2(Z, T). \end{aligned} \quad (3.48)$$

Applying all the transformations considered up until now, the bacterial density reads

$$n(x, y, t) = n_0 + \frac{\varepsilon}{z_0} \sqrt{\frac{\varepsilon_1 P}{Q \varepsilon_0}} \text{Real} \left[ \psi \left( \frac{\varepsilon}{z_0} (Kx + Ly - (KV_x + LV_y)t), \frac{2P\varepsilon^2}{z_0^2} t \right) e^{i(k_x x + k_y y - \omega t)} \right] \quad (3.49)$$

Besides the parameters of the original model that are known,  $L$ , and  $z_0$  appear to be the only free parameters of the solution Eq. (3.49). While  $\varepsilon$  and  $L$  impact the amplitudes, thickness, and velocity of the wave,  $z_0$  is expected to influence the wave thickness and its velocity. Furthermore, the finiteness of the solution Eq. (3.49) requires that  $Q \neq 0$ . In other words, the nonlinearity brought by cubic and the crossing terms must not cancel out. Moreover, the positivity of the bacterial densities enforces that  $P \cdot Q > 0$ , a criterium governing the rise of coherent modes in the nonlinear Schroedinger equation Eq. (3.46). The latter inequality also means that competition between dispersive and nonlinear effects is compelling to generate localized structures in the model Eqs. (2.19). Hereafter, Solutions Eqs. (3.49) are used to assess spatiotemporal evolutions of bacterial density in the model Eqs. (2.19). In Fig. 3.14 are displayed the bacterial wave solutions of Eqs. (2.19) generated by plugging the rational solutions (3.47)-(3.48) into Eq. (3.49). To be precise, the top panels of Fig. 3.14 are recovered by inserting the first-order rational solutions Eq. (3.47) into Eq. (3.49). In the same way, the bottom panels of Fig. 3.15 are obtained after injecting the second-order rational solution Eq. (3.48) into Eq. (3.49). The profiles hence depicted are new ones in the sense they have not yet been obtained in chemotaxis-fluids models, to the best of our knowledge. Both first, and second-order waves have a commonality: They oscillate along the y-axis and present localized periodic breathing patterns centered at the origin along the x-direction. This says at certain positions, our solutions are simple periodic functions while at others, they periodically breathe. Though the role and the importance of breathing behaviors have not yet been reported in chemotaxis-fluids systems, we point out the fact that such behavior may explain the signal regulation, intercellular communication which is often necessary to achieve collective dynamics. The different breathing patterns portrayed in Fig. 3.14 are representative of the dependence of these solutions on system parameters. In addition to the asymmetry in their profiles, the features of these solutions are reminiscent of plume patterns recovered through numerical simulations in [68, 77] and experimental works [74]. For instance, in the left-hand panels of Fig. 3.14, it is observed

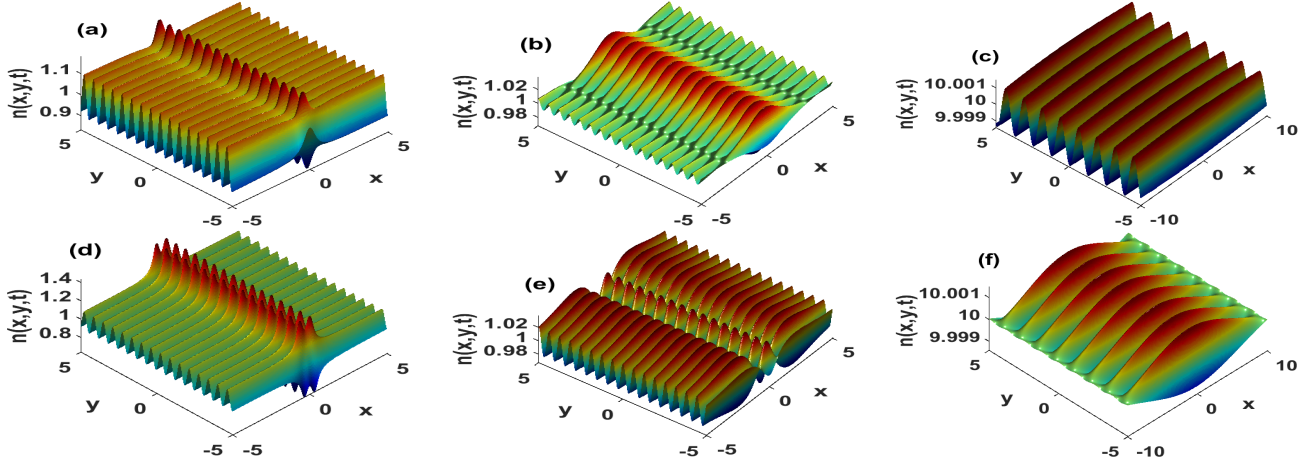


Figure 3.15: Top panels display bacterial waves profile generated by inserting the first order rational solution Eqs. (3.48) into Eq. (3.50). Bottom panels represent the bacterial profile recovered by plugging the second order rational solution Eq. (3.49) into Eq. (3.50). In top and bottom panels, solutions are displayed at the same time  $t = 5 \cdot 10^{-3}$ .  $L = 0.09, z_0 = 0.1, k_x = 0.01, k_y = 10, \varepsilon = 10^{-3}$ . Left panels  $\mu_0 = 1, \nu = 2$ . Middle panels  $\mu_0 = 0.1, \nu = 2, L = 0.009$  and right panels  $n_0 = 10, \gamma_0 = 1, \gamma = 10, \mu_0 = 0.1; Pe = 100, k_y = 5$ .

that breathers are highly localized at the position  $x = 0$ . When the parameter networks changes, the middle panels show that the first-order solutions (b) give structures with bigger volumes while the second-order rational solution (e) tends to separate the periodic from breathing profiles. By increasing the traction, and reducing the modulation wave number  $k_y$ , we obtain periodic (c) and breathing (f) profiles. The coalescence of periodic and breathing modes progressively gives rise to periodic profile in one case (c) and to breathers on the other hand (f). These results enforce that cells are continuously collected into high and low-concentration layers that are mediated by nonuniform fluid flows. These results are also indicative of how one can achieve cellular distribution in an optimized fashion way. In fact, breather carries energy during their propagation and the fact that their volumes augment implies that their thickness increase as well, an outcome that may optimize cellular redistribution across the medium. Furthermore, as the breathers increase their volumes, the sharp distribution of cells located at  $x = 0$  scatters towards the edges, a result that is consistent with numerical simulations presented in [68, 77], and experimental works of [76].

A better understanding of the dynamical behaviors of our solutions may be attained considering the individual effects system parameters have on the proposed solutions. Up until now, results presented rely on the choice  $\alpha = 1$ , which in other words means that chemoattractant and bacteria diffuse at the same rate. However, by increasing the diffusion ratio (d), the breathing behavior tends to

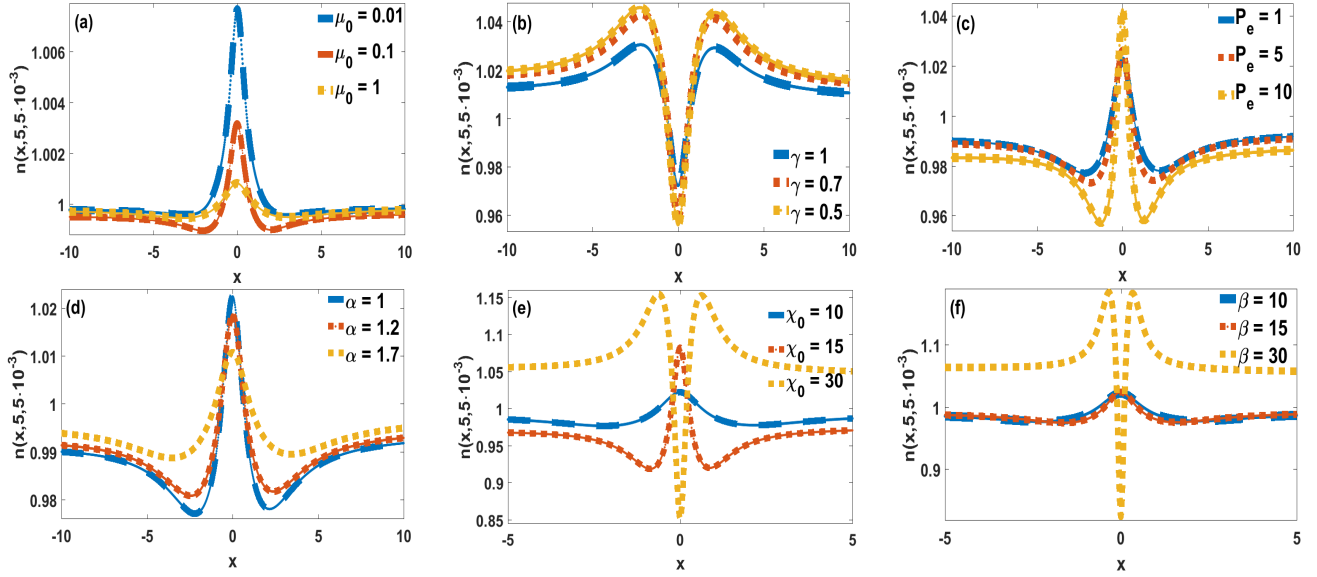


Figure 3.16: Influences of proportion of cells vertically transported (a), friction (b), traction (c), diffusion ratio (d), chemotaxis (e), and chemoattractant consumption rate (f) on the thicknesses and amplitudes of the wave. Parameters taken as in Fig. 3.14(b).

give place to a pulsatory pattern, with a consequence of the diminution of the breathing frequency, the number of bacteria carried by the wave as well as the wave thickness. In other words, when the chemoattractant diffuses faster than bacteria, the number of particles transported by the wave decreases, and their spatial distribution is also affected. The latter features are also reported when traction decreases (c), while friction (b) and the proportion of cells vertically transported (a) increase. In their study of active fluids [70], the authors showed that fast diffusing species up-regulate the stress. Our results extend these observations by stating that when one of the diffusive species is active, the density of the fast diffusing species is expected to reduce, and the characteristics of structures ensuring transport in the medium are slightly modified. On the other hand, the contribution of chemotaxis and chemoattractant consumption have more dramatic effects on the wave profiles. As these parameters increase, they incur several damages to the wave structures to the point that the latter change their profiles. We understand these sudden wave profile changes as a mechanism for shifting the primary transport mode. In addition to the fact that chemotaxis has stabilizing/destabilizing properties on the system Eqs. (2.19), its effects on our solutions are on the line with results experimentally obtained by [97], which stated that chemotactic bacteria transit towards the formation of unsteady plumes that penetrated deeply into the medium with the consequence of enhancing their transport. However, the symmetry of the wave is globally preserved, enforcing some compelling implications: Chemotaxis strength must be high enough such that cells may overcome the instabilities incurred by the medium

within which they are immersed. In other words, by controlling the chemotactic activity of cells in fluids, one can prevent and disseminate fluid instabilities.

### 3.5.4 Confirmation through direct numerical simulations

This section presents our numerical simulations, the aim being an ascertainment of the ability of the solutions proposed above to propagate in a stable fashion in the model Eqs. (2.19). Using pseudo-spectral methods, direct numerical integrations of Eqs. (2.19) on a domain of length  $l = 10$  are performed. Along each spatial direction,  $N = 1024$  points are considered and the time step is  $dt = 10^{-6}$ , and we ran simulations over the final dimensional time  $t_{fin} = 2 \cdot 10^{-2}$ . As said earlier, this time corresponds to a time  $t = 2 \cdot 10^4$  s in the real space-time frame. Our initial conditions are the analytical solutions Eqs. (3.49) taken at  $t = 0$ . Simulations are launched by perturbing the analytical solutions with small perturbations of strength 10 percent of the wave amplitude, taken at time  $t = 0$ . Panels (a), (b), (c) of Fig. 3.16 (resp. panels (d), (e), (f)) depict snapshots of bacterial

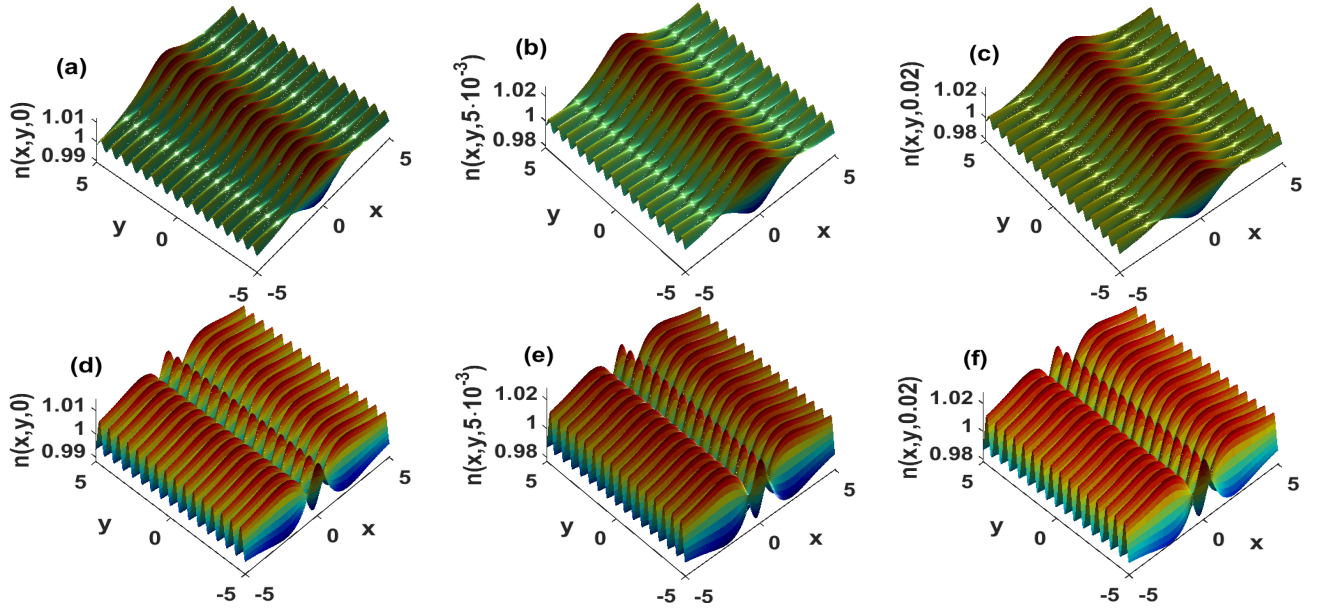


Figure 3.17: Stable numerical solutions for first (second) order bacterial wave at  $t = 0$  (a) [(d)],  $t = 5 \cdot 10^{-3}$  (b) [(e)], and  $t = 0.02$  (c) [(f)]. Parameters as in Figs. 5(b) [(f)].

densities whose analytical solutions are recovered by inserting the first (resp. second) order rational solution Eq. (3.46) (resp. Eq. (3.47)) into Eq. (3.48). Our solutions have initially been perturbed, but the results displayed in Fig. 3.16 indicate that their numerical counterpart evolves without neither collapses nor explosions. In that sense, our solutions are numerically stable and are likely to be observed in experiments. Chemotaxis-fluids systems are the seat of highly nonlinear events where

gravity, friction, viscosity, chemotaxis, and diffusion are more likely to interact in either constructive or destructive ways to produce interesting spatiotemporal behaviors. Numerical analyses performed in this section do confirm that while in the vertical line, cells fluctuate around their reference state. The density remains quasi-constant along the horizontal axis, with their distribution reaching its peak at the origin. These results are quite interesting and are new ones since two-dimensional waves modulation in chemotaxis-fluids systems has never been carried before, to the best of our knowledge. We, therefore, expect the investigations carried here to spark the light toward experimental studies of chemotaxis systems where traction, friction, viscous, and gravity forces are at play.

### 3.6 Conclusion

In this chapter, we have considered several physical considerations and construct their relative mathematical models. We start with a model where cells are immersed in a uniform flow, analytical solutions have been constructed and their existence conditions specified. We discussed the experimental feasibility of those solutions, and found that the background flow constitutes the compact support on which non-stationary traveling structures emerge. The flow also contribute to the colonization of large domains even when the chemotactic sensitivity of cells drastically decreases. Further, we considered the coupled dynamics between chemotaxis and haptotaxis. The resulting model is shown to be presenting viscoelastic properties and we identified the parameter regions where nonlinear excitations either expand or counter-propagate. It is observed that traction and adhesion have competing effects on wave amplitude and thickness. In a fluid with nonuniform flows, we derived an extended two-dimensional model for chemotaxis taking into consideration gravity, friction, and viscous forces. A linear stability showed that instability reduces when friction and gravity increase. On the other hand, traction increases the instability domains in addition to the fact that the systems remain unstable at long wave vectors in both spatial directions. In deep water, our analysis reveals that the emergence of oscillatory instability when the perturbations considered deviate from the vertical axis. In presence of transversal perturbations, the type of instability does not absolutely depend on the depth of the suspension. Finite sums of nonlinear modulated waves showed that bacterial waves are asymmetric breathing patterns interacting with periodic vertical structures. It is shown that of the wave is enhanced when bacterial diffusion, chemotaxis, friction, traction, chemoattractant consumption rate increase while the number of cells vertically transported in the system decreases. In each of our manufacturings, numerical simulations show that analytical and numerical solutions remain closed to one another, meaning that solutions constructed are stable.

---

# Conclusion and future research plans

The objective of this work was to discuss spatiotemporal behaviors of collective motion exhibited by chemotactic systems where mechanical, body and traction forces are at play. In that end, mathematical models taking these aspects have been derived. Analytical solutions of those models have been constructed and their existence conditions discussed with great details. Our investigations point that in a situation where traction forces and long-range diffusion are at play, the whole system is significantly modified. We predict the existence of a minimal chemoattractant concentration in the system, in order for waves to be generated. It is also proved that the fluid constitutes the compact support through which propagation happens, and the wave velocity depends on the flow rate of the fluid. Our study reveals that in a situation where cortical flows are taken into consideration, optimal characteristics of cells transport are observed through step and dip waves. The former carries a high number of cells while the latter ensures their fast collective displacement. Furthermore, coupling chemotaxis with mechanical actions allows us to show that traction and adhesion have competing effects on the transport of cells. In addition, we predict the existence of a threshold value of traction above which nonlinearly modulated waves are compressive. In a nonuniform fluid flow where traction, friction and body forces are simultaneously at play, we predict that non-transversal perturbations favor the emergence of oscillatory stable patterns in deep suspensions. To the best of our knowledge, the results discussed in this document are new and have not yet been obtained before. However, there still remain unanswered questions that we aim at pursuing in a near future.

- Use the kinetic theory to derive a multiscale model through which effects of rheological forces would be fully clarified.
  - Apply the Lagrangian mechanics to determine the contribution of shape changing of cells on the collective dynamic of the bulk population.
  - Study a multi-populations system to show how their interactions shape their respective evolution.
-

---

# Appendices: Derivation of the cubic complex Ginzburg-Landau Equation Eq. (3.25) and the Davey-Stewartson equation Eqs. (3.45)

## Appendix A: Derivation of the cubic complex Ginzburg-Landau Equation Eq. (3.25)

We insert the expansions Eqs. (2.19) into Eqs. (2.14) and collect resulting terms in power of  $\epsilon$ . Doing so leads to the first order harmonics

$$C_1^{(1)} = \Gamma_1 m, \quad \rho_1^{(1)} = B_1 m, \quad U_1^{(1)} = A_1 m \quad (\text{A.1})$$

where we set  $m = n_1^{(1)}$ , given that the dispersion relation

$$A_0 \omega^3 + B_0 \omega^2 + C_0 \omega + D_0 = 0. \quad (\text{A.2})$$

is satisfied. This last one depends on the parameters of the system and we can solve it for  $\omega$  as function of the wave vector  $k$ .  $A_0, B_0, C_0$ , and  $D_0$  are given by

$$\begin{aligned} A_0 &= -ik\mu N_0, & B_0 &= N_0 a_0 k \mu - ia_{01}, & C_0 &= a_{03} + a_0 a_{01} - ia_{02}, & \text{and } D_0 &= a_0 a_{02} + a_{04}, \\ K_0 &= 1 - \lambda n_0^2, & N_0 &= (1 + \lambda n_0^2)^2, & M_0 &= n_0(1 + \lambda n_0^2), & a_0 &= D_c k^2 + \beta_0 n_0 - \alpha_0, \\ a_{01} &= ik^3 \mu N_0 D_n - ik \rho_0 \tau_0 n_0 K_0 + i N_0 (s \rho_0 + k^2) - ik^2 \rho_0 \tau_0 M_0 (1 - \gamma k^2), \\ a_{02} &= D_n k^2 [k^2 \rho_0 \tau_0 M_0 (1 - \gamma k^2) - N_0 (s \rho_0 + k^2)] - \rho_0^2 \tau_0 n_0 K_0 \alpha_1 k, \\ a_{03} &= ik^3 \chi_0 n_0 c_0 (\mu N_0 \beta - \rho_0 \tau_0 K_0 k^2), & a_{04} &= \chi_0 n_0 c_0 k^2 \beta [k^2 \rho_0 \tau_0 M_0 (1 - \gamma k^2) - N_0 (s \rho_0 + k^2)]. \end{aligned}$$

Eq. (3.25) admits three complex solutions. Hereafter in the present study we discuss our results

---



for the solution of Eq. (3.25) that is

$$\omega = \frac{4\omega_2(1+i\sqrt{3}) - (1-i\sqrt{3})\omega_1^{\frac{2}{3}}}{12A_0\omega_1^{\frac{1}{3}}}, \quad \text{where} \quad \omega_2 = 3A_0C_0 - B_0^2, \quad (\text{A.3})$$

$$\omega_1 = 36A_0(B_0C_0 - 3D_0A_0^2) - 8B_0^3 + 12A_0\sqrt{27A_0D_0(3A_0D_0 - 2B_0C_0) + 12A_0C_0^3 + 3B_0^2(4D_0B_0 - C_0^2)}$$

The coefficients  $A_1$ ,  $B_1$  and  $\Gamma_1$  are given by

$$A_1 = \frac{-ik\tau_0\rho_0K_0}{N_0(ik\omega\mu - s\rho_0 - k^2) + k^2\rho_0\tau_0M_0(1 - \gamma k^2)}, \quad B_1 = -ik\rho_0A_1, \quad \Gamma_1 = \frac{-c_0(\beta + k\omega A_1)}{D_c k^2 + \beta n_0 - \alpha - i\omega}, \quad (\text{A.4})$$

We continue as at the first order of  $\epsilon$ , and obtain the second-order and constant terms as function of the first harmonics. At  $O(\epsilon^2)$ , for  $l = 0$ , we obtain

$$U_0^{(2)} = \frac{1}{\rho_0 s N_0} [ik\delta_0(B_1 - B_1^*) - 4\lambda n_0(1 + \lambda n_0^2)(s\rho_0 - k^2)(A_1 + A_1^*) - N_0 s(A_1 B_1^* + B_1 A_1^*)] |m|^2, \\ \delta_0 = \tau_0(1 - \gamma k^2)(1 + 3\lambda n_0^2 K_0 - K_0). \quad (\text{A.5})$$

For sake of simplicity, we rewrite  $U_0^{(2)} = A|m|^2$ . For  $l = 1$ , we have the

$$C_1^{(2)} = \Gamma_1 m + \Gamma_{21} \frac{\partial m}{\partial \xi}, \quad \rho_1^{(2)} = B_1 m + B_{21} \frac{\partial m}{\partial \xi}, \quad U_1^{(2)} = A_1 m + A_{21} \frac{\partial m}{\partial \xi}, \quad (\text{A.6})$$

with

$$A_{21} = \frac{\omega\tau_0 M_0(1 - \gamma k^2)(-B_1 + ik\rho_0 A_1) - \omega\tau_0 K_0 - 2i\omega k N_0 A_1(1 - i\omega\mu)}{\omega N_0(ik\omega\mu - s\rho_0 - k^2) + \omega k^2 \rho_0 \tau_0 M_0(1 - \gamma k^2)} \\ + \frac{V_g[-\mu\omega k^2 N_0 A_1 + k\tau_0 M_0(1 - \gamma k^2)(B_1 + ik\rho_0 A_1)]}{\omega N_0(ik\omega\mu - s\rho_0 - k^2) + \omega k^2 \rho_0 \tau_0 M_0(1 - \gamma k^2)}, \\ B_{21} = -\left[\rho_0 A_1 + ik\rho_0 A_{21} + \frac{V_g}{i\omega}(B_1 + ik\rho_0 A_1)\right], \\ \Gamma_{21} = \frac{V_g(\Gamma_1 - ikc_0 A_1) + c_0 k\omega A_{21} - i\omega c_0 A_1 + 2ikD_c \Gamma_1}{D_c k^2 + \beta n_0 - \alpha - i\omega}, \quad (\text{A.7})$$

The group velocity  $V_g$  takes the form:

$$V_g = \frac{\delta_1 - \delta_3}{\delta_4 - \delta_2}, \quad \delta_1 = \frac{c_0 k\omega\beta_1 - i\omega c_0 A_1 + 2ikD_c \Gamma_1}{D_c k^2 + \beta n_0 - \alpha - i\omega}, \quad \delta_2 = \frac{\Gamma_1 - ikc_0 A_1 + c_0 k\omega\beta_2}{D_c k^2 + \beta n_0 - \alpha - i\omega}, \\ \delta_3 = -\frac{2ik(D_n - \chi_0 n_0 \Gamma_1 - n_0 \alpha_1 B_1) + n_0 A_1(i\omega - \alpha_1 \rho_0 k^2) - n_0 k\beta_1(\omega + i\alpha_1 \rho_0)}{\chi_0 n_0 k^2}, \\ \delta_4 = -\frac{\omega[1 + ikn_0 A_1 - n_0 k\beta_2(\omega + i\alpha_1 \rho_0)] + i\alpha_1 n_0 k^2(B_1 + ik\rho_0 A_1)}{\chi_0 n_0 \omega k^2}, \\ \beta_1 = \frac{\tau_0 M_0(1 - \gamma k^2)(-B_1 + i\rho_0 A_1) - \tau_0 K_0 - ikN_0 A_1(1 - i\omega\mu)}{N_0(ik\omega\mu - s\rho_0 - k^2) + k^2 \rho_0 \tau_0 M_0(1 - \gamma k^2)}, \\ \beta_2 = \frac{-\mu\omega k^2 N_0 A_1 + k\tau_0 M_0(1 - \gamma k^2)(B_1 + ik\rho_0 A_1)}{\omega N_0(ik\omega\mu - s\rho_0 - k^2) + \omega k^2 \rho_0 \tau_0 M_0(1 - \gamma k^2)}. \quad (\text{A.8})$$

Further, At  $l = 2$ , we have to solve a system of the form

$$\begin{aligned} a_{11}n_2^{(2)} + b_{11}C_2^{(2)} + c_{11}U_2^{(2)} - e_{11}m^2 &= 0 \\ a_{22}n_2^{(2)} + b_{22}C_2^{(2)} + c_{22}U_2^{(2)} - e_{22}m^2 &= 0 \\ a_{33}n_2^{(2)} + c_{33}U_2^{(2)} - e_{33}m^2 &= 0, \end{aligned} \quad (\text{A.9})$$

in order to determine  $n_2^{(2)}, C_2^{(2)}, U_2^{(2)}$ . The  $(a, b, c, e)_{jj}$  coefficients are:

$$\begin{aligned} a_{11} &= 4D_n k^2 - 2i\omega, & b_{11} &= -4\chi_0 n_0 k^2, & c_{11} &= 4n_0 k(\omega + 2ik\rho_0\alpha_1), \\ e_{11} &= 2\chi_0 k^2 \Gamma_1 + 2\alpha_1 k^2 B_1 - 2\omega k A_1 - 4i\alpha_1 n_0 k^3 A_1 B_1, \\ a_{22} &= \beta c_0, & b_{22} &= 4D_c k^2 + \beta n_0 - \alpha - 2i\omega, & c_{22} &= 4c_0 k\omega, & e_{22} &= -\Gamma_1(\beta + 2\omega k A_1), \\ a_{33} &= 2ik\tau_0 \rho_0 K_0, & c_{33} &= N_0(8ik\omega\mu - s\rho_0 - k^2) + 4k^2\tau_0 M_0 \rho_0(1 - \gamma k^2), \\ e_{33} &= N_0 s A_1 B_1 + 2ik\tau_0 \rho_0 n_0 \lambda + 4\lambda n_0 A_1(1 + \lambda n_0^2)(k^2 - s\rho_0 - i\omega k\mu) \\ &\quad - ik\tau_0 B_1(1 - \gamma k^2)(K_0 - 1 + 3\lambda n_0^2) - 2k^2\tau_0 M_0 A_1 B_1(1 - \gamma k^2). \end{aligned}$$

Solutions of Eq. (A.9) can be written as

$$\begin{aligned} n_2^{(2)} &= D_2 m^2, & C_2^{(2)} &= \Gamma_2 m^2, & \rho_2^{(2)} &= B_2 m^2, & U_2^{(2)} &= A_2 m^2, \\ A_2 &= \frac{a_{11}b_{22}e_{33} - a_{22}b_{11}e_{33} + a_{33}b_{11}e_{22} - a_{33}b_{22}e_{11}}{a_{11}b_{22}c_{33} - a_{22}b_{11}c_{33} + a_{33}b_{11}c_{22} - a_{33}b_{22}c_{11}}, & B_2 &= -ik(A_1 B_1 + 2\rho_0 A_2), \\ D_2 &= \frac{b_{11}c_{22}e_{33} - b_{11}c_{33}e_{22} - b_{22}c_{11}e_{33} + b_{22}c_{33}e_{11}}{a_{11}b_{22}c_{33} - a_{22}b_{11}c_{33} + a_{33}b_{11}c_{22} - a_{33}b_{22}c_{11}}, \\ \Gamma_2 &= \frac{(a_{11}c_{22} - a_{22}c_{11})e_{33} + (-a_{11}c_{33} + a_{33}c_{11})e_{22} + (a_{22}c_{33} - a_{33}c_{22})e_{11}}{a_{11}b_{22}c_{33} - a_{22}b_{11}c_{33} + a_{33}b_{11}c_{22} - a_{33}b_{22}c_{11}} \end{aligned} \quad (\text{A.10})$$

Moreover, expressions for the zeroth harmonic have not been completely determined within the second order. We therefore consider the third-order equations. The  $(l = 0)$ -components of the third order are given by:

$$\begin{aligned} V_g \frac{\partial n_0^{(2)}}{\partial \xi} &= [i\omega(A_1^* - A_1 + ik\chi_0(\Gamma_1 - \Gamma_1^*) + ik\alpha_1(B_1 - B_1^*))] \frac{\partial |m|^2}{\partial \xi}, \\ V_g \frac{\partial \rho_0^{(2)}}{\partial \xi} &= i\omega(B_1 A_1^* - A_1 B_1^*) \frac{\partial |m|^2}{\partial \xi}. \end{aligned} \quad (\text{A.11})$$

After integration, Eq. (A.11) becomes

$$\begin{aligned} n_0^{(2)} &= D|m|^2 + h(\tau), & \rho_0^{(2)} &= B|m|^2 + g(\tau), & C_0^{(2)} &= \Gamma|m|^2 - \frac{\beta c_0 h(\tau)}{\beta n_0 - \alpha}, \\ D &= \frac{i\omega(A_1^* - A_1 + ik\chi_0(\Gamma_1 - \Gamma_1^*) + ik\alpha_1(B_1 - B_1^*))}{V_g}, & B &= \frac{i\omega}{V_g}(B_1 A_1^* - A_1 B_1^*), & \Gamma &= -\frac{\beta(c_0 D + \Gamma_1 + \Gamma_1^*)}{\beta n_0 - \alpha} \end{aligned} \quad (\text{A.12})$$

$h(\tau)$  and  $g(\tau)$  being two arbitrary real functions of the slow time variable  $\tau$ . The  $(l = 1)$ -components yield the system

$$\begin{aligned} a_1 n_1^{(3)} + b_1 C_1^{(3)} + c_1 \rho_1^{(3)} + d_1 U_1^{(3)} - e_1 &= 0, & a_2 n_1^{(3)} + b_2 C_1^{(3)} + c_2 \rho_1^{(3)} + d_2 U_1^{(3)} - e_2 &= 0, \\ c_3 \rho_1^{(3)} + d_3 U_1^{(3)} - e_3 &= 0, & a_4 n_1^{(3)} + c_4 \rho_1^{(3)} + d_4 U_1^{(3)} - e_4 &= 0. \end{aligned} \quad (\text{A.13})$$

The coefficients  $(a, b, c, d)_j$  of Eq. (A.13) are

$$\begin{aligned}
a_1 &= D_n k^2 - i\omega, & b_1 &= -\chi_0 n_0 k^2, & c_1 &= -\alpha_1 n_0 k^2, & d_1 &= n_0 k \omega, & a_2 &= \beta c_0, \\
b_2 &= D_c k^2 + \beta n_0 - \alpha - i\omega, & d_2 &= c_0 k \omega, & c_3 &= -i\omega, & d_3 &= \rho_0 k \omega, \\
a_4 &= ik\tau_0 \rho_0 K_0, & c_4 &= ik\tau_0 M_0 (1 - \gamma k^2), & d_4 &= N_0 (ik\omega\mu - s\rho_0 - k^2), \\
p_1 &= -(1 + ikn_0 A_1), & p_2 &= -(\Gamma_1 + ikc_0 A_1), & p_3 &= -(B_1 + ik\rho_0 A_1), & p_4 &= N_0 \mu k^2 A_1; \\
q_1 &= D_n - \chi_0 n_0 \Gamma_1 + n_0 A_1 V_g - n_0 \alpha_1 B_1 + in_0 A_{21} (\omega + kV_g) - 2ik\chi_0 n_0 \Gamma_{21} - 2ikn_0 \alpha_1 B_{21}, \\
q_2 &= D_c \Gamma_1 + c_0 V_g A_1 + ic_0 A_{21} (\omega + kV_g) + \Gamma_{21} (V_g + 2ikD_c), \\
q_3 &= \rho_0 V_g A_1 + i\rho_0 A_{21} (\omega + kV_g) + V_g B_{21}, \\
q_4 &= -N_0 A_{21} (\mu k^2 V_g + 2\mu k \omega + 2ik) - \tau_0 M_0 B_{21} (1 - \gamma k^2) - N_0 A_1 (1 - i\omega\mu) - 3ik\tau_0 M_0 \gamma B_{11}; \\
R_1 &= \chi_0 k^2 \Gamma_1 + \alpha_1 k^2 B_1 - k\omega A_1, & R_2 &= \frac{\beta c_0 (\beta + \omega k A_1)}{\beta n_0 - \alpha} - \beta \Gamma_1, & R_3 &= -\omega k A_1; \\
R_{41} &= (N_0 s A_1 - ik\tau_0 K_0), \\
R_{42} &= 2ik\tau_0 \rho_0 n_0 \lambda - ik\tau_0 B_1 (1 - \gamma k^2) (1 + 3\lambda n_0^2) - 4n_0 A_1 \lambda (1 + \lambda n_0^2) (i\omega\mu - k^2 - s\rho_0); \\
S_1 &= \chi_0 k^2 (2\Gamma_2 - D_2 \Gamma_1^* + D\Gamma_1) + \alpha_1 k^2 (2B_2 - D_2 B_1^* + DB_1) - \omega k (2A_2 - D_2 A_1^* + DA_1), \\
S_2 &= \omega k (\Gamma_2 A_1^* - 2A_2 \Gamma_1^* - \Gamma A_1) - \beta (D_2 \Gamma_1^* + \Gamma_2 + \Gamma + D\Gamma_1), & S_3 &= \omega k (B_1 A_1^* - 2A_2 B_1^* - BA_1), \\
S_4 &= D [2ik\tau_0 n_0 \rho_0 \lambda - ik\tau_0 B_1 (1 - \gamma k^2) (1 + 3\lambda n_0^2) - 4n_0 \lambda A_1 (1 + \lambda n_0^2) (i\omega\mu - s\rho_0 - k^2)] \\
&+ DB (ik\tau_0 K_0 - N_0 s A_1) - ik\tau_0 (1 - \gamma k^2) [n_0 \lambda (6B_1 - 5B_1^*) - D_2 B_1^* (1 + 3\lambda n_0 - 2K_0)] \\
&+ ik\tau_0 B_2 (1 - 4\gamma k^2) (K_0 - 2 - 6\lambda n_0^2) + N_0 s (A_2 B_1^* + B_2 A_1^*) + ik\tau_0 \rho_0 \lambda (1 + 2n_0 D_2) \\
&+ 4\lambda n_0 (1 + \lambda n_0^2) [ik\mu (D_2 - 8\mu\omega B_2) + D_2 A_1^* (k^2 + s\rho_0) + s (B_1 + \rho_0 A_2 + A_1 B_1^* + B_1 A_1^*) + 4k^2 A_2]; \\
T_1 &= V_g + 2ik (D_n - \chi_0 n_0 \Gamma_1 - n_0 \alpha_1 B_1) + in_0 A_1 (\omega + kV_g), & T_2 &= \Gamma_1 (V_g + 2ikD_c) + ic_0 A_1 (\omega + kV_g), \\
T_3 &= B_1 V_g + i\rho_0 A_1 (\omega + kV_g), & T_4 &= -[\tau_0 K_0 \rho_0 + \tau_0 M_0 B_1 (1 - \gamma k^2) - N_0 A_{21} (\mu k^2 V_g + 2\mu k \omega + 2i\omega)], \\
e_1 &= p_1 \frac{\partial m}{\partial \tau} + q_1 \frac{\partial^2 m}{\partial \xi^2} + R_1 h(\tau) m + S_1 |m|^2 m + T_1 \frac{\partial n_1^{(2)}}{\partial \xi}, \\
e_2 &= p_2 \frac{\partial m}{\partial \tau} + q_2 \frac{\partial^2 m}{\partial \xi^2} + R_2 h(\tau) m + S_2 |m|^2 m + T_2 \frac{\partial n_1^{(2)}}{\partial \xi}, \\
e_3 &= p_3 \frac{\partial m}{\partial \tau} + q_3 \frac{\partial^2 m}{\partial \xi^2} + R_3 g(\tau) m + S_3 |m|^2 m + T_3 \frac{\partial n_1^{(2)}}{\partial \xi}, \\
e_4 &= p_4 \frac{\partial m}{\partial \tau} + q_4 \frac{\partial^2 m}{\partial \xi^2} + [R_{41} g(\tau) + R_{42} h(\tau)] m + S_4 |m|^2 m + T_4 \frac{\partial n_1^{(2)}}{\partial \xi} + 2ik\mu N_0 A_1 V_g \frac{\partial m}{\partial \xi}.
\end{aligned}$$

Using all the above determined expressions, we use the solvability condition provided by the dispersion relation Eq. (A.3) into Eq. (A.8), and after gathering all remaining expressions, we arrive at the cubic complex nonlinear partial differential equation

$$i \frac{\partial m}{\partial \tau} + P \frac{\partial^2 m}{\partial \xi^2} + R \frac{\partial m}{\partial \xi} + Q |m|^2 m + H(\tau) m = 0. \quad (\text{A.14})$$

which governs the evolution of weakly nonlinear excitations in the original model Eqs. (2.14). The coefficients P, Q, R, are complex and so do the linear gain/loss coefficient  $H(\tau)$ . Explicitly their

analytical expressions are:

$$\begin{aligned}
P &= \frac{\Delta_1 q_1 + \Delta_2 q_2 + \Delta_3 q_3 + \Delta_4 q_4}{\Delta_1 p_1 + \Delta_2 p_2 + \Delta_3 p_3 + \Delta_4 p_4}, & R &= \frac{2ik\mu N_0 V_g A_1}{\Delta_1 p_1 + \Delta_2 p_2 + \Delta_3 p_3 + \Delta_4 p_4}, \\
Q &= \frac{\Delta_1 S_1 + \Delta_2 S_2 + \Delta_3 S_3 + \Delta_4 S_4}{\Delta_1 p_1 + \Delta_2 p_2 + \Delta_3 p_3 + \Delta_4 p_4}, & H(\tau) &= R_h h(\tau) + R_g g(\tau), \\
R_h &= \frac{\Delta_1 R_1 + \Delta_2 R_2 + \Delta_3 R_{42}}{\Delta_1 p_1 + \Delta_2 p_2 + \Delta_3 p_3 + \Delta_4 p_4}, & R_g &= \frac{\Delta_3 R_3 + \Delta_4 R_{41}}{\Delta_1 p_1 + \Delta_2 p_2 + \Delta_3 p_3 + \Delta_4 p_4}, \\
\Delta_1 &= b_2 c_3 d_4 - b_2 c_4 d_3, & \Delta_2 &= b_1 c_4 d_3 - b_1 c_3 d_4, & \Delta_3 &= b_2 c_4 d_1 - b_2 c_1 d_4 - b_1 c_4 d_2, \\
\Delta_4 &= b_1 c_3 d_2 + b_2 c_1 d_3 - b_2 c_3 d_1.
\end{aligned} \tag{A.15}$$

we introduce the transformation  $m(\xi, \tau) = \psi(\xi, \tau)e^{i(\chi_1 \xi + \chi_2(\tau))}$ , and Eq. (A.17) becomes Eq. (3.24) in the main document, provided that  $\chi_1 = \frac{R_r}{2P_i}$ ,  $R_{11} = R_i + 2\chi_1 P_r$ ,  $\chi_2(\tau) = -\chi_1 \tau (R_i + \chi_1 P_r)$ .  $h(\tau)$  and  $g(\tau)$  are chosen so that the real part of  $H(\tau)$  is zero.  $\varphi(\tau) = \text{Im}(H(\tau)) + \chi_1 (R_r - P_i \chi_1)$ . If we simultaneously set  $h(\tau) = 0$  and  $g(\tau) = 0$ , Eq. (A.17) reduces to the traditional cubic complex nonlinear Schroedinger equation. Eq. (A.17), is the reduced form of Eqs. (2.14).

## Appendix B: Derivation of the complex Davey-Stewartson Equation Eqs. (3.45)

Substituting Eqs. (3.45) into Eqs. (2.19) and assembling the terms with the same exponential yields the first harmonics

$$\begin{aligned}
C_1^{(1)} &= \Gamma_1 n_1^{(1)}, & u_1^{(1)} &= A_1 n_1^{(1)}, & v_1^{(1)} &= B_1 n_1^{(1)}, \\
\Gamma_1 &= \frac{-i\omega - ik_y \mu_0 \gamma_0 (\gamma - n_0 - \frac{n_0}{1+\nu k^2}) + k^2 \left(1 + \frac{n_0 P_e}{N_0^2 (1+\nu k^2)}\right)}{n_0 k^2 \left(\chi_0 + \frac{\chi_1}{1+\nu k^2}\right)}, & A_1 &= \frac{1}{1+\nu k^2} \left[ ik_x \left( \chi_1 \Gamma_1 - \frac{P_e}{N_0^2} \right) - \frac{\mu_0 \gamma_0 k_x k_y (1-\nu)}{1+k^2} \right], \\
B_1 &= \frac{1}{1+\nu k^2} \left[ ik_y \left( \chi_1 \Gamma_1 - \frac{P_e}{N_0^2} \right) - \frac{\mu_0 \gamma_0 (1+k_y^2 + \nu k_x^2)}{1+k^2} \right], & N_0 &= 1 + n_0,
\end{aligned} \tag{B.1}$$

provided that the dispersion relation is given by

$$\begin{aligned}
&\left[ -i\omega + ik_y \mu_0 \gamma_0 \left( \gamma - n_0 - \frac{n_0}{1+\nu k^2} \right) + k^2 \left( 1 + \frac{n_0 P_e}{N_0^2 (1+\nu k^2)} \right) \right] \left[ -i\omega - ik_y \mu_0 \gamma_0 n_0 + \beta n_0 + k^2 \left( \alpha - \frac{\chi_1 c_0}{1+\nu k^2} \right) \right] \\
&+ n_0 c_0 k^2 \left( \chi_0 + \frac{\chi_1}{1+\nu k^2} \right) \left[ \beta + \frac{P_e k^2 - ik_y \mu_0 \gamma_0 N_0^2}{N_0^2 (1+\nu k^2)} \right] = 0.
\end{aligned} \tag{B.2}$$

As expected, it is observed from Eqs. (B.2) that real and imaginary parts of  $\omega$  depends on system's parameters as well as modulation wave vectors  $k_x$  and  $k_y$ . The imaginary part of  $\omega$  coincides with the growth rate factor earlier discussed in the linear stability section. At the second order, we continue and determine the amplitudes of the second harmonics, the constant terms and the non vanishing

terms. The constant terms corresponding to  $l = 0$  yield

$$\begin{aligned} C_0^{(2)} &= -\frac{c_0}{n_0} n_0^{(2)} + \frac{2}{n_0 N_0^2} \frac{n_0 P_e + N_0^2 (1 + \nu k^2)}{\chi_1 + n_0 (1 + \nu k^2)} |n_1^{(1)}|^2, \quad u_0^{(2)} = A |n_1^{(1)}|^2, \quad \text{with} \\ A &= \frac{2}{N_0} [k_x k_y (1 - \nu) (B_1 + B_1^*) - (1 + k_y^2 + \nu k_x^2) (A_1 + A_1^*) + 2i k_x \chi_1 (\Gamma_1 - \Gamma_1^*)], \\ B &= \frac{2}{N_0} [k_x k_y (1 - \nu) (A_1 + A_1^*) - 2\mu_0 \gamma_0 + (1 + k_y^2 + \nu k_x^2) (B_1 + B_1^*)]. \end{aligned} \quad (\text{B.3})$$

The  $l = 1$  terms are reduced into

$$\begin{aligned} C_1^{(2)} &= \Gamma_1 n_1^{(2)} + \Gamma_{21} \frac{\partial n}{\partial \xi} + \Gamma_{22} \frac{\partial n}{\partial \eta}, \quad u_1^{(2)} = A_1 n_1^{(2)} + A_{21} \frac{\partial n}{\partial \xi} + A_{22} \frac{\partial n}{\partial \eta}, \quad v_1^{(2)} = B_1 n_1^{(2)} + B_{21} \frac{\partial n}{\partial \xi} + B_{22} \frac{\partial n}{\partial \eta}, \\ \text{with } \Gamma_{21} &= \frac{\Gamma_1 [V_x + i k_x (2\alpha - \frac{\chi_1 c_0}{1 + \nu k^2})] - c_0 A_1 \left(1 + \frac{k_y^2 (1 - \nu) - 2\nu k_x^2}{1 + \nu k^2}\right) + \frac{c_0 k_x}{1 + \nu k^2} \left[B_1 k_y (1 + \nu) + \frac{i P_e}{N_0^2}\right]}{\beta c_0 + \frac{c_0 P_e k^2 - i k_y \mu_0 c_0 \gamma_0 N_0^2}{N_0^2 (1 + \nu k^2)}}, \\ \Gamma_{22} &= \frac{\mu_0 \gamma_0 n_0 + \Gamma_1 [V_y + i k_y (2\alpha - \frac{\chi_1 c_0}{1 + \nu k^2})] - c_0 B_1 \left(1 + \frac{k_x^2 (1 - \nu) - 2\nu k_y^2}{1 + \nu k^2}\right) + \frac{c_0 k_y}{1 + \nu k^2} \left[A_1 k_x (1 + \nu) + \frac{i P_e}{N_0^2}\right]}{\beta c_0 + \frac{c_0 P_e k^2 - i k_y \mu_0 c_0 \gamma_0 N_0^2}{N_0^2 (1 + \nu k^2)}}, \\ B_{21} &= \frac{1 + k_y^2 + \nu k_x^2}{(1 + k^2)(1 + \nu k^2)} \left[ \frac{i k_y \chi_1 (1 + k^2)}{1 + k_y^2 + \nu k_x^2} \Gamma_{21} - i k_y (1 - \nu) A_1 + 2i k_x B_1 \right] \\ &\quad - \frac{k_x k_y (1 - \nu)}{(1 + k^2)(1 + \nu k^2)} \left[ \frac{P_e}{N_0^2} + i k_y (1 - \nu) B_1 - \chi_1 \Gamma_1 - 2i k_x \nu A_1 \right], \\ B_{22} &= \frac{1 + k_y^2 + \nu k_x^2}{(1 + k^2)(1 + \nu k^2)} \left[ \frac{i k_y \chi_1 \Gamma_{22} (1 + k^2)}{1 + k_y^2 + \nu k_x^2} - \frac{P_e}{N_0^2} - i k_x A_1 (1 - \nu) + \chi_1 \Gamma_1 + 2i k_y \nu B_1 \right] \\ &\quad - \frac{k_x k_y (1 - \nu)}{(1 + k^2)(1 + \nu k^2)} [i k_x B_1 (1 - \nu) - 2i k_y A_1], \\ A_{21} &= -\frac{i k_x (\chi_1 \Gamma_{21} + 2\nu A_1) + (1 - \nu) (k_x k_y B_{21} - i k_y B_1) + \chi_1 \Gamma_1 - \frac{P_e}{N_0^2}}{1 + k_y^2 + \nu k_x^2}, \\ A_{22} &= \frac{i k_x [\chi_1 \Gamma_{22} - B_1 (1 - \nu)] + k_x k_y B_{22} (1 - \nu) + 2i k_y A_1}{1 + k_y^2 + \nu k_x^2}, \end{aligned} \quad (\text{B.4})$$

provided that  $V_x$  and  $V_y$  take the form

$$\begin{aligned} V_x &= \frac{N_x}{D_x}, \quad \text{and} \quad V_y = \frac{N_y}{D_y}, \\ N_x &= -n_0 k^2 \left(\chi_0 + \frac{\chi_1}{1 + \nu k^2}\right) \left\{ i k_x \left[ \frac{c_0 P_e}{N_0^2 (1 + \nu k^2)} + \Gamma_1 \left(2\alpha - \frac{\chi_1 c_0}{1 + \nu k^2}\right) \right] - c_0 A_1 \left[ 1 + \frac{k_y^2 (1 - \nu) - 2\nu k_x^2}{1 + \nu k^2} \right] + \frac{c_0 k_x k_y B_1 (1 + \nu)}{1 + \nu k^2} \right\} \\ &\quad - \left\{ i k_x \left[ 2 + \frac{n_0 P_e}{N_0^2 (1 + \nu k^2)} - n_0 \Gamma_1 \left(2\chi_0 + \frac{\chi_1}{1 + \nu k^2}\right) \right] + \frac{k_x k_y n_0 B_1 (1 + \nu)}{1 + \nu k^2} - n_0 A_1 \left(1 - \frac{2\nu k_x^2}{1 + \nu k^2}\right) \right\} \times \\ &\quad \left[ -i\omega - i k_y \mu_0 \gamma_0 n_0 + \beta n_0 + k^2 \left(\alpha - \frac{\chi_1 c_0}{1 + \nu k^2}\right) \right], \\ D_x &= -i\omega - i k_y \mu_0 n_0 \gamma_0 + \beta n_0 + k^2 \left(\alpha - \frac{\chi_1 c_0}{1 + \nu k^2}\right) + n_0 k^2 \left(\chi_0 + \frac{\chi_1}{1 + \nu k^2}\right), \\ D_y &= -2i\omega - i k_y \mu_0 \gamma_0 \left(\gamma - n_0 - \frac{n_0}{1 + \nu k^2}\right) + (\alpha + 1) k^2 + \frac{k^2 (n_0 P_e - N_0^2 c_0 \chi_1)}{N_0^2 (1 + \nu k^2)}, \\ N_y &= -n_0 k^2 \left(\chi_0 + \frac{\chi_1}{1 + \nu k^2}\right) \left\{ \mu_0 \gamma_0 n_0 - c_0 B_1 \left[ 1 + \frac{(1 - \nu) k_x^2 - 2\nu k_y^2}{1 + \nu k^2} \right] + \frac{c_0 k_x k_y A_1 (1 + \nu)}{1 + \nu k^2} \right\} \\ &\quad - i k_x n_0 k^2 \left(\chi_0 + \frac{\chi_1}{1 + \nu k^2}\right) \left[ \frac{c_0 P_e}{N_0^2 (1 + \nu k^2)} + \Gamma_1 \left(2\alpha - \frac{\chi_1 c_0}{1 + \nu k^2}\right) \right] - \left[ -i\omega - i k_y \mu_0 n_0 \gamma_0 + \beta n_0 + k^2 \left(\alpha - \frac{\chi_1 c_0}{1 + \nu k^2}\right) \right] \times \\ &\quad \left\{ \frac{k_x k_y n_0 A_1 (1 + \nu)}{1 + \nu k^2} - \mu_0 n_0 \gamma_0 - n_0 B_1 \left(1 + \frac{(1 - \nu) k_y^2 - 2\nu k_x^2}{1 + \nu k^2}\right) + i k_y \left[ 2 + \frac{P_e n_0}{N_0^2 (1 + \nu k^2)} - n_0 \Gamma_1 \left(2\chi_0 + \frac{\chi_1}{1 + \nu k^2}\right) \right] \right\}. \end{aligned} \quad (\text{B.5})$$

We continue the resolution of the second order. For  $l = 2$ , components of the second harmonics are recovered by solving the system

$$\begin{aligned} a_{11}n_2^{(2)} + b_{11}C_2^{(2)} + c_{11}V_2^{(2)} &= d_{11} \left(n_1^{(1)}\right)^2, & a_{22}n_2^{(2)} + b_{22}C_2^{(2)} + c_{22}V_2^{(2)} &= d_{22} \left(n_1^{(1)}\right)^2, \\ a_{33}n_2^{(2)} + b_{33}C_2^{(2)} + c_{33}V_2^{(2)} &= d_{33} \left(n_1^{(1)}\right)^2, & U_2^{(2)} &= a_{44}n_2^{(2)} + b_{44}C_2^{(2)} + c_{44}V_2^{(2)} + d_{44} \left(n_1^{(1)}\right)^2, \end{aligned} \quad (\text{B.6})$$

where

$$\begin{aligned} a_{44} &= -\frac{2ik_x P_e}{N_0^2(1+4k_y^2+4\nu k_x^2)}, & b_{44} &= -\frac{k_x k_y(1-\nu)}{1+4k_y^2+4\nu k_x^2}, & c_{44} &= \frac{2ik_x \chi_1}{1+4k_y^2+4\nu k_x^2}, & c_{22} &= 2ik_y c_0(1+c_{44}), \\ d_{44} &= -\frac{2N_0 A_1(1+k_y^2+\nu k_x^2)+2N_0 k_x k_y B_1(\nu-1)-2ik_x \chi_1 \Gamma_1}{N_0^2(1+4k_y^2+4\nu k_x^2)}, & b_{11} &= -4\chi_0 n_0 k^2 + 2ik_x n_0 b_{44}, \\ a_{11} &= -2i\omega + 4k^2 + 2ik_y \mu_0 \gamma_0(\gamma - n_0) + 2ik_x n_0 a_{44}, & c_{11} &= 2ik_y n_0 + 2ik_x n_0 c_{44}, \\ d_{11} &= 2\chi_0 k^2 \Gamma_1 - 2ik_x A_1 - 2ik_y B_1 - 2ik_x n_0 d_{44}, \\ a_{22} &= \beta c_0 + 2ik_y c_0 a_{44}, & b_{22} &= -2i\omega + 4\alpha k^2 + \beta n_0 + 2ik_y(\mu_0 n_0 \gamma_0 + c_0 b_{44}), \\ d_{22} &= -\Gamma_1 [\beta + 2i(k_x A_1 + k_y B_1)] - 2ik_y c_0 d_{44}, & a_{33} &= 4N_0^2 a_{44} k_x k_y(1-\nu) - 2ik_y P_e - \mu_0 \gamma_0 N_0^2, \\ b_{33} &= 2ik_y \chi_1 N_0^2 + 4k_x k_y N_0^2 b_{44}(1-\nu), & c_{33} &= 4k_x k_y N_0^2 c_{44}(1-\nu) - N_0^2 - 4N_0^2(k_x^2 + \nu k_y^2), \\ d_{33} &= 2N_0 B_1(1+k_x^2 + \nu k_y^2) + \mu_0 \gamma_0 + 2k_x k_y N_0 - 2ik_y N_0 \chi_1 \Gamma_1 - 4d_{44} k_x k_y N_0^2(1-\nu). \end{aligned}$$

The system Eqs. (B.6) is solved for the dependent variables  $n_2^{(2)}$ ,  $C_2^{(2)}$ ,  $V_2^{(2)}$  and  $U_2^{(2)}$ , and the solutions are given as functions of  $\left(n_1^{(1)}\right)^2$ , thus we write

$$\begin{aligned} n_2^{(2)} &= D_2 \left(n_1^{(1)}\right)^2, & C_2^{(2)} &= \Gamma_2 \left(n_1^{(1)}\right)^2, & U_2^{(2)} &= A_2 \left(n_1^{(1)}\right)^2, & V_2^{(2)} &= B_2 \left(n_1^{(1)}\right)^2, & \text{where} \\ A_2 &= -\frac{2N_0 A_1(1+k_y^2+\nu k_x^2)+2N_0 k_x k_y B_1(\nu-1)-2ik_x \chi_1 \Gamma_1+2ik_x(P_e D_2-N_0^2 \chi_1 \Gamma_2)+4N_0^2 k_x k_y B_2(1-\nu)}{N_0^2(1+4k_y^2+4\nu k_x^2)}, \\ D_2 &= \frac{b_{11}c_{22}d_{33}-b_{11}c_{33}d_{22}-b_{22}c_{11}d_{33}+b_{22}c_{33}d_{11}+b_{33}c_{11}d_{22}-b_{33}c_{22}d_{11}}{a_{11}b_{22}c_{33}-a_{11}b_{33}c_{22}-a_{22}b_{11}c_{33}+a_{22}b_{33}c_{11}+a_{33}b_{11}c_{22}-a_{33}b_{22}c_{11}}, \\ \Gamma_2 &= -\frac{a_{11}c_{22}d_{33}-a_{11}c_{33}d_{22}-a_{22}c_{11}d_{33}+a_{22}c_{33}d_{11}+a_{33}c_{11}d_{22}-a_{33}c_{22}d_{11}}{a_{11}b_{22}c_{33}-a_{11}b_{33}c_{22}-a_{22}b_{11}c_{33}+a_{22}b_{33}c_{11}+a_{33}b_{11}c_{22}-a_{33}b_{22}c_{11}}, \\ B_2 &= \frac{a_{11}b_{22}d_{33}-a_{11}b_{33}d_{22}-a_{22}b_{11}d_{33}+a_{22}b_{33}d_{11}+a_{33}b_{11}d_{22}-a_{33}b_{22}d_{11}}{a_{11}b_{22}c_{33}-a_{11}b_{33}c_{22}-a_{22}b_{11}c_{33}+a_{22}b_{33}c_{11}+a_{33}b_{11}c_{22}-a_{33}b_{22}c_{11}}. \end{aligned} \quad (\text{B.7})$$

At the third order of  $\epsilon$ , the  $l = 0$  components of the third order allows us to establish that the dependent variable  $n_0^{(2)}$  we could not explicitly determine a the second order for  $l = 0$  satisfies

$$\sigma_1 \frac{\partial^2 n_0^{(2)}}{\partial \xi^2} + \sigma_2 \frac{\partial^2 n_0^{(2)}}{\partial \eta^2} = \sigma_3 \frac{\partial^2 |n_1^{(1)}|^2}{\partial \xi^2} + \sigma_2 \frac{\partial^2 |n_1^{(1)}|^2}{\partial \eta^2}. \quad (\text{B.8})$$

The parameters  $\sigma_1$ ,  $\sigma_2$ ,  $\sigma_3$ , and  $\sigma_4$  are given by

$$\begin{aligned} \alpha_1 &= n_0 A + A_1 + A_1^* + ik_x \chi_0(\Gamma_1 - \Gamma_1^*), & \alpha_2 &= n_0 B + B_1 + B_1^* + ik_y \chi_0(\Gamma_1 - \Gamma_1^*), & \sigma_1 &= V_{x_i} V_{x_r}, \\ \sigma_2 &= -V_{y_i} [V_{y_r} - \mu_0 \gamma_0(\gamma - 2n_0)], & \sigma_3 &= \frac{V_{x_i} V_{y_i} \alpha_1^2}{\alpha_1 V_{y_i} + \alpha_2 V_{x_i}}, & \sigma_4 &= -\frac{V_{x_i} V_{y_i} \alpha_2^2}{\alpha_1 V_{y_i} + \alpha_2 V_{x_i}}. \end{aligned}$$

$\sigma_1, \sigma_2, \sigma_3$  and  $\sigma_4$  are all reals. The  $l = 1$ -components of the third order yields the system

$$\begin{aligned}
a_1 n_1^{(3)} + b_1 C_1^{(3)} + c_1 U_1^{(3)} + d_1 V_1^{(3)} &= -\frac{\partial n_1^{(1)}}{\partial \tau} + P_1 \frac{\partial^2 n_1^{(1)}}{\partial \xi^2} + P_2 \frac{\partial^2 n_1^{(1)}}{\partial \eta^2} + P_3 \frac{\partial^2 n_1^{(1)}}{\partial \xi \partial \eta} + P_4 n_1^{(1)} n_0^{(2)} \\
&\quad + P_5 n_1^{(1)} |n_1^{(1)}|^2 + P_6 \frac{\partial n_1^{(2)}}{\partial \xi} + P_7 \frac{\partial n_1^{(2)}}{\partial \eta}, \\
a_2 n_1^{(3)} + b_2 C_1^{(3)} + c_2 U_1^{(3)} + d_2 V_1^{(3)} &= -\Gamma_1 \frac{\partial n_1^{(1)}}{\partial \tau} + Q_1 \frac{\partial^2 n_1^{(1)}}{\partial \xi^2} + Q_2 \frac{\partial^2 n_1^{(1)}}{\partial \eta^2} + Q_3 \frac{\partial^2 n_1^{(1)}}{\partial \xi \partial \eta} + Q_4 n_1^{(1)} n_0^{(2)} \\
&\quad + Q_5 n_1^{(1)} |n_1^{(1)}|^2 + Q_6 \frac{\partial n_1^{(2)}}{\partial \xi}, \\
a_3 n_1^{(3)} + b_3 C_1^{(3)} + c_3 U_1^{(3)} + d_3 V_1^{(3)} &= R_1 \frac{\partial^2 n_1^{(1)}}{\partial \xi^2} + R_2 \frac{\partial^2 n_1^{(1)}}{\partial \eta^2} + R_3 \frac{\partial^2 n_1^{(1)}}{\partial \xi \partial \eta} + R_4 n_1^{(1)} n_0^{(2)} + R_5 n_1^{(1)} |n_1^{(1)}|^2 \\
&\quad + R_6 \frac{\partial n_1^{(2)}}{\partial \xi} + R_7 \frac{\partial n_1^{(2)}}{\partial \eta}, \\
a_4 n_1^{(3)} + b_4 C_1^{(3)} + c_4 U_1^{(3)} + d_4 V_1^{(3)} &= S_1 \frac{\partial^2 n_1^{(1)}}{\partial \xi^2} + S_2 \frac{\partial^2 n_1^{(1)}}{\partial \eta^2} + S_3 \frac{\partial^2 n_1^{(1)}}{\partial \xi \partial \eta} + S_4 n_1^{(1)} n_0^{(2)} + S_5 n_1^{(1)} |n_1^{(1)}|^2 \\
&\quad + S_6 \frac{\partial n_1^{(2)}}{\partial \xi} + S_7 \frac{\partial n_1^{(2)}}{\partial \eta}, \quad (\text{B.9})
\end{aligned}$$

with

$$\begin{aligned}
a_1 &= -i\omega + k^2 + ik_y \mu_0 \gamma_0 (\gamma - n_0), \quad b_1 = \chi_0 n_0 c_0 k^2, \quad c_1 = ik_x c_0, \quad a_2 = \beta c_0, \\
b_2 &= -i\omega + \alpha k^2 + \beta n_0 - ik_y \mu_0 n_0 \gamma_0, \quad c_2 = ik_x c_0, \quad d_2 = ik_y c_0, \quad a_3 = -ik_x P_e, \quad b_3 = ik_x \chi_1 N_0^2, \\
c_3 &= -N_0^2 (1 + k_y^2 + \nu k_x^2), \quad d_3 = N_0^2 k_x k_y (1 - \nu), \quad a_4 = -i(k_y P_e + \mu_0 \gamma_0 N_0^2), \quad b_4 = ik_y \chi_1 N_0^2, \\
c_4 &= k_x k_y N_0^2 (1 - \nu), \quad d_4 = -N_0^2 (1 + k_x^2 + \nu k_y^2), \quad P_1 = 1 - \chi_0 n_0 \Gamma_1 - 2ik_x \chi_0 n_0 \Gamma_{21} - n_0 A_{21}, \\
P_2 &= 1 - \chi_0 n_0 \Gamma_1 - 2ik_y \chi_0 n_0 \Gamma_{22} - n_0 B_{22}, \quad P_3 = -2i\chi_0 n_0 (k_x \Gamma_{22} + k_y \Gamma_{21}) - n_0 (A_{22} + B_{21}), \\
P_4 &= \chi_0 k^2 \Gamma_1 - ik_x A_1 - ik_y (B_1 - \mu_0 \gamma_0), \quad P_5 = \chi_0 k^2 (2\Gamma_2 - D_2 \Gamma_1^*) - ik_x (A_2 + A + D_2 A_1^*) - ik_y (B_2 + D_2 B_1^* + B), \\
P_6 &= V_x + 2ik_x (1 - \chi_0 n_0 \Gamma_1) - n_0 A_1, \quad P_7 = V_y + 2ik_y (1 - \chi_0 n_0 \Gamma_1) + \mu_0 \gamma_0 (n_0 - \gamma) - n_0 B_1, \\
Q_1 &= \alpha \Gamma_1 + \Gamma_{21} (V_x + 2i\alpha k_x) - c_0 A_{21}, \quad Q_2 = \alpha \Gamma_1 + \Gamma_{22} (V_y + 2i\alpha k_y + \mu_0 \gamma_0 n_0) - c_0 B_{22}, \\
Q_3 &= \Gamma_{21} (V_y + 2i\alpha k_y + \mu_0 n_0 \gamma_0) - c_0 B_{21} + \Gamma_{22} (V_x + 2i\alpha k_x) - c_0 A_{22}, \\
Q_4 &= \Gamma_1 (ik_y \mu_0 n_0 \gamma_0 - \beta) + \frac{c_0}{n_0} (\beta + ik_x A_1 + ik_y B_1),
\end{aligned}$$

$$\begin{aligned}
Q_5 &= -\beta(\Gamma + \Gamma_2 + D_2\Gamma_1^*) - ik_y(B\Gamma + B_2\Gamma_1^* + B_1^*\Gamma_2 + \Gamma B_1) - ik_x(A\Gamma_1 + A_2\Gamma_1^* + A_1^*\Gamma_2 + \Gamma A_1), \\
Q_6 &= -c_0A_1 - \Gamma_1(V_x + 2ik_x\alpha), \quad Q_7 = -c_0B_1 - \Gamma_1(V_y + 2i\alpha k_y + \mu_0n_0\gamma_0), \\
R_1 &= -N_0^2B_1 + ik_yN_0^2A_{21}(1-\nu) - 2ik_xN_0^2B_{21}, \quad R_2 = -\nu N_0^2B_1 + ik_xN_0^2A_{22}(1-\nu) - 2ik_y\nu N_0^2B_{22} - \chi_1N_0^2\Gamma_{22}, \\
R_3 &= N_0^2A_1(1-\nu) - \chi_1N_0^2\Gamma_{21} + ik_xN_0^2A_{21}(1-\nu) - 2ik_y\nu N_0^2B_{21} + ik_yN_0^2A_{22} - 2ik_xN_0^2B_{22}, \\
R_4 &= 2N_0B_1(1 + k_x^2 + \nu k_y^2) + 2N_0k_xk_yA_1(\nu - 1) + 2N_0\mu_0\gamma_0 - 2ik_y\chi_1N_0\Gamma_1, \\
R_5 &= (1 + k_x^2 + \nu k_y^2)(B_1^* + 2B_1 + 2N_0D_2B_1^*) + k_xk_y(\nu - 1)(A_1^* + 2A_1 + 8N_0A_2 + 2N_0D_2A_1^*) + \mu_0\gamma_0(3 + 4N_0D_2) \\
&\quad + 2N_0B_2(1 + 4k_x^2 + 4\nu k_y^2) + ik_y\chi_1(\Gamma_1^* - 2\Gamma_1) + 2ik_yN_0\Gamma_1(D_2\Gamma_1^* - 2\Gamma_2), \\
R_6 &= N_0^2[ik_yA_1(1-\nu) - 2ik_xB_1], \quad R_7 = N_0^2[ik_xA_1(1-\nu) - 2ik_yB_1 - \chi_1\Gamma_1], \\
S_1 &= N_0^2[\nu A_1 - \chi_1\Gamma_{21} + ik_xB_{21}(1-\nu) - 2ik_x\nu A_{21}], \quad S_2 = N_0^2[A_1 + ik_xB_{22}(1-\nu) - 2ik_ya_{22}], \\
S_3 &= N_0^2[(1-\nu)(B_1 + ik_yB_{22} + ik_xB_{21}) - \chi_1\Gamma_{22} - 2ik_x\nu A_{22} - 2ik_yA_{21}], \\
S_4 &= -2\nu N_0k_xk_yB_1(1-\nu) - 2N_0A_1(1 + k_x^2 + \nu k_y^2) + 2ik_xN_0\chi_1\Gamma_1, \\
S_5 &= 2N_2A_1 + ik_x\chi_1(\Gamma_1^* + 2N_0D_2\Gamma_1^* - 2\Gamma_1 - 4N_0\Gamma_2) + (1 + k_x^2 + \nu k_y^2)(A_1^* + 2A_1 + 2N_0D_2A_1^*) \\
&\quad + k_xk_y(\nu - 1)(B_1^* + 2N_0D_2B_1^* + 2B_1 + 8N_0B_2) + 2N_0A_2(1 + 4k_y^2 + 4\nu k_x^2), \\
S_6 &= P_e - \chi_1N_0^2\Gamma_1 + ik_yN_0^2B_1(1-\nu) - 2ik_xN_0^2\nu A_1, \quad S_7 = iN_0o_0^2[k_xB_1(1-\nu) - 2k_yA_1].
\end{aligned}$$

Eq. (B.10) is solved with respect to the dependent variables  $X_1^{(3)}$ ,  $X = n, c, U, V$ . Taking in to consideration the solvability conditions given by Eq. (B.2) and Eq. (B.5) leads to the equation

$$i\frac{\partial n_1^{(1)}}{\partial \tau} + P_\xi \frac{\partial^2 n_1^{(1)}}{\partial \xi^2} + P_\eta \frac{\partial^2 n_1^{(1)}}{\partial \eta^2} + P_{\xi\eta} \frac{\partial^2 n_1^{(1)}}{\partial \xi \partial \eta} + Q|n_1^{(1)}|^2 n_1^{(1)} + Q_0 n_1^{(1)} n_0^{(2)} = 0. \quad (\text{B.10})$$

The coefficients  $P_\xi, P_\eta, P_{\xi\eta}, Q$  and  $Q_0$  are complex constants, and given by

$$\begin{aligned}
P_\xi &= -i\frac{P_1\Delta_1 + Q_1\Delta_2 + R_1\Delta_3 + S_1\Delta_4}{\Delta_1 + \Gamma_1\Delta_2}, \quad P_\eta = -i\frac{P_2\Delta_1 + Q_2\Delta_2 + R_2\Delta_3 + S_2\Delta_4}{\Delta_1 + \Gamma_1\Delta_2}, \quad P_{\xi\eta} = -i\frac{P_3\Delta_1 + Q_3\Delta_2 + R_3\Delta_3 + S_3\Delta_4}{\Delta_1 + \Gamma_1\Delta_2}, \\
Q_0 &= -i\frac{P_4\Delta_1 + Q_4\Delta_2 + R_4\Delta_3 + S_4\Delta_4}{\Delta_1 + \Gamma_1\Delta_2}, \quad Q_1 = -i\frac{P_5\Delta_1 + Q_5\Delta_2 + R_5\Delta_3 + S_5\Delta_4}{\Delta_1 + \Gamma_1\Delta_2}, \quad \text{and} \\
\Delta_1 &= b_2c_4d_3 + b_3c_2d_4 + b_4c_3d_2 - b_2c_3d_4 - b_3c_4d_2 - b_4c_2d_3, \\
\Delta_2 &= b_3c_4d_1 + b_4c_1d_3 + b_1c_3d_4 - b_1c_4d_3 - b_3c_1d_4 - b_4c_3d_1, \\
\Delta_3 &= b_1c_4d_2 + b_2c_1d_4 + b_4c_2d_1 - b_1c_2d_4 - b_2c_4d_1 - b_4c_1d_2, \\
\Delta_4 &= b_1c_2d_3 + b_3c_1d_2 + b_2c_3d_1 - b_1c_3d_2 - b_3c_2d_1 - b_2c_1d_3.
\end{aligned}$$

Combining Eq. (B.8) and Eq. (B.10) yields the reduced model Eqs. (3.46) (of the main document) which stands for the complex Davey-Stewartson equation.



---

# Bibliography

- [1] Min Li, Shuya Li, Han Zhou, Xinfeng Tang, Yi Wu, Wei Jiang, Zhigang Tian, Xuechang Zhou, Xianzhu Yang, Yucai Wang, Nature Communication **2020** 11:1126.
  - [2] J. Murray, *Mathematical Biology II : Spatial Models and Biomedical Applications*, 2nd ed., (Springer, New York, 2002).
  - [3] Y. Kim, S. Lawler, M. O. Nowicki, E. A. Chiocca, A. Friedman, J. Theor. Biol. **2009**, 260:359-371.
  - [4] C. Jiang, C. Cui, L. Li, Y. Shao, PLoS ONE, **2014** 9(10):e109784.
  - [5] J. F. Jikeli, L. Alvarez, B. M. Friedrich, G. L. Wilson, R. Pascal, R. Colin, M. Pichlo, A. Rennhack, C. Brenker, U. B. Kaupp, Nature Communications. **2015**, 6:7985.
  - [6] L. Zhicheng, B. Quaife, H. Salman H, N. O. Zoltan, Sci. Rep. **2017**, 7:12855.
  - [7] W. G. Stetler-Stevenson, S. Aznavoorian, L. A. Liotta, Annu. Rev. Cell. Biol. **1993**, 9:541-573.
  - [8] Y. Kim, M. A. Stolarska, H. G. Othmer, Prog. Biophys. Mol. Biol. **2011** 106:353-379.
  - [9] U. P. Thorgeirsson, C. K. Lindsay, D. W. Cottam, D. E. Gomez, J. Neurooncol. **1994**, 18:89-103.
  - [10] S. R. McDougall, A. R. A. Anderson, M. A. J. Chaplain, J. A. Sherratt, Bull. Math. Biol. **2002**, 64:673-702.
  - [11] J. Adler, Science. **1966**, 153:708.
  - [12] C. S. Patlak, Bull. Math. Biophys. **1953**, 15.
  - [13] E. F. Keller, L. A. Segel, J. Theor. Biol. **1970**, 26:399.
  - [14] J. Murray, G. Oster, A. Harris, J. Math. Biol. **1983**, 17:125-129.
  - [15] M. A. J. Chaplain, G. Lolas, Net. and Heter. Med. **2006**; 1(3):399-439.
-

- [16] M. A. J. Chaplain, G. Lolas, *Math. Mod. and Meth. in App Sci.* **2005**, 15(11):1685-1734.
- [17] A. J. Perumpanani, H. M. Byrne, *Eur. J. Can.*, **1999**, 35(8):1274-1280.
- [18] T. B. Issa, R. B. Salako, W. Shen, arXiv:2010.11335v1 [math.AP] **21 Oct 2020**
- [19] C. Emako, C. Gayraud, A. Buguin, L. Neves de Almeida, N. Vauchelet, *PLoS. Comput. Biol.* **2016**, 12(4):e1004843.
- [20] M. Seyrich, A. Palugniok, H. Stark, *New J. Phys.* **2019**, 21:103001.
- [21] J. Long, S. W. Zucker, T. Emonet, *PLoS. Comput. Biol.* **2017**, 13(3):e1005429.
- [22] M. Ben Amar, C. Bianca, *Sci. Rep.* **2016**, 6:33849.
- [23] A. Chertock, K. Fellner, A. Kurganov, A. Lorz, P. A. Markowich, *J. Fluid Mech.* **2012**, 694:155-190.
- [24] J. E. Bear, J. M. Haugh, *Curr. Opin. Cell. Biol.*, **2014 October**, 0:74-82.
- [25] J. Saragosti, V. Calvez, N. Bournaveas, A. Buguin, P. Silberzan, *PLoS. Comput. Biol.* **2010**, 6:e1000890.
- [26] C. Walker, *Eur. J. Appl. Math.* **2008**, 19:113-147.
- [27] C. Walker, G. F. Webb, *SIAM J. Math. Anal.* **2007**, 38:1694-1713.
- [28] G. Litcanu, C. Morales-Rodrigo, *Nonlinear Anal.* **2010**, 72:77-98.
- [29] Jian-Guo Liu, A. Lorz, *Ann. I. H. Poincaré Anal. Nonlinéaire.* **2011**, 28:643-652.
- [30] T. Black. J. Lankeit, M. Mizukami, arXiv:1707.05528v1 [math.AP], **18 Jul 2017**.
- [31] T. Engelmann, *Pflugers Arch. Gesamte Physiol. Menschen. Tiere.* **1881**, 25:285-292.
- [32] T. Engelmann, *Pflugers Arch. Gesamte Physiol.* **1881**, 26:537.
- [33] W. Pfeffer, *Unters. Bot. Inst. Tübingen.* **1888**, 2:582.
- [34] M. J. Tindall, S. L. Porter, P. K. Maini, G. Gaglia, J. P. Armitage, *Bull. Math. Biol.* **2008**, 70:1525-1569
- [35] M. J. Tindall, E. A. Gaffney, P. K. Maini, J. P. Armitage, *Syst. Biol. Med.* **2012**, 4:247-259.
- [36] G. Wadhams, J. Armitage, *Nat. Rev. Mole. Cell Biol.* **2004**, 5(12):1024-1037.

- [37] M. Welch, K. Oosawa, S. Aizawa, M. Eisenbach, PNAS USA, **1993** 90(19):8787-8791.
- [38] K. Lipkow, PLoS Comput Biol. **2006** 2(4):e39.
- [39] L. Hall-Stoodley, J. W. Costerton, P. Stoodley, Nat. Rev. Microbiol. **2004**, 2:95-108.
- [40] J. Adler, J. Bacteriol. **1966**, 92:121.
- [41] C. Liu, X. Fu, L. Liu, X. Ren, C. K. Chau, S. Li et al. Science. **2011**, 334:238-241.
- [42] X. Fu, L. H. Tang, C. Liu, J. D. Huang, T. Hwa et al. Phys. Rev. Lett. **2012**, 108:198102
- [43] M. C. Marchetti, J. F. Joanny, S. Ramaswamy, T. B. Liverpool, J. Prost, Madan Rao, R. Aditi Simha, arXiv:1207.2929v1 [cond-mat.soft] **12 Jul. 2012**.
- [44] T. Vicsek, A. Czirok, E. Ben-Jacob, I. Cohen, O. Shochet, Phys. Rev. Lett. **1995**, 75:1226.
- [45] T. Emonet, C. Macal, M. North, C. Wickersham, P. Cluzel, Bioinf. **2005**, 21(11):2714-2721.
- [46] L. Zonia D. Bray, J. R. Soc. Interface. **2009**, 6(40):1035-1046.
- [47] D. Bray, M. Levin, K. Lipkow, Curr. Biol. **2007** 17(1):12-19.
- [48] S. Setayeshgar, C. Gear, H. Othmer, I. Kevrekidis, Mult. Mod. Sim. **2005**, 4(1):307-327.
- [49] R. Erban H. Othmer, SIAM J. Appl. Math. **2004**, 65(2):361-391.
- [50] W. Alt, J. Math. Biol., **1980**, 9(2):147-177.
- [51] K. Nishinari, K. Abe, J. Satsuma, J. Phys, Soc. Japan. **1993**, 62(6):2021-2029.
- [52] A. Davey, K. Stewartson, Proc. R. Soc. Lond. A. **1974**, 338:101-110.
- [53] C. B. Tabi, C. S. Panguetna, T. C. Kofané Physica B: Condensed Matter. **2018**, 545:370-376.
- [54] C. D. Bansi Kamdem, C. B. Tabi, Alidou Mohamadou, chaos, Fractals, and Solitons. **2018**, 109:170-183.
- [55] C.B. Tabi, A. S. Etémé, A. Mohamadou, Physics A. **2017**, 474:186-198.
- [56] W. Domgno Kuipou, A. Mohamadou, under review at Chaos, Fractals and Solitons **2021**.
- [57] W. Domgno Kuipou, A. Mohamadou, E. Kengne Chaos. Fractals and Solitons. **2021**, 152:111321.
- [58] Giovanna De Palo, D. Yi, R. G. Endres arXiv:1801.03707v1 [q-bio.CB] 11 Jan **2018**

- [59] E. O. Budrene, H. C. Berg, *Nature*. **1991**, 349:630-633.
- [60] E. O. Budrene, H. C. Berg, *Nature*, **1995** 376:49-53.
- [61] G. J. Kimmel, M. Dane, L. Heiser, P. M. Altrock, Noemi Andor, bioRxiv preprint
- [62] V. Calvez, B. Perthame, S. Yasuda, *Kin. Rel. Mod. AIMS*, **2018**, 11(4):891-909.
- [63] E. F. Keller, L. A. Segel *J. Theor. Biol.* **1971**, 2(30):235.
- [64] H. Wioland, E. Lushi, R. E. Goldstein, *New J. Phys.* **2016**, 18:075002.
- [65] E. Lushi, R. E. Goldstein, M. J. Shelley, *Phys. Rev. E.* **2018**, 98:052411
- [66] A. J. Perumpanani, J. A. Sherratt, J. Norbury, H. M. Byrne, *Physica D.* **1999**, 126:145-149.
- [67] T. Youshan, C. Cui. *J. Math. Anal. Appl.* **2010**, 367:612-624.
- [68] Y. Deleuze, C. Chen-Yu, M. Thiriet, T. W. H. Sheu. arXiv:1502.05374v1. **2014**.
- [69] J. S. Bois, F. Jülicher, S. W. Grill, *Phys. Rev. Lett.* **2011**, 106:028103.
- [70] K. Vijay Kumar, J. S. Bois, F. Jülicher, S. W. Grill, *Phys. Rev. Lett.* **2014**, 112:208101.
- [71] M. Mayer, M. Depken, J. S. Bois, F. Jülicher, S. W. Grill, *Nature* **2010**, 467:617.
- [72] G. Salbreux, J. Prost, J. F. Joanny, *Phys. Rev. Lett.* **2009**, 103:058102.
- [73] T. J. Pedley, J. O. Kessler, *Annu. Rev. Fluid Mech.* **1992**, 24:13-358
- [74] A. J. Hillesdon, T. J. Pedley, J. O. Kessler, *Bul. of Math. Biol.* **1995**, 57(2):299-344.
- [75] A. J. Hillesdon, T. J. Pedley, *J. Fluid Mech.* **1996**, 324:23-259.
- [76] A. M. Metcalfe, T. J. Pedley, *J. Fluid Mech.* **1998**, 370:249-270.
- [77] A. Chertock, K. Fellner, A Kurganov, A. Lorz, P. A. Markowich *J. Fluid Mech.* **2012**, 694:155-190.
- [78] A. Darwish, E. F. G. Fang, *Chaos, Solitons and Fractals.* **2004**, 20:609.
- [79] D. Belobo Belobo, T. Meier, *Sci. Rep.* **2018**, 8:3706.
- [80] H. Triki, H. Leblond, D. Mihalache, *Nonlinear Dyn.* **2016**, 86:2115.
- [81] A. V. Mikhailov, *Integrability*, Lect. Notes Phys. 767 (Springer, Berlin Heidelberg 2009).

- [82] R. Hirota *The Direct Method in Soliton Theory*, (Cambridge University Press, New York 2004).
- [83] T. Eckstein, E. Vidal-Henriquez, A. Bae, V. Zykov, E. Bodenschatz, PLoS ONE. **2018**, 13:e0194859.
- [84] R. Karmakar, T. Man-Ho, Y. Haicen Yue, D. Lombardo, A. Karanam, B. A. Camley, A. Groisman, Wouter-Jan Rappel, Phys. Rev. E. **2021**, 103:012402.
- [85] W. Domgno Kuipou, D. Belobo Belobo, A. Mohamadou, Eur. Phys. J. Plus. **2021**, 136:701.
- [86] A. Bhowmik, Wouter-Jan Rappel, H. Levine, Phys. Biol. **2016**, 13:016002.
- [87] M. Kærn, M. Menzinger, J. Phys. Chem. B. **2002**, 14:3751.
- [88] E. A. Ermakova, E. E. Shnol, M. A. Panteleev, A. A. Butylin, V. Volpert, F. I. Ataullakhanov, PloS One. **2009**, 2:4.
- [89] M. Leconte, J. Martin, N. Rakotomalala, D. Salin, Y. Yortsos, J. Chem. Phys. **2004**, 16:7314.
- [90] K. Ishihara, P. A. Nguyen, M. Waehr, A. C. Groen, C. M. Field, T. J. Mitchison. Philos. Trans. R. Soc. Lond. B. Biol. Sci. **2014**, 369.
- [91] M. J. Ablowitz, H. Segur, J. Fluid Mech. **1979**, 92:691-715
- [92] Y. B. Liu, C. Qian, D. Mihalache, J. S. He, Nonlinear Dynam. **2019**, 95:839-857.
- [93] N. Akhmediev, A. Ankiewicz, M. Taki, Physics Letters A. **2009**, 373:675-678.
- [94] N. Akhmediev, J. M. Soto-Crespo, A. Ankiewicz, Physics Letters A. **2009**, 373:2137-2145.
- [95] N. Akhmediev, A. Ankiewicz, J. M. Soto-Crespo, J. M. Dudley, Physics Letters A. **2011**, 375:541-544.
- [96] W. P. Zhong, M. R. Belic, T. Huang Phys. Rev. E. **2013**, 87:065201.
- [97] A. Sokolov, R. E. Goldstein, F. I. Feldchtein, I. S. Aranson, Phys. Rev. E. **2009**, 80:031903.


---

# List of publications

1. **W. Domgno Kuipou**, D. Belobo Belobo, A. Mohamadou, "New traveling waves for a  $(2 + 1)$ -dimensional chemotactic system with uniform flow" Eur. Phys. J. Plus (2021) 136:701.
  2. **W. Domgno Kuipou**, A. Mohamadou, E. Kengne "Cellular transport through nonlinear mechanical waves in fibrous and absorbing biological tissues." Chaos, Solitons and Fractals (2021) 152:111321.
  3. **W. Domgno Kuipou**, D. Belobo Belobo, A. Mohamadou, H. P. Ekobena Fouda "Step, dip, and bell-shape traveling waves in a  $(2 + 1)$ -chemotaxis model with traction and long-range diffusion" Eur. Phys. J. Plus (2022)
  4. **W. Domgno Kuipou**, A. Mohamadou, "Management of invasive cells in soft biological tissues through modulated nonlinear excitations: Long-range effects." Communications in Nonlinear Science and Numerical Simulation (2022) 110:106360.
  5. **W. Domgno Kuipou**, A. Mohamadou "Engineering of nonlinear breathing structures in an extended chemotaxis-fluid model." Chaos Solitons and Fractals (To be published).
-



# Step, dip, and bell-shape traveling waves in a $(2 + 1)$ -chemotaxis model with traction and long-range diffusion

W. Domgno Kuipou<sup>1,2,a</sup> , D. Belobo Belobo<sup>1,2,3</sup>, A. Mohamadou<sup>4</sup>, H. P. Ekobena Fouda<sup>1,2</sup>

<sup>1</sup> Laboratory of Biophysics, Department of Physics, Faculty of Science, University of Yaounde I, P.O. Box 812, Yaounde, Cameroon

<sup>2</sup> African Centre for Advanced Studies, P.O. Box 4477, Yaounde, Cameroon

<sup>3</sup> Department of Mathematics and Physical Sciences, National Advanced School of Engineering of Yaounde, University of Yaounde I, P.O. Box 8390, Yaounde, Cameroon

<sup>4</sup> National Advanced School of Engineering of Maroua, University of Maroua, P.O. Box 46, Maroua, Cameroon

Received: 12 August 2021 / Accepted: 15 February 2022

© The Author(s), under exclusive licence to Società Italiana di Fisica and Springer-Verlag GmbH Germany, part of Springer Nature 2022

**Abstract** In this paper, a new  $(2 + 1)$ -dimensional chemotaxis model is introduced, the focus being the understanding of influences of cooperative mechanisms from traction forces, long-range diffusion to chemotaxis on the dynamical characteristics of waves and their transport. Applying the F-expansion method, three families of new traveling wave solutions of bacterial density and chemoattractant concentration are constructed, including step, dip, and bell-shape wave profiles. The dependence of the conditions of existence of our solutions with respect to the model parameters is fully clarified. We found that traction and long-range diffusion slow down the waves and entail the transport of a small number of particles. Surprisingly, the long-range diffusion increases the thickness of the wave but does not alter its magnitude. Among families of solutions constructed, dip waves travel faster may be used to explain fast coordination among particles. As they support the transport of large amounts of cells, step waves could explain the transport of particles in high dense media. Intensive numerical simulations corroborate with a pretty much good accuracy our theoretical analysis, confirming the robustness of our predictions. Traction and long-range diffusion deeply affect the wave dynamics, they must be taken into account for a better understanding of chemotaxis systems.

## 1 Introduction

Studies on the dispersal of active particles have shed light on different mechanisms associated with their response when placed under various mechanical and/or chemical conditions. An example of active particles is given by a distribution of bacteria in a uniform flow whose collective motion allows them to spread and colonize outward regions. Depending on their sensitivity and acquaintance with the local environment composition, such a collective motion has been characterized qualitatively and quantitatively [1–14]. When placed in chemical fields with attractive properties, ciliated particles, for example, synchronize their flagella's rotation, the resulting quasi-linear run allows them to efficiently reach the core of higher chemical concentrations. Such a collective behavior termed chemotaxis has been widely studied since the pioneering work of Adler [1]. Besides the importance of chemotaxis in the cellular realm where it plays a major role in fertilization [2–4], intercellular communication [5,6], wound repair [2,3], and pattern formation [3,7], it has also been reported in animal and insect ecology [4], large-scale collective behavior [1,8–14] and synchronization processes [5,8]. Though the literature is well furnished when it comes to chemotaxis, various issues associated with a combination of chemical and mechanical constraints cells might feature in their natural habitats that has just recently started receiving attention [10,12–22]. It is known that the latter interactions may lead to interesting holistic dynamical behaviors that to the best of our knowledge remain to be fully understood.

The collective dynamic entailed by chemotaxis indicates that bacteria are social entities and are therefore prone to communicate with one another. In some extreme cases, communication is made possible through chemoattractant production. The latter is responsible for the attraction of other distant entities. This phenomenon significantly different from chemotaxis at the molecular level can be termed auto-chemotaxis and was recently observed through lenses of experimental settings [5]. Though the authors were not able to provide full and satisfying explanations of its specific contribution at the local level, they showed that it has the potential of biasing the primary chemotactic signal at the onset of bacterial motion. Depending on the strength of the bias, cells rearrange themselves and exhibit a different moving pattern. Independently, a theoretical approach to the question was addressed to demonstrate that auto-chemotaxis is a factor of instability [15,16], while friction and proliferation in the system have stabilizing effects. Such an antagonism is at the onset of pattern selection with a well-defined wave number [15]. On the other side, the fact that cells can become attractive by producing their own chemoattractant implies that in a given population, certain cells are more

<sup>a</sup> e-mail: [dkwilliam90@gmail.com](mailto:dkwilliam90@gmail.com) (corresponding author)

chemotactic than others, therefore may exert distant actions like traction forces. In cancer invasion for example, those distant actions allow cancerous melanocytic cells to escape tumorous regions and undergo metastasis [17]. In the dynamic of micro-swimmers assembly, distant traction forces were also reported. This means that the existence of traction forces might be a common feature in reactive systems, especially for higher active particles densities [16].

Apart from interspecies communication mechanisms, cells are also involved in hydrodynamic interactions which ensure an active transport of diffusive and non-active components over long distances. In aqueous media, swimming patterns of cells that consist of pulling, pushing, gliding, and scrawling imply that cells interactions with fluids constituents may lead to a variety of spatiotemporal patterns. Experimental and theoretical evidence showed that bacteria are collectively transported through wavy structures like solitary pulses [18–20, 24–30]. Furthermore, other experimental findings suggest that hydrodynamic interactions coupled to the chemoattractant concentration gradient may guide traveling bands of bacteria at a constant speed [18–20]. Therefore, the inclusion of advection rate while modeling chemotactic behaviors is expected to substantially improve our knowledge of the system. Mathematical modeling in this view requires to couple the Keller–Segel chemotaxis model to Navier–Stokes equations [16, 21–23]. Another simple and realistic approach consists at collecting contributions emanating from stresses and traction cells exert upon each other in addition to the uniform flow coming from the background field within which cells are immersed in. In fact, recent evidences demonstrate that the collective motion of cells in a fluid generates flows mediated by the hydrodynamics interactions in between them [10, 22, 23]. It is therefore natural to wonder how both chemotaxis and traction forces contribute to producing structures like traveling waves observed from the Keller–Segel formulation for chemotaxis [24]. The latter model initially introduced to describe slime mold showed drawbacks and later experimental findings suggest that the issues may be circumvented when cells create their own chemoattractant gradient [25]. This implies that the collective motion of cells modifies the average flow of the medium, which in turn affects cellular response. In this way, cells' response to an excitatory source ceases to be proportional to the concentration gradient of the excitation. Another way of looking at the problem consists at considering the nonlocal character of bacterial response [3, 26, 31] which is responsible for the nucleation of long-range diffusion. In this work, we introduce a mathematical model that extends the existing ones, with the aim to fill in the above-mentioned gaps. To this end, we consider a chemotactic system where long- and short-range diffusion, chemotaxis, traction forces, cellular proliferation, and uniform advection are accounted for; dynamical behaviors of new traveling waves shall be investigated.

The rest of the manuscript is organized as follows. In Sect. 2 we derive the model and construct its analytical solutions. Secondly, we evaluate the effects of key parameters of the system on the proposed solutions and then make some predictions on the dynamical behavior of the system. In Sect. 3, numerical simulations are performed to ascertain our predictions. Some biological implications are discussed. Section 4 concludes the paper.

## 2 Main results and discussion

### 2.1 The model

In this description of collective behavior, we are interested in a bacterial population in a two-dimensional frame, immersed in a fluid experiencing a uniform flow. Besides the chemotactic velocity and the medium flow rate, the bulk bacterial motion also has a drift-velocity contribution emanating from the stress cells exert upon each other. Recent studies show that many energy sources simultaneously influence cells motion [30], but in the present paper, we consider the case where bacteria are in the presence of only one chemoattractant source. The timescale is large enough such that cells undergo proliferation, the nonlocal response ensures long-distance communications, and the cellular protrusion is also accounted for. The resulting model is an extended set of coupled partial differential equations that reads [3, 24, 28–31]

$$\frac{\partial c}{\partial t} + \nabla \cdot (c\delta) = D_3 \nabla^2 n + \frac{k_0 n}{k_1 + k_2 n^2} - \beta n c. \quad (1a)$$

$$\frac{\partial n}{\partial t} + \nabla \cdot (n\delta) = D_1 \nabla^2 n - D_2 \nabla^4 n - \chi_0 \nabla \cdot (n \nabla c) + r n (\sigma - n), \quad (1b)$$

In Eq. (1),  $t$  is the time variable in seconds (s),  $\nabla = \left( \frac{\partial}{\partial x}, \frac{\partial}{\partial y} \right)^T$  is two-dimensional gradient,  $\nabla^2 = \frac{\partial^2}{\partial x^2} + \frac{\partial^2}{\partial y^2}$ , the two-dimensional Laplacian.  $n$  is the bacterial density, while  $c$  is the chemoattractant concentration.  $D_1$  and  $D_3$  are short-range diffusion while  $D_2$  stands for the long-range diffusion of bacteria.  $\chi_0$  represents the chemotaxis strength,  $r$  is the proliferation rate of cells,  $\sigma$ , the medium's carrying capacity. The term  $\frac{k_0 n}{k_1 + k_2 n^2}$  describes the chemoattractant production. Numerical values of  $k_0, k_1, k_2$  are not known to the best of our knowledge.  $\beta$  is the chemoattractant consumption's rate.  $\delta = (\delta_x, \delta_y)^T$  is the two-dimensional bulk velocity field of the system. Recent studies of bacterial migration in a confined one-dimensional racetrack showed nucleation of strong flows emanating from cells closes to channel boundaries [14]. These flows were capable of swerving the bulk dynamic of cells placed far from channel walls. In this sense, the bulk velocity field in the system comprises an active part generated by the collective motion of cells and a passive part emanating from the perturbations of the medium within which cells are immersed. We propose a velocity field in the medium with the form



$$\delta = \nabla_0 + \nabla H(n, c), \quad \text{with } \delta_0 = \delta_{0_x} + \delta_{0_y}, \quad \text{and } H(n, c) = \frac{\tau_0 n}{1 + \lambda n}. \tag{2}$$

$\delta_{0_x}$ , and  $\delta_{0_y}$  are components of the uniform flow imposed by the medium within which cells and the chemoattractant are immersed. The function  $H$  takes into account the effects of traction forces generated by active particles present in the medium (here the bacterial cells).  $\tau_0$  is the maximum traction force ensuring a finite velocity at higher cellular density when the population increases in a quasi-dilute medium.  $\lambda$  measures the velocity decrease due to a higher density of cellular aggregation. In the thermodynamic limit, this choice of  $H$  ensures that the velocity remains finite both at low and high densities. The current model diverges from the classical Keller–Segel models [3,24,29–31], since the chemotactic velocity drift, as well as wave profiles, remains bounded. This further sets the stepping stone to find relevant physical solutions for the model under consideration. In that endeavor, we assume a quasi-dilute medium, corresponding to  $\lambda \rightarrow 0$ , meaning that hydrodynamic properties of bacteria are weak but non-null. Under this configuration, experimental studies revealed that one might still expect complicated patterns [7,32], and bacterial distribution per unit area may be very small but non-null. Hence, only a small amount of cells are expected to contribute to chemoattractant production, a situation entailing  $\frac{k_2 n^2}{k_1} \ll 1$ . Considering lower power series of the saturating term from Eq. (1b) and plugging Eq. (2) into Eq. (1) yield the (2 + 1)-modified extended chemotaxis model

$$\frac{\partial n}{\partial t} + \nabla \cdot (n\delta) = D_1 \nabla^2 n - D_2 \nabla^4 n - \tau_0 \nabla \cdot (n\nabla n) - \chi_0 \nabla \cdot (n\nabla c) + rn(\sigma - n), \tag{3a}$$

$$\frac{\partial c}{\partial t} + \nabla \cdot (c\delta_0) = D_3 \nabla^2 n - \tau_0 \nabla \cdot (c\nabla n) + \beta_1 n - \beta_3 n^3 - \beta nc, \tag{3b}$$

$\beta_1 = \frac{k_0}{k_1}$ ,  $\beta_3 = \frac{k_0 k_2}{k_1^2}$  are arbitrary real constants and are also not known as the  $k'_j$ s. Nevertheless, they will be chosen in accordance with biological relevance.  $\beta_1$ ,  $\beta_3$  are referred to as the new chemoattractant production rate parameters. More than a simple reaction–diffusion–advection process, the system of Eq. (3) is dynamically interesting. It takes into consideration simple and nonlinear cross diffusion, in addition to incorporating two active transport mechanisms, namely chemotaxis and traction. Though traction has been the subject of intensive experimental studies [5,15,16,25], its contribution has not yet been mathematically formulated in chemotactic systems, to the best of our knowledge. Model Eq. (3) indicates that taking into account traction forces enhances both cellular and chemical displacement toward one another. In this sense, Eq. (3) can be used to explain a broad range of phenomena in systems made of composite materials. For example, it may describe the spreading behavior of two chemotactic subpopulations of bacteria moving toward each other with different velocities. Such a differential velocity may lead to rich phenomena like instabilities and new patterns formation just to name a few. We propose Eq. (3) as a viable generalized chemotaxis model that incorporates several aspects of bacterial collective motion not discussed in previous models [3,15,28–31,33–42].

### 2.2 Analytical solutions through the extended F-expansion method

The F-expansion method is a scheme used to solve nonlinear ordinary differential equations. In order to solve Eq. (3) using an extended F-expansion method, the traveling wave variable  $\xi = kx + ly - \omega t$  is assumed. In the latter transformation,  $\frac{1}{k}$  and  $\frac{1}{l}$  are the wave widths along the  $x$ - and  $y$ - directions, respectively,  $\omega$  the wave velocity taken in the laboratory frame. Thus, Eq. (3) become

$$D_2 K^2 \frac{d^4 n}{d\xi^4} - D_1 K \frac{d^2 n}{d\xi^2} + \Omega_0 \frac{dn}{d\xi} + \chi_0 K \frac{d}{d\xi} \left( n \frac{dc}{d\xi} \right) + \tau_0 K \frac{d}{d\xi} \left( n \frac{dn}{d\xi} \right) - rn(\sigma - n) = 0, \tag{4a}$$

$$-D_3 K \frac{d^2 c}{d\xi^2} + \Omega_0 \frac{dc}{d\xi} + \tau_0 K \frac{d}{d\xi} \left( c \frac{dn}{d\xi} \right) - \beta_1 n + \beta nc + \beta_3 n^3 = 0, \tag{4b}$$

with

$$K = k^2 + l^2, \quad \text{and } \Omega_0 = \delta_{0_x} k + \delta_{0_y} l - \omega.$$

Solutions of Eq. (4) are sought for a chemoattractant concentration of the form

$$c(\xi) = G(n(\xi), \xi). \tag{5}$$

Inserting Eq. (5) into Eq. (4) leads to the fourth- order nonlinear ordinary differential equation

$$D_2 K^2 \frac{d^4 n}{d\xi^4} + \chi_0 \left( \frac{\Omega_0}{\chi_0 - \tau_0} \right)^2 + \left[ \frac{\beta \chi_0 \Omega_0 \xi}{K(\chi_0 - \tau_0)^2} + \frac{\beta}{\tau_0} \frac{D_1(\chi_0 - \tau_0) + \tau_0 D_3}{\chi_0 - \tau_0} - r\sigma + \beta_1 \right] n + \left( r + \frac{\beta \tau_0}{\chi_0 - \tau_0} \right) n^2 - \beta_3 n^3 = 0, \tag{6}$$

provided that

$$c(\xi) = -\frac{\tau_0 n(\xi) + D_3}{\chi_0 - \tau_0} - \frac{\Omega_0 \chi_0 \xi}{K(\chi_0 - \tau_0)^2} - \frac{D_1}{\tau_0}. \tag{7}$$

We restrict ourselves to the case where  $\omega = k\delta_{0x} + l\delta_{0y}$ , (which implies  $\Omega_0 = 0$ ) to avoid nonphysical solutions that diverge at infinity. Such a choice is also consistent with recent numerical and theoretical results presented in [19,42,43] where the authors proved that the wave velocity in the Martiel–Golbeter chemotaxis model (for *Dictyostelium discoideum* dynamics) varies linearly with the imposed flow. On the other hand, Eq. (7) tells that variations of chemoattractant and bacterial waves are directly linked; hence, the corroborating results are obtained in the analysis of chemotactic *Dictyostelium* colonies [40]. The same study showed that by increasing background level, the directed propagation can be suppressed, due to memory inactivation. In other words, cells can be swept or their direction propagation swerved, enforcing the conclusion that medium flow rate has the potential of favoring the rise of progressive or regressive waves. In the present study, the transition from forward to backward propagation is attained when parameters are chosen such that the critical line  $\frac{\delta_{0x}}{\delta_{0y}} = \frac{-l}{\sqrt{K-l^2}}$  corresponding to stationary patterns is violated. In the latter configuration, our solutions may be either progressive ( $\omega > 0$ ) or regressive ( $\omega < 0$ ). The former is responsible for faster bacterial colonization of unoccupied regions, while the latter may be the signature of backward waves. In the flux limiting cases, the backward waves in a chemotactic system were shown to be responsible for a population saturation in a stable state accompanied by a transition toward unstable modes [44].

Physically acceptable solutions of Eq. (3) correspond to positive bacterial and chemoattractant wave amplitudes. In addition, both bacterial densities and chemoattractant concentrations must remain finite; hence, using Eq. (7) and assuming that  $n(\xi) \geq 0$ , the finiteness of the chemoattractant concentration implies the following restrictions

$$\tau_0 > \chi_0, \quad \tau_0 \neq 0, \quad c(\xi) \geq \frac{D_3}{\tau_0 - \chi_0} - \frac{D_1}{\tau_0} = c_{\min}, \quad D_1 \leq \frac{D_3\tau_0}{\tau_0 - \chi_0}. \tag{8}$$

Before proceeding further, Eq. (8) provides important characteristics about the solutions to be found below. The traction forces must be non-null and greater than the chemotaxis strength implying that the experimenter must choose an appropriate chemoattractant substance that is consistent with Eq. (8). Moreover, there exists a critical chemoattractant concentration that completely depends on system parameters  $(\tau_0, \chi_0, D_1, D_3)$ , below which the corresponding solutions are unphysical. The solutions will be viable only if the chemoattractant concentration is at least equal to  $c_{\min}$ , a situation which means that chemoattractant diffusion rate is always greater or equal than a minimal value  $D_3 \geq D_1 \left(1 - \frac{\chi_0}{\tau_0}\right) = D_{3\min}$ . The fact that  $D_1 > D_{3\min}$  implies bacteria diffuse faster than the minimum chemoattractant diffusion rate that is necessary to generate traveling chemical and bacterial waves. Furthermore, the minimal chemoattractant diffusion rate  $D_{3\min}$  broadly depends on the ratio between chemotaxis strength and traction forces, enforcing that the latter substantially modify the behavior of chemotactic systems. Taking into account the above considerations, Eqs. (6), (7) become

$$D_2 K^2 \frac{d^4 n}{d\xi^4} + \sigma_1 n + \sigma_2 n^2 - \beta_3 n^3 = 0, \tag{6'}$$

$$c(\xi) = c_{\min} - \frac{\tau_0 n(\xi)}{\chi_0 - \tau_0}, \tag{7'}$$

where

$$\sigma_1 = \beta_1 - \beta c_{\min} - r\sigma, \quad \sigma_2 = r + \frac{\beta\tau_0}{\chi_0 - \tau_0}.$$

The next step of the F-expansion method consists at looking to solutions of Eq. (6') in a polynomial expansion [45–50]. We determine the order of the expansion by balancing the higher-order derivative with the higher-order nonlinear terms in Eq. (6'). Doing so permits a finite polynomial expansion

$$n = a_0 + a_1 F(\xi) + a_2 F(\xi)^2, \tag{9}$$

where  $a_0, a_1, a_2$  are real constants to be determined later. The function  $F(\xi)$  is a solution of the auxiliary equation

$$\left(\frac{dF(\xi)}{d\xi}\right)^2 = P_4 F(\xi)^4 + P_3 F(\xi)^3 + P_2 F(\xi)^2 + P_1 F(\xi) + P_0. \tag{10}$$

$P_4, P_3, P_2, P_1, P_0$  are real constants. Solutions of Eq. (10) may be found in [27,45–50]. As explained in [45–50], solutions of Eq. (10) admit unbounded and localized structures. The latter ones are excellent candidates for describing real physical phenomena. We continue the methodology by plugging Eq. (9) into Eq. (6') and making use of Eq. (10). Further, we collect all the coefficients of power of  $F$  ( $F^m(\xi)$ ,  $m = 0, 1, 2, 3, 4$ ), and setting each coefficients to zero yields a set of algebraic equations that we solve for the variables  $a_0, a_1, a_2, K, \beta_3$  and obtain different families of solutions presented below.

*Family A:*  $P_0 = P_1 = P_3 = 0, P_2 > 0, P_4 < 0, F(\xi) = \sqrt{-\frac{P_2}{P_4}} \cosh^{-1}(\sqrt{P_2}\xi)$

$$a_0 = 0, \quad a_1 = 0, \quad a_2 = \frac{15\sigma_1 P_4}{2\sigma_2 P_2}, \quad K = \frac{1}{4P_2} \sqrt{-\frac{\sigma_1}{D_2}}, \quad \beta_3 = -\frac{2\sigma_2^2}{15\sigma_1}, \tag{11a}$$

$$\begin{aligned}
 a_0 &= \frac{\sigma_1(3 + \epsilon\sqrt{105})}{\sigma_2(7 + \epsilon\sqrt{105})}, & a_1 &= 0, & a_2 &= -\frac{3\sigma_1 P_4(35 + \epsilon\sqrt{105})}{28P_2\sigma_2}, \\
 K &= \frac{1}{4P_2} \sqrt{\frac{\sigma_1(7 + \epsilon\sqrt{105})}{14D_2}}, & \beta_3 &= -\frac{2\sigma_2^2(7 + \epsilon\sqrt{105})}{3\sigma_1(19 + \epsilon\sqrt{105})}.
 \end{aligned}
 \tag{11b}$$

Family B:  $P_0 = P_1 = P_3 = 0, P_2 < 0, P_4 > 0, F(\xi) = \sqrt{-\frac{P_2}{P_4}} \sec(\sqrt{-P_2}\xi)$

$$a_0 = 0, \quad a_1 = 0, \quad a_2 = \frac{15\sigma_1 P_4}{2\sigma_2 P_2}, \quad K = -\frac{1}{4P_2} \sqrt{-\frac{\sigma_1}{D_2}}, \quad \beta_3 = -\frac{2\sigma_2^2}{15\sigma_1},
 \tag{12a}$$

$$\begin{aligned}
 a_0 &= \frac{\sigma_1(3 + \epsilon\sqrt{105})}{\sigma_2(7 + \epsilon\sqrt{105})}, & a_1 &= 0, & a_2 &= -\frac{3\sigma_1 P_4(35 + \epsilon\sqrt{105})}{28P_2\sigma_2}, \\
 K &= -\frac{1}{4P_2} \sqrt{\frac{\sigma_1(7 + \epsilon\sqrt{105})}{14D_2}}, & \beta_3 &= -\frac{2\sigma_2^2(7 + \epsilon\sqrt{105})}{3\sigma_1(19 + \epsilon\sqrt{105})}.
 \end{aligned}
 \tag{12b}$$

Family C:  $P_0 = \frac{P_2^2}{4P_4}, P_1 = P_3 = 0, P_2 < 0, P_4 > 0, F(\xi) = \sqrt{-\frac{P_2}{2P_4}} \tanh\left(\sqrt{-\frac{P_2}{2}}\xi\right)$

$$a_0 = -\frac{15\sigma_1}{2\sigma_2}, \quad a_1 = 0, \quad a_2 = \frac{15\sigma_1 P_4}{2\sigma_2 P_2}, \quad K = -\frac{1}{2P_2} \sqrt{-\frac{\sigma_1}{D_2}}, \quad \beta_3 = -\frac{2\sigma_2^2}{15\sigma_1}
 \tag{13a}$$

$$\begin{aligned}
 a_0 &= -\frac{\sigma_1(543 + \epsilon 53\sqrt{105})}{\sigma_2(133 + \epsilon 13\sqrt{105})}, & a_1 &= 0, & a_2 &= \frac{30\sigma_1 P_4(11 + \epsilon\sqrt{105})}{\sigma_2 P_2(35 + \epsilon 3\sqrt{105})}, \\
 K &= -\frac{1}{2P_2} \sqrt{\frac{\sigma_1(7 + \epsilon\sqrt{105})}{14D_2}}, & \beta_3 &= -\frac{2\sigma_2^2(133 + \epsilon 13\sqrt{105})}{3\sigma_1(113 + \epsilon 11\sqrt{105})}.
 \end{aligned}
 \tag{13b}$$

Family D:  $P_0 = \frac{P_2^2}{4P_4}, P_1 = P_3 = 0, P_2 > 0, P_4 < 0, F(\xi) = \sqrt{-\frac{P_2}{2P_4}} \tan\left(\sqrt{\frac{P_2}{2}}\xi\right)$

$$a_0 = -\frac{15\sigma_1}{2\sigma_2}, \quad a_1 = 0, \quad a_2 = \frac{15\sigma_1 P_4}{2\sigma_2 P_2}, \quad K = \frac{1}{2P_2} \sqrt{-\frac{\sigma_1}{D_2}}, \quad \beta_3 = -\frac{2\sigma_2^2}{15\sigma_1}
 \tag{14a}$$

$$\begin{aligned}
 a_0 &= -\frac{\sigma_1(543 + \epsilon 53\sqrt{105})}{\sigma_2(133 + \epsilon 13\sqrt{105})}, & a_1 &= 0, & a_2 &= \frac{30\sigma_1 P_4(11 + \epsilon\sqrt{105})}{\sigma_2 P_2(35 + \epsilon 3\sqrt{105})}, \\
 K &= \frac{1}{2P_2} \sqrt{\frac{\sigma_1(7 + \epsilon\sqrt{105})}{14D_2}}, & \beta_3 &= -\frac{2\sigma_2^2(133 + \epsilon 13\sqrt{105})}{3\sigma_1(113 + \epsilon 11\sqrt{105})}.
 \end{aligned}
 \tag{14b}$$

Family E:  $P_0 = \frac{1}{4}, P_1 = P_3 = 0, P_2 = \frac{1}{2}, P_4 = \frac{1}{4}, F(\xi) = \sin(\xi) + \epsilon \cos(\xi)$

$$\begin{aligned}
 a_0 &= -\frac{8\sigma_1(111 + 11\epsilon\sqrt{105})}{\sigma_2(203 + 23\epsilon\sqrt{105})}, & a_1 &= 0, & a_2 &= -\frac{60\sigma_1(49 + 5\epsilon\sqrt{105})}{7\sigma_2(85 + 9\epsilon\sqrt{105})}, \\
 K &= \sqrt{\frac{\sigma_1(7 + \epsilon\sqrt{105})}{14D_2}}, & \beta_3 &= -\frac{2\sigma_2^2}{15\sigma_1}
 \end{aligned}
 \tag{15}$$

Family F:  $P_0 = P_1 = 0, P_2 > 0, P_3 = 2\epsilon\sqrt{P_2P_4}, P_4 > 0, F(\xi) = \frac{\epsilon\sqrt{\frac{P_2}{P_4}}}{\cosh\left(\frac{\sqrt{P_2}}{2}\xi\right)\left[\epsilon\sinh\left(\frac{\sqrt{P_2}}{2}\xi\right) - \cosh\left(\frac{\sqrt{P_2}}{2}\xi\right)\right]}$

$$a_0 = -\frac{\sigma_1(\sqrt{105} + 21)}{14\sigma_2}, \quad a_1 = \epsilon\sqrt{\frac{P_4}{P_2}}\frac{3\sigma_1(35 - \sqrt{105})}{7\sigma_2}, \quad a_2 = -\frac{3\sigma_1P_4(35 - \sqrt{105})}{7P_2\sigma_2}$$

$$\beta_3 = -\frac{28\sigma_2^2}{3\sigma_1(7 + 3\sqrt{105})} \quad K = \frac{1}{P_2}\sqrt{-\frac{\sigma_1(\sqrt{105} - 7)}{14D_2}}, \tag{16a}$$

$$a_0 = 0, \quad a_1 = \frac{30\sigma_1\sqrt{P_2P_4}}{\sigma_2P_2}, \quad a_2 = \frac{30\sigma_1P_4}{\sigma_2P_2}, \quad K = \frac{\sqrt{-D_2\sigma_1}}{\sigma_2P_2}, \quad \beta_3 = -\frac{2\sigma_2^2}{15\sigma_1} \tag{16b}$$

Family G:  $P_0 = P_1 = 0, P_2 < 0, P_3 = 2\epsilon\sqrt{P_2P_4}, P_4 > 0, F(\xi) = \frac{\epsilon\sqrt{\frac{-P_2}{P_4}}}{\cos\left(\frac{\sqrt{P_2}}{2}\xi\right)\left[\epsilon\sin\left(\frac{\sqrt{P_2}}{2}\xi\right) + \cos\left(\frac{\sqrt{P_2}}{2}\xi\right)\right]}$

$$a_0 = -\frac{\sigma_1(\sqrt{105} + 21)}{14\sigma_2}, \quad a_1 = \epsilon\sqrt{\frac{P_4}{P_2}}\frac{3\sigma_1(35 - \sqrt{105})}{7\sigma_2}, \quad a_2 = -\frac{3\sigma_1P_4(35 - \sqrt{105})}{7P_2\sigma_2}$$

$$\beta_3 = -\frac{28\sigma_2^2}{3\sigma_1(7 + 3\sqrt{105})} \quad K = -\frac{1}{P_2}\sqrt{-\frac{\sigma_1(\sqrt{105} - 7)}{14D_2}}, \tag{17a}$$

$$a_0 = 0, \quad a_1 = \frac{30\sigma_1\sqrt{P_2P_4}}{\sigma_2P_2}, \quad a_2 = \frac{30\sigma_1P_4}{\sigma_2P_2}, \quad K = -\frac{\sqrt{-D_2\sigma_1}}{\sigma_2P_2}, \quad \beta_3 = -\frac{2\sigma_2^2}{15\sigma_1} \tag{17b}$$

For the sake of simplicity, the parameters  $\sigma_1, \sigma_2$  and  $\epsilon$  appearing in Eqs. (11)–(17) have been defined as:

$$\sigma_1 = \beta_1 - r\sigma - \beta c_{\min} \neq 0, \quad \tau_0 \neq \chi_0, \quad \text{and} \quad \epsilon = \pm 1.$$

### 2.3 Existence and dynamical behavior of solutions Eqs. (11)–(17)

A straightforward analysis of Eqs. (11)–(17) shows that bacterial and chemoattractant solutions exist if  $D_2 \neq 0, \sigma_1 < 0, \sigma_2 > 0$  which lead to the constraints

$$\beta_1 < r\sigma + \beta c_{\min} = \beta_{1\max}, \quad \text{and} \quad r > \frac{\beta}{D_3}(\tau_0 c_{\min} + D_1) = r_{\min}. \tag{18}$$

The first inequality of Eq. (18) proves that the linear chemoattractant production rate  $\beta_1$  possesses a maximum value given by  $r\sigma$  (in the absence of chemoattractant production) and linearly increases with chemoattractant consumption rate  $\beta$ . Though the F-expansion method allows a large number of analytical solutions for the auxiliary equation Eq. (10), we just keep above families of solutions that are physically relevant as they satisfy the existence conditions Eqs. (8) and (18). The fact that the maximum chemoattractant production rate depends on the nominal chemoattractant consumption rate enforces to hypothesize the existence of a critical chemoattractant production–consumption line that may impede the wave generation process if violated. The second inequality of Eq. (18) shows that our system admits a minimal proliferation rate always greater than the threshold value  $r_{\min}$ . Equations (8) and (18) describe the general conditions of the existence of bacterial and chemoattractant concentration waves but, do not provide any details on dynamical properties. We discuss below some dynamical properties of both bacterial and chemoattractant waves such as their profiles, velocities, amplitudes, and thicknesses, and we analyze effects of  $\tau_0, \chi_0, D_2, D_1,$  and  $\beta$ . To this end, we take  $\beta_1 = \frac{\beta_{1\max}}{10}, r = r_{\min} + r_0, r_0 = 1.69 \times 10^{-9}$  being the proliferation rate given in [3]. Table 1 displays the parameters values used in our analyses.

#### 2.3.1 Bell-shaped bacterial and chemoattractant: family A

The bell-shaped profile corresponds to Family A. Using parameters of Eq. (11a), explicit analytical expressions are given by

$$n(x, y, t) = -\frac{15\sigma_1}{2\sigma_2} \left( \frac{1}{\cosh[\sqrt{P_2}(kx + ly - \omega t)]} \right)^2, \tag{19a}$$

$$c(x, y, t) = c_{\min} - \frac{15\sigma_1\tau_0}{2\sigma_2(\chi_0 - \tau_0)} \left( \frac{1}{\cosh[\sqrt{P_2}(kx + ly - \omega t)]} \right)^2, \tag{19b}$$

**Table 1** Parameter network values

Parameters	Values	References
$D_1$	$8.9 \times 10^{-6} \text{ cm}^2 \text{ s}^{-1}$	[3, 19, 29, 30]
$D_2$	$1.69 \times 10^{-9} \text{ cm}^4 \text{ s}^{-1}$	N/A
$D_3$	$4 \times 10^{-6} \text{ cm}^2 \text{ s}^{-1}$	[3, 19, 29, 30]
$\chi_0$	$6.49 \times 10^{-5} \text{ cm}^2 \text{ M}^{-1} \text{ s}^{-1}$	[3, 19, 29, 30]
$\tau_0$	$1.62 \times 10^{-3} \text{ cm}^2 \text{ s}^{-1} \text{ cell}^{-1}$	N/A
$r_0$	$(1 - 3) \times 10^{-9} \text{ s}^{-1} \text{ cell}^{-1}$	[3]
$\sigma$	$2.4231 \times 10^8 \text{ s}^{-1}$	[3]
$\beta$	$3.5 \times 10^{-8} \text{ s}^{-1} \text{ cell}^{-1}$	[3]
$\delta_{0x}, \delta_{0y}$	$10^{-4} - 10^{-6} \text{ cm s}^{-1}$	[18–20, 29, 30]

where the associated velocity reads:

$$\omega = \delta_{0x} \sqrt{\frac{1}{4P_2} \sqrt{-\frac{\sigma_1}{D_2}} - l^2} + \delta_{0y} l = \omega_{bs}. \tag{20}$$

From Eq. (20), one deduces the existence of minimal/maximal wave velocities

$$\omega_{\min} = 0 \leq \omega \leq \omega_{\max} = \sqrt{\frac{\delta_{0x}^2 + \delta_{0y}^2}{4P_2} \sqrt{-\frac{\sigma_1}{D_2}}},$$

where  $\omega_{\min} = \omega(l = l_{\text{crit}})$  and  $\omega_{\max} = \omega(l = l_0)$ .  $l_{\text{crit}}$  is recovered by solving  $\omega|_{l=l_{\text{crit}}} = 0$ , and the maximum velocity  $\omega_{\max}$  is reached at  $l_0$ . The latter is determined by solving  $\frac{d\omega}{dl}|_{l=l_0} = 0$ ; hence, we have

$$l_{\text{crit}} = \delta_{0x} \sqrt{\frac{\omega_0}{\delta_0^2}}, \quad l_0 = \delta_{0y} \sqrt{\frac{\omega_0}{\delta_0^2}}, \quad \delta_0^2 = \delta_{0x}^2 + \delta_{0y}^2, \quad \omega_0 = \frac{1}{4P_2} \sqrt{-\frac{\sigma_1}{D_2}}.$$

$l_0$  and  $l_{\text{crit}}$  depend on the system parameters, which means the experimenter has the potential of controlling fast or slow wave propagation if he accurately tunes the experimental setups. From Eq. (19)  $n_{\infty_{bs}} = \lim_{\xi \rightarrow \infty} n(x, y, t) \rightarrow 0$  and  $c_{\infty_{bs}} = \lim_{\xi \rightarrow \infty} c(x, y, t) \rightarrow c_{\min}$  which mean that bacterial and chemoattractant wave amplitudes are finite as their associated velocity. This confirms that bell-shaped solutions Eq. (19) are physical objects. The bell-shape profile Eq. (19) is displayed in Fig. 1 at the time  $t = 100$ . Bell-shape waves have been predicted analytically [24, 26–30, 36–38, 42], numerically [16, 19, 28, 30, 36, 40, 43, 51], and experimentally observed [15, 19, 20, 30] in one-dimensional chemotactic systems. Traveling waves in reactive systems are either matter carriers or information conveyors, the bell-shaped profile obtained here may explain collective bands of bacteria usually observed in reactive systems. Its velocity is depicted in panels (c)–(e) of Fig. 1. It is seen that the amplitude of  $\omega_{bs}$  decreases with increasing values of traction and long-range diffusion, respectively (see Fig. 1c–d), meaning that the traction and the long-range diffusion slow down the waves. Conversely, the amplitude of  $\omega_{bs}$  increases with increasing values of  $\chi_0$  implying that the chemotaxis strength accelerates the wave propagation.  $\tau_0$ ,  $D_2$ , and  $\chi_0$  have competing effects on the velocity of the wave. This property may be used in experiments to detect or characterize the waves. In all the cases, the velocity reduces with increasing values of  $l$ , thus thinner waves move faster than wider ones.

Considering the influences of system parameters on the bell-shaped wave, one observes that when long-range diffusion increases (Fig. 2a), the wave thickness widens, hence the cellular distribution occupies a larger spatial domain. At high values of long-range diffusion  $D_2$ , the coordination degree among units of the bacterial population decreases, resulting in a diminution of the global velocity of the aggregation. Such a result is in accordance with the idea that diffusion of particles should break up coordination and communication degree among particles. Wave thickness variations are a common feature in reactive systems as extensively discussed in [19, 42, 51], and its occurrence in the present study signifies that cells do not lose their active properties, but rather rearrange themselves to accommodate chemoattractant concentrations across the medium. In panels (b)–(e) of Fig. 2, wave thickness variations are accompanied by an amplitude variation. Amplitude and thickness increase are observed when traction Fig. 2b and short-range diffusion Fig. 2d increase, while chemotaxis Fig. 2c as well as the chemoattractant consumption rate Fig. 2e decreases. Wave thickness reduction or increase coupled with amplitude variations in systems with uniform flows have also been reported in autocatalytic fronts [52], the Fitz–Hugh–Nagumo model [53], and the Belousov–Zhabotinsky reaction [54, 55]. We propose such a coupled dynamic between wave thickness and amplitude as a tool to slice spatial domains in intervals within which cells activity remains optimized, and above which cellular density drastically reduces.

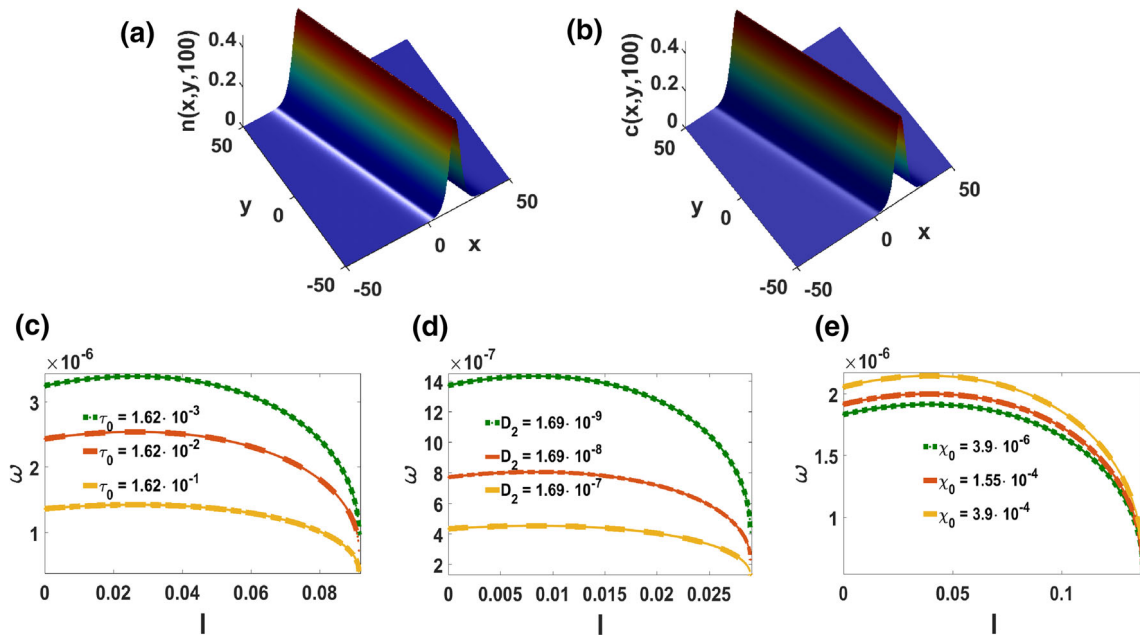


**Fig. 1** Snapshots at  $t = 100$  s of bell-shaped solutions Eq. (19) for density (a) and chemoattractant concentration (b). Wave velocity increases with chemotaxis (e) or when long-range diffusion (d), traction (c) reduce.  $\delta_{0x} = 1.5 \times 10^{-5}$ ,  $\delta_{0y} = 4.5 \times 10^{-4}$ ,  $P_2 = 4$

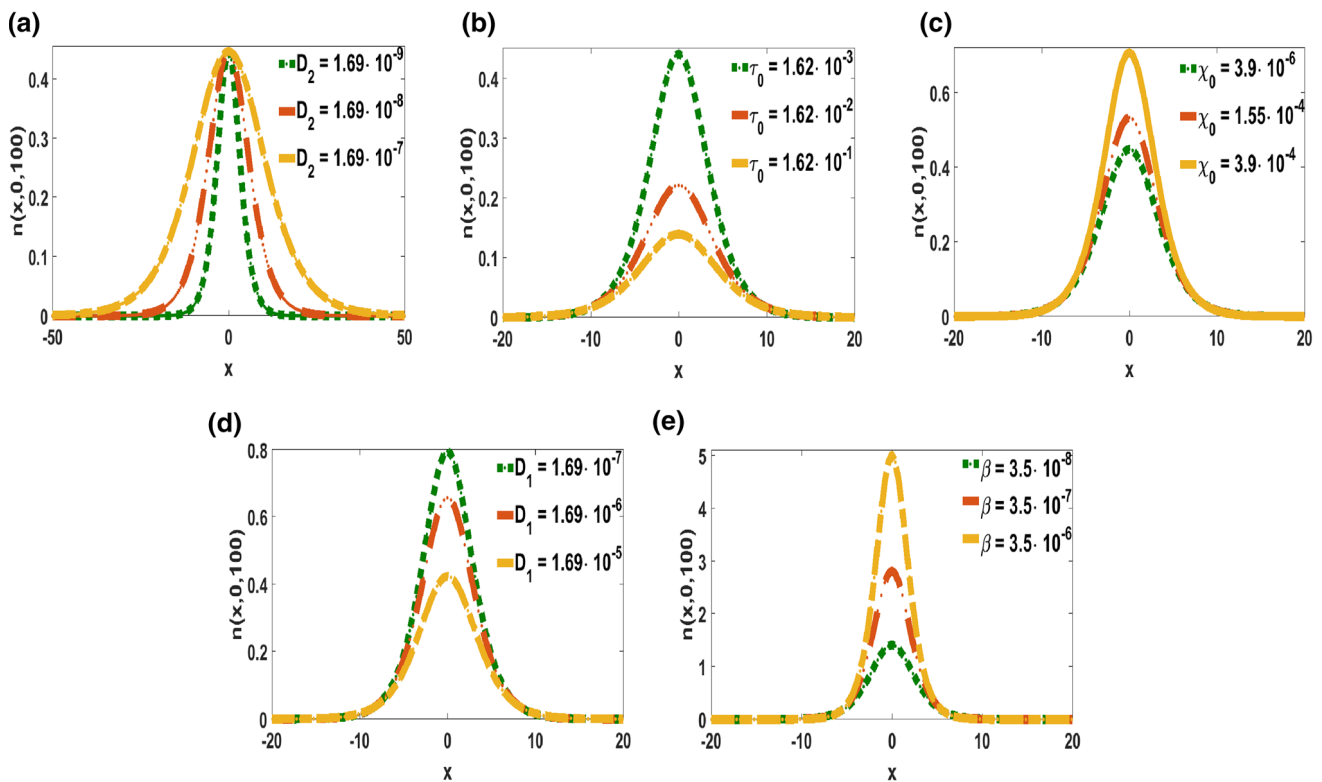
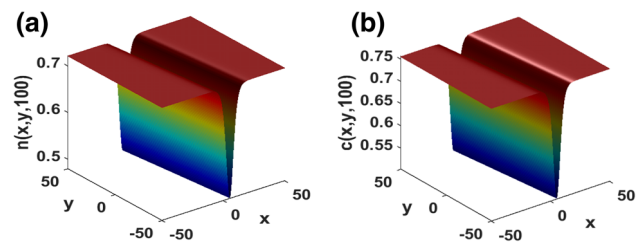


**Fig. 2** Influence of long-range diffusion (a), traction (b), chemotaxis (c), short-range diffusion (d) and chemoattractant consumption rate (e) upon the bell-shaped bacterial wave at  $y = 0$  and time  $t = 100$ .s Except where mentioned, parameters are taken as in Fig. 1

**Fig. 3** Dip traveling waves for bacterial density (a) and chemoattractant concentration (b) given by Eq. (23). Same parameters as in Fig. 1 except for  $P_2 = -2$ .



2.3.2 Dip bacterial and chemoattractant waves: family C

Using the parameters given in Eq. (13a) into Eq. (9) and Eq. (7') permits to recover the dip traveling wave solutions

$$n(x, y, t) = -\frac{15\sigma_1}{4\sigma_2} \left[ 2 + \tanh \left( \sqrt{-\frac{P_2}{2}}(kx + ly - \omega t) \right)^2 \right], \tag{21a}$$

$$c(x, y, t) = c_{\min} + \frac{15\tau_0\sigma_1}{4\sigma_2(\chi_0 - \tau_0)} \left[ 2 + \tanh \left( \sqrt{-\frac{P_2}{2}}(kx + ly - \omega t) \right)^2 \right]. \tag{21b}$$

In the long time/large space limits,  $n_{\infty_{dw}} = \lim_{\xi \rightarrow \infty} n(x, y, t) \rightarrow -\frac{45\sigma_1}{4\sigma_2} > 0$  and  $c_{\infty_{dw}} = \lim_{\xi \rightarrow \infty} c(x, y, t) \rightarrow c_{\min} - \frac{45\sigma_1\tau_0}{4\sigma_2(\tau_0 - \chi_0)} > 0$ . The velocity associated with solutions Eq. (21) reads

$$\omega = \delta_{0,x} \sqrt{-\frac{1}{2P_2} \sqrt{-\frac{\sigma_1}{D_2}} - l^2} + \delta_{0,y} l = \omega_{dw}. \tag{22}$$

Figure 3a, b shows the snapshots at time  $t = 100$  of bacterial density (Eq. (21a)) and chemoattractant concentration (Eq. (21b)). The dip waves travel faster than the bell-shape waves since  $\omega_{dw} > \omega_{bs}$ . A straightforward comparison of Eqs. (20) and (22) allows to figure out that the model parameters have similar effects on dip waves and their velocity  $\omega_{dw}$  as on the bell-shape wave presented above.

2.3.3 Step bacterial and chemoattractant waves: family F

Plugging the parameters Eq. (16a) into Eq. (7') and Eq. (8) allows us to construct step traveling waves whose analytical formula are

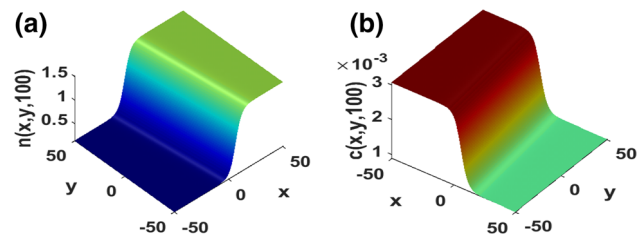
$$n(x, y, t) = -\frac{\sigma_1(21 + \sqrt{105})}{14\sigma_2} - \frac{3\sigma_1(35 - \sqrt{105})}{28\sigma_2} \frac{\cosh \left( \sqrt{\frac{P_2}{4}}(kx + ly - \omega t) \right)^{-2}}{\tanh \left( \sqrt{\frac{P_2}{4}}(kx + ly - \omega t) \right) - 1} \times \left[ -2 + \frac{\cosh \left( \sqrt{\frac{P_2}{4}}(kx + ly - \omega t) \right)^{-2}}{\tanh \left( \sqrt{\frac{P_2}{4}}(kx + ly - \omega t) \right) - 1} \right], \tag{23a}$$

$$c(x, y, t) = c_{\min} + \frac{\tau_0\sigma_1(21 + \sqrt{105})}{14\sigma_2(\chi_0 - \tau_0)} + \frac{3\sigma_1\tau_0(35 - \sqrt{105})}{28\sigma_2(\chi_0 - \tau_0)} \frac{\cosh \left( \sqrt{\frac{P_2}{4}}(kx + ly - \omega t) \right)^{-2}}{\tanh \left( \sqrt{\frac{P_2}{4}}(kx + ly - \omega t) \right) - 1} \left[ -2 + \frac{\cosh \left( \sqrt{\frac{P_2}{4}}(kx + ly - \omega t) \right)^{-2}}{\tanh \left( \sqrt{\frac{P_2}{4}}(kx + ly - \omega t) \right) - 1} \right]. \tag{23b}$$

The corresponding velocity associated with solutions Eq. (23) is

$$\omega = \delta_{0,x} \sqrt{\frac{1}{P_2} \sqrt{\frac{7 - \sqrt{105}}{14D_2}} \sigma_1 - l^2} + \delta_{0,y} l = \omega_{sw}. \tag{24}$$

**Fig. 4** Step traveling waves for bacterial density (a) and chemoattractant concentration (b) (Eq. (23)).  $P_2 = 4$ , other parameters taken as in Fig. 1



Furthermore,  $n_{-\infty_{sw}} = \lim_{\xi \rightarrow -\infty} n(x, y, t) \rightarrow -\frac{\sigma_1(21+\sqrt{105})}{14\sigma_2}$ ,  $c_{-\infty_{sw}} = \lim_{\xi \rightarrow -\infty} c(x, y, t) \rightarrow c_{\min} - \frac{\sigma_1\tau_0(21+\sqrt{105})}{14\sigma_2(\tau_0-\chi_0)}$ , and  $n_{+\infty_{sw}} = \lim_{\xi \rightarrow +\infty} n(x, y, t) \rightarrow -\frac{\sigma_1(420-11\sqrt{105})}{14\sigma_2}$ ,  $c_{+\infty_{sw}} = \lim_{\xi \rightarrow +\infty} c(x, y, t) \rightarrow c_{\min} - \frac{\sigma_1\tau_0(420-11\sqrt{105})}{14\sigma_2(\tau_0-\chi_0)}$ . Step waves obtained here translate the transition process happening between two different levels of bacteria as well as chemoattractant distribution. The gap between the levels depends on system parameters, which means that the experimenter has the potential of choosing how and the position at which the transition happens. Figure 4 displays bacterial and chemoattractant step waves Eq. (23) in panels (a), (b), respectively.

Numerical values of short-range diffusion  $D_1$ ,  $D_3$ , chemotaxis strength  $\chi_0$ , chemoattractant consumption rate  $\beta$ , and medium carrying capacity  $\sigma$  were chosen as in [3, 19, 29, 30]. The fluids flow rate was taken according to experimental studies [18–20, 29, 30]. The other parameters  $\tau_0$ ,  $D_2$ ,  $\beta_1$ ,  $\beta_3$  to the best of our knowledge are not yet available. While the analytical formalism used allows to determine  $\beta_3$  as given by Eqs. (11)–(17), the existence of solutions discussed yields a minimum value of  $\beta_1$ . Though traction forces dominate the chemotaxis strength, the latter is shown to still have strong effects on wave characteristics namely the velocity, amplitude, and thickness. These observations are consistent with conclusions reported in [30]. More importantly, for the same set of parameter values, comparison of Eq. (20), Eqs. (22) and (24) yields  $\omega_{dw} > \omega_{sw} > \omega_{bs}$ : The dip waves travel faster than the step and the bell-shaped waves. In other words, dip waves are better candidates to achieve fast coordination of cells or to quickly convey a piece of information within a bacterial population. From Eqs. (19), (21) and (23), one derives the inequalities  $n_{sw} > n_{dw} > n_{bs}$ . Step waves carry a higher number of particles compared to dip and bell-shaped waves. Generally speaking, an optimal transport is expected for higher velocities and wave amplitudes, but the results obtained here draw the roadmap to characterizing an optimal transport as follows: while step waves ensure the transport of a higher number of particles, a faster transport is guaranteed through dip wave structures. In reactive systems without traction and long-range diffusion, it has been shown that optimal transport necessitates the coupled dynamic between short-range diffusion and feedback [56, 57]. However, the present study stresses that traction and long-range diffusion deeply alter the optimal transport of waves, hence must be taken into account for a better description of waves propagation.

### 3 Numerical experiments

In this section, we ascertain the ability of waves discussed above to propagate in a stable fashion way in model Eq. (3). To this end, direct numerical integrations of Eq. (3) on a square spatial domain of length  $L = 100$  are performed. We take  $N = 512$  points along each spatial direction with a time step is  $dt = 10^{-2}$ . Integrations are performed through the pseudo-spectral method. We initially launched the simulations by introducing perturbed analytical solutions with a noise strength of ten percent of the initial amplitude of the wave. Simulations ran over a final time  $t_{\text{fin}} = 200$  s and results are displayed in Figs. 5, 6, 7. To be precise, panels (a), (b), (c) of Figs. 5, 6, 7 (resp. panels (d), (e), (f)) display snapshots of the bacterial density (resp. chemoattractant concentration) at  $t = 0$  s, 100 s, 200 s, respectively, obtained with the analytical solutions Eqs. (19), (21), (23) as initial conditions. Though we inserted a random perturbation at the initial time, the results depicted in Figs. 5, 6, 7 show that initial solutions evolve without undergoing any collapses nor explosions. Our solutions are numerically stable ones. In addition, from Eqs. (19), (21), and (23), the analytical solutions found above predict waves whose profiles, widths, amplitudes, and velocities remain unchanged during their evolutions, but are slightly displaced due to small fluid velocities of magnitude about  $10^{-5}$ . Snapshots of waves displayed in Figs. 5, 6, 7 are in good agreement with analytical predictions. Our solutions are therefore stable ones, such that they are likely to be observed in experiments. Interestingly, analyzing Fig. 6 reveals that the heights of dip bacterial and chemical waves are slightly shifted by a magnitude of  $\sim 10^{-2}$ . The latter observation forces us to determine the absolute errors for bacterial and chemoattractant concentrations and found that  $|n_{\text{ana}}(x, y, t) - n_{\text{num}}(x, y, t)| \sim 10^{-2}$ ,  $|c_{\text{ana}}(x, y, t) - c_{\text{num}}(x, y, t)| \sim 10^{-2}$ . Dip waves have not yet been recovered in chemotactic systems, to the best of our knowledge. The fact that their height slightly increases may be the signature of some biophysical features whose stability properties are beyond the scope of the present work. Our results are new ones and we do believe this work may motivate further two-dimensional experimental investigations in chemotaxis systems where traction forces, advection, and long-range diffusion are at play. To the best of our knowledge, such experimental investigations that take into account the latter effects are still missing.

In the above numerical simulations, we show that solutions constructed here are stable, even though families of solutions B, D, E, G are not presented. The solutions corresponding to Families B, D, E, and G exhibit periodic and triangular periodic waves. They



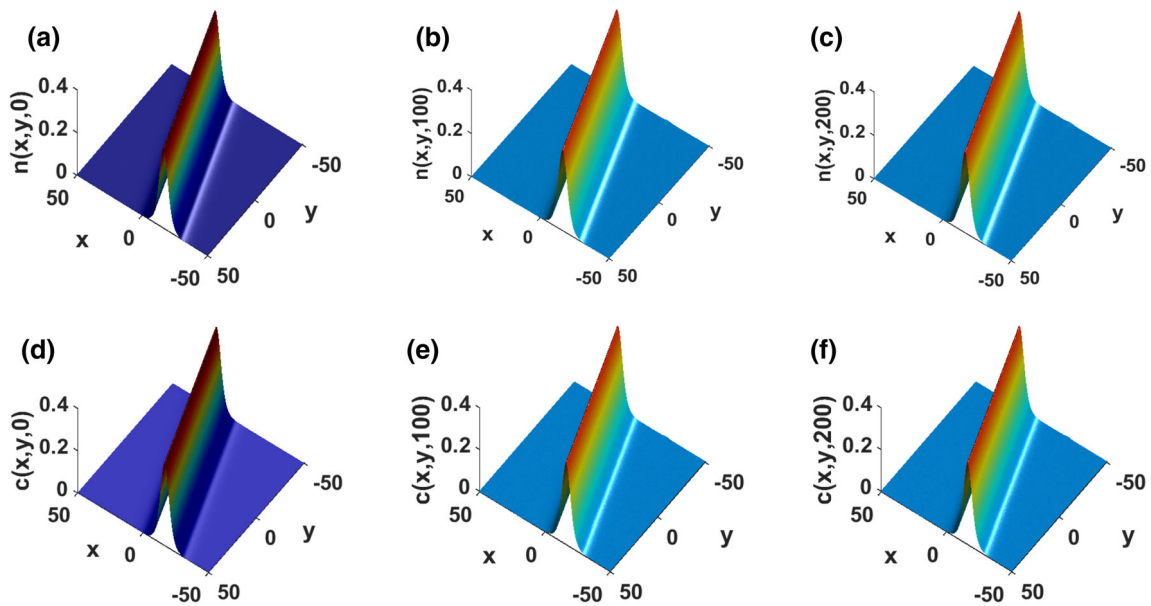


**Fig. 5** Snapshots of stable numerical bell-shape solutions for bacterial (chemoattractant) wave at  $t = 0$  s (a) [(d)],  $t = 100$  s (b) [(e)], and  $t = 200$  s (c) [(f)]. Parameters as in Fig. 1

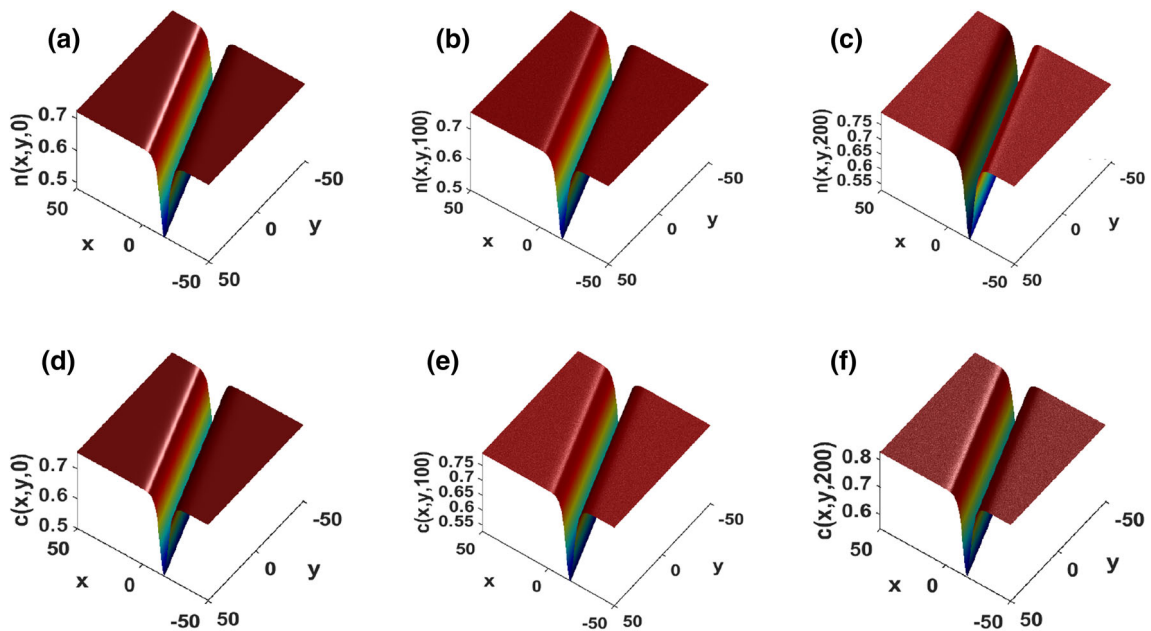


**Fig. 6** Stable propagation of dip bacterial (chemoattractant) wave at  $t = 0$  s (a) [(d)],  $t = 100$  s (b) [(e)], and  $t = 200$  s (c) [(f)]. Parameters as in Fig. 1

actually represent important ways by which bacteria and chemoattractant are transported, in addition to the fact that they substantially match recent experimental results [18–20]. Periodic bacterial waves were proposed as a mechanism to inhibit the runaway fashions due to catalysis response of cells to chemoattractant they might produce [43,57]. In this sense, periodic waves corresponding to Families B, D, E, and G are stable solutions that could be used in the assessment of other aspects of the transport of chemotactic particles in fluids.

#### 4 Conclusion

We discussed the existence and the dynamical behaviors of bacterial and chemical waves propagating in a  $(2 + 1)$ -dimensional chemotactic system. We introduced a new model that takes into consideration several processes including a uniform advection,

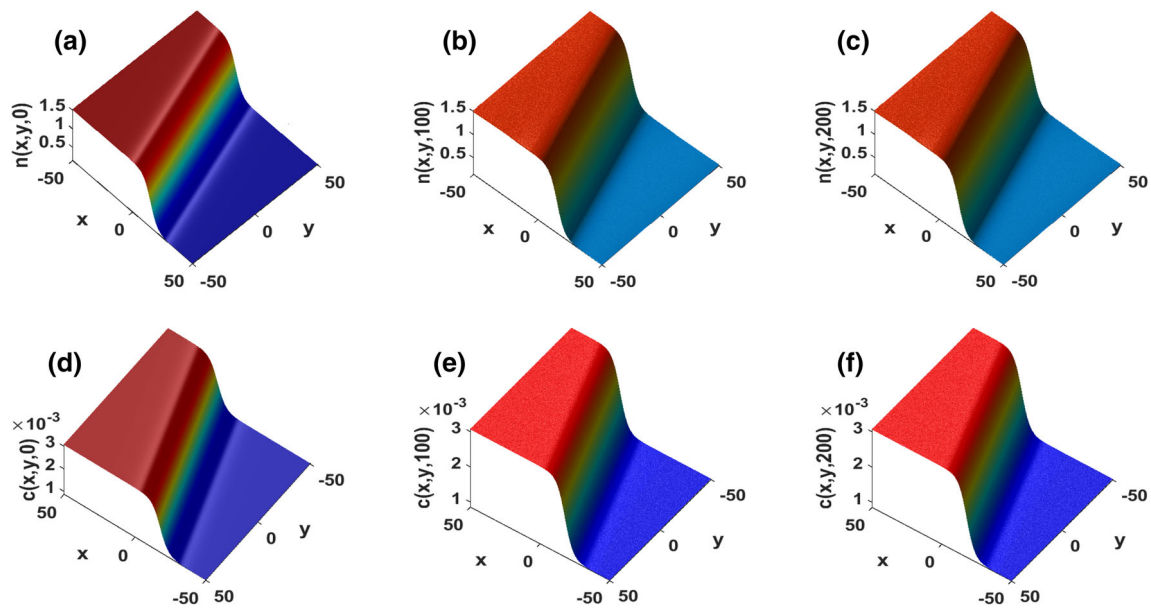


**Fig. 7** Stable evolutions of step waves of bacterial (chemoattractant) at  $t = 0$  s (a) [(d)],  $t = 100$  s (b) [(e)], and  $t = 200$  s (c) [(f)]. Parameters as in Fig. 1

long-range diffusion, chemotaxis, traction, cellular proliferation, and chemoattractant production degradation. The traveling wave variable is assumed and an extended F-expansion method is used to construct new traveling wave solutions like step, dip, and bell-shape waves. The quest for physically acceptable solutions enforces the existence of a minimum chemoattractant concentration which depends on both traction, chemotaxis strength, bacterial and chemical short-range diffusion. We showed that traction, short-range diffusion, chemotaxis, and chemoattractant consumption rate have competing effects on the number of particles transported. The former parameters decrease the number of particles transported while the latter ones increase wave amplitudes. Increasing values of long-range diffusion decrease wave velocity but increase the wave width, the amplitude remaining unchanged. Besides, by comparing velocities and amplitudes of solutions presented, we observed that while dip waves travel faster hence are better candidates to explaining fast bacterial coordination, step waves have the potential of carrying a higher number of cells, hence may be considered as robust structures to perform transport in a highly dense system. The stability of solutions constructed is analyzed through direct numerical integration of the original model. Both numerical and analytical solutions remain very close hence ascertaining our theoretical predictions.

**Data Availability Statement** This manuscript has associated data in a data repository. This manuscript has associated data in a data repository. [Authors' comment: The data that support the findings of this study are available in GitHub at <https://github.com/wil-09/Codes/blob/master/Code.m>.]

#### Declarations

**Conflict of interest** The authors declare that they have no conflict of interest.

#### References

1. J. Adler, *Science* **153**, 708 (1966)
2. M. Eisenbach, *Chemotaxis* (Imperial Colleges Press, London, 2004)
3. J. Murray, *Mathematical Biology II: Spatial Models and Biomedical Applications*, 2nd edn. (Springer, New York, 2002)
4. J. Murray, *Mathematical Biology I. An Introduction*, 1st edn. (Springer, New York, 1993)
5. L. Zhicheng, B. Quaife, H. Salman, N.O. Zoltan, *Sci. Rep.* **7**, 12855 (2017)
6. L. Long, S.W. Zucker, T. Emonet, *PLoS Comput. Biol.* **13**, 3 (2017)
7. H. Berg, E.O. Budrene, *Nature* **376**, 6 (1995)
8. N. Mittal, E.O. Budrene, M.P. Brenner, A. Van Oudenaarden, *Proc. Natl. Acad. Sci. USA* **100**, 13259 (2003)
9. C. Dombrowski, L. Cisneros, S. Chatkaew, R.E. Goldstein, J.O. Kessler, *Phys. Rev. Lett.* **93**, 098103 (2004)
10. A. Sokolov, I. Aranson, *Phys. Rev. Lett.* **109**, 248109 (2012)
11. H. Wioland, F.G. Woodhouse, J. Dunkel, R.E. Goldstein, *Nat. Phys.* **12**, 341 (2016)
12. J. Gachelin, A. Rousselet, A. Lindner, E. Clement, *New J. Phys.* **16**, 025003 (2014)
13. E. Lushi, H. Wioland, R.E. Goldstein, *Proc. Natl. Acad. Sci. USA* **111**, 9733 (2014)
14. H. Wioland, E. Lushi, R.E. Goldstein, *New J. Phys.* **18**, 075002 (2016)
15. M. Ben Amar, C. Bianca, *Sci. Rep.* **3**, 33849 (2016)
16. E. Lushi, R.E. Goldstein, M.J. Shelley, *Phys. Rev. E* **98**, 052411 (2018)

17. A.J. Muinonen-Martin, PLoS Biol. **12**, e1001966 (2014)
18. A. Gholami, V. Zykov, O. Steinbock, E. Bodenschatz, New J. Phys. **17**, 093040 (2015)
19. T. Eckstein, E. Vidal-Henriquez, A. Bae, V. Zykov, E. Bodenschatz, A. Gholami, PLoS ONE **3**, 13 (2018)
20. E. Vidal-Henriquez, V. Zykov, E. Bodenschatz, A. Gholami, Chaos **27**, 103110 (2017)
21. A. Chertock, K. Fellner, A. Kurganov, A. Lorz, P.A. Markowich, J. Fluid Mech. **694**, 155 (2012)
22. D. Saintillan, M.J. Shelley, Phys. Rev. Lett. **100**, 178103 (2008)
23. A. Sokolov, I.S. Aranson, Phys. Rev. Lett. **109**, 248109 (2012)
24. L. Cisneros, R. Cortez, C. Dombrowski, R.E. Goldstein, J.O. Kessler, Exp. Fluids. **43**, 737 (2007)
25. E.F. Keller, J. Theor. Biol. **2**, 30235 (1971)
26. M.P. Brenner, L.S. Levitov, E.O. Budrene, Biophys. J. **74**, 1677 (1998)
27. H. Triki, H. Leblond, D. Mihalache, Nonlinear Dyn. **86**, 2115 (2016)
28. P. Zupanovic, M. Brumen, M. Jagodic, D. Juretic, Phil. Trans. R. Soc. B. **365**, 1397 (2010)
29. M. Seyrich, A. Palugniok, H. Stark, New J. Phys. **21**, 103001 (2019)
30. C. Emako, C. Gayraud, A. Buguin, L. Neves de Almeida, N. Vauchelet, PLoS Comput. Biol. **12**, 4 (2016)
31. J. Saragosti, V. Calvez, N. Bournaveas, A. Buguin, P. Silberzan, PLoS Comput. Biol. **8**, 6 (2010)
32. A. Mishra, R.S. Kaushal, A. Prasad, Pramana. J. Phys. **86**, 5 (2016)
33. E.O. Budrene, H. Berg, Nature **349**, 630 (1991)
34. C.S. Patlak, Bull. Math. Biophys. **15**(1953)
35. E.F. Evelyn, F. Keller, L.A. Segel, J. Theor. Biol. **2**, 225 (1971)
36. K.J. Painter, T. Hillen, Physica D **240**, 363–375 (2011)
37. C. Xue, H. Ju Hwang, K.J. Painter, R. Erban, Bull. Math. Biol. **73**, 16951733 (2011)
38. B. Franz, C. Xue, K.J. Painter, R. Erban, Bull. Math. Biol. **76**, 377 (2014)
39. T. Hillen, K.J. Painter, J. Math. Biol. **58**, 183 (2009)
40. M. Ben Amar, Sci. Rep. **6**, 21269 (2016)
41. R. Karmakar, T. Man-Ho, Y. Haicen Yue, D. Lombardo, A. Karanam, B.A. Camley, A. Groisman, W.-J. Rappel, Phys. Rev. E. **103**, 012402 (2021)
42. T. B. Issa, R. B. Salako, W. Shen, [arXiv:2010.11335v1](https://arxiv.org/abs/2010.11335v1) [math.AP] 21 Oct (2020)
43. W. DomgnoKuipou, D. Belobo Belobo, A. Mohamadou, Eur. Phys. J. Plus. **136**, 701 (2021)
44. V. Calvez, B. Perthame, S. Yasuda, AIMS **4**, 11 (2018)
45. A. Darwish, E.F.G. Fang, Chaos Solit. Fract. **20**, 609 (2004)
46. D. Belobo Belobo, T. Meier, Sci. Rep. **8**, 3706 (2018)
47. Y. Zhou, M. Wang, Y. Wang, Phys. Lett. A **308**, 31 (2003)
48. S.K. Liu, Z.T. Fu, S.D. Liu, Q. Zhao, Phys. Lett. A **289**, 69 (2001)
49. Z.T. Fu, S.K. Liu, S.D. Liu, Q. Zhao, Phys. Lett. A **290**, 72 (2001)
50. M.L. Wang, Y.M. Wang, Phys. Lett. A **287**, 211 (2001)
51. E.F. Keller, L.A. Segel, J. Theor. Biol. **26**, 399 (1970)
52. A. Bhowmik, W.-J. Rappel, H. Levine, Phys. Biol. **13**, 016002 (2016)
53. M. Kærn, M. Menzinger, J. Phys. Chem. B. **14**, 3751 (2002)
54. E.A. Ermakova, E.E. Shnol, M.A. Panteleev, A.A. Butylin, V. Volpert, F.I. Ataulkhanov, PloS One **2**, 4 (2009)
55. M. Leconte, J. Martin, N. Rakotomalala, D. Salin, Y. Yortsos, J. Chem. Phys. **16**, 7314 (2004)
56. K. Ishihara, P.A. Nguyen, M. Waehr, A.C. Groen, C.M. Field, T., J. Mitchison. Philos. Trans. R. Soc. Lond. B. Biol. Sci. **369**(2014)
57. L. Gelens, G.A. Anderson, J.E. Ferrell Jr., Mol. Biol. Cell. **25**, 3486 (2014)